105

DESIGN, FABRICATION, AND TESTING OF A PULVERIZED FUEL COMBUSTION FACILITY

by

Lawrence Patrick Nelson

B.S., Pittsburg State University, 1977

A MASTER'S THESIS

submitted in partial fulfillment of the

requirements for the degree

MASTER OF SCIENCE

Department of Nuclear Engineering

KANSAS STATE UNIVERSITY

Manhattan, Kansas

1979

Approved:

Thomas W. Lester

Major Professor

TABLE OF CONTENTS

LIST OF FIGURES

LIST OF TABLES

1 INTRODUCTION

1.1 General Considerations

Increasing the use of coal in utility boilers is important insofar as the United States is estimated to have between 25 to 30 percent of the world's unexploited coal reserves[1]. In energy content the coal reserves of the United States represent nearly 80% of our fossil fuel reserves, and yet, in 1973 coal accounted for only 24% of the total fossil fuels extracted, well below both natural gas and petroleum. Accompanying this growth in coal utilization will be a potentially disastrous rise in the levels of noxious emissions such as oxides of nitrogen (NO_x), sulfur dioxide (SO_2), particulate matter, and trace elements. To minimize detrimental effects to the population and property, steps must be taken to control these emissions. To accomplish this, research into the combustion characteristics of and pollutant formation mechanisms from coal is needed.

A large number of variables exert an influence on the behavior of a coal fired boiler. Among these are the properties of the coal being fired, the physical condition of the boiler, the aerodynamics and stoichiometry within the combustion zone, and the boiler surface and air temperatures. The individual influences of each of these parameters on emissions and combustion efficiency are not well known, save in the grossest sense. Experimentation in full scale, operating boilers is prohibitively expensive, time consuming, and not likely to yield information of a basic nature that can be applied to different boiler designs.

Small scale combustion facilities were conceived originally as a means of conducting preliminary investigations into proposed emission control schemes without expending the effort and capital necessary to facilitate full scale testing. These apparatus are designed to simulate as closely as practicable the conditions within larger boilers. In this manner, promising methods may be developed for further testing in larger units and concepts of dubious merit may be screened out.

The advantages of utilizing a small scale burner facility are manifold. Equipment modifications and replacements are cheaper and simpler to accomplish. It is expected that conditions within the region of interest are easier to control on a smaller scale. By making minor modifications the same facility may be employed to simulate different boiler designs or to perform basic combustion research. In addition, it may be utilized in the study of a wide range of alternative solid fuels and fuel mixtures without jeopardizing the integrity of a full scale unit. The laboratory scale furnace thus has the advantages of being much more versatile and easier to operate and maintain. One possible disadvantage is the lack of knowledge concerning the applicability of results obtained from the smaller apparatus to full scale furnaces. At least one concern performing investigations sponsored by the Environmental Protection Agency routinely tests its emission control techniques on small, medium, and large scale experimental apparatus to determine any effect of scaling on the results.

This project was motivated by the need for an experimental test bed to study the emission and firing characteristics of high sulfur midwestern

bituminous coals and agricultural residue when fired under conditions comparable to those encountered in a utility boiler. Significant basic combustion research on coal and agricultural dusts has previously been performed employing the single pulse chemical shock tube at Kansas State University, but facilities for more applied research were not available. The purpose of this project was to design, construct, and demonstrate the utility of a laboratory scale combustion facility for pulverized solid fuels.

Design of the facility involved a review of similar equipment with respect to the particular demands of this investigation. Several goals served to guide the design procedure. First, the combustion environment created (temperatures, residence time, and burner configuration) had to be suitably representative of larger scale equipment designs. Second, the apparatus had to be versatile enough that a wide range of experiments could be accommodated. Third, the equipment had to be engineered to be compatible with the surroundings. For example, it was necessary to keep pulverized fuel dusts and noxious exhaust gases confined to the laboratory furnace and exhaust system. Fourth, it was necessary to plan the project in such a way that the equipment could be modified or dismantled with a reasonable expenditure of effort in order to increase the flexibility of the facility and allow for alternative uses of the laboratory facilities.

The construction phase of the project overlapped with both the design and demonstration phases as more experience was accrued and

better design ideas incorporated. There were two guidelines that steered construction of the facility. One was to follow the design specifications as closely as possible and recommend improvements where needed. The second and most important objective was to construct the facility with continual emphasis on safety. This included not only careful assembly and installation of the designed safety equipment, but diligence in the installation of all systems, particularly those separating the combustion products from the laboratory environment.

The demonstration phase of the project primarily sought to establish that the data obtained from the facility could be applied to conventional equipment. As a means of satisfying this goal, NO_x and SO_2 emissions were measured from coal flames and compared with results from earlier EPA sponsored research. There was no attempt made to directly compare this facility's performance characteristics to those of a full scale operating boiler since variations in boiler design and conditions have a significant effect on their performance. A secondary objective was to investigate the suitability of an agricultural waste product, wheat straw, as a boiler fuel. This portion of the study established the effects of cofiring various amounts of straw and coal on gaseous emissions, and discerned whether burning the mixtures had any noticeable bearing on flame stability and luminosity.

In the sections that follow, the general theory of pulverized fuel combustion will be covered, with particular emphasis on the parameters germane to construction of the furnace. The harmful effects of

some of the emissions from coal flames will be discussed in order to underscore the importance of emissions control. A description of the apparatus and reports on the results of testing low and high sulfur coals and wheat straw will be presented and compared where possible to similar work. Finally, based on the firing results, the potential for firing wheat straw in utility boilers will be addressed and possible problems discussed.

1.2 Particle Combustion

The combustion of pulverized solid fuel is a complicated physical and chemical reaction involving conductive, convective, and radiative heat transfer, particle pyrolysis, mass transfer, and ignition and burning of matter in the gaseous and solid states. Furthermore, it is dependent on a multitude of properties of the fuel, the combustion chamber, and conditions such as temperature, aerodynamics, and local stoichiometry. The explanation offered in this section must thus be recognized as a simplification of the actual process and not a comprehensive technical review. Several recent publications[2,3] provide excellent overviews which the interested reader may consult for a more rigorous analysis.

The pulverized fuel is introduced usually to the combustion chamber as a suspension in the primary air which also serves as a portion of the oxidizer. The balance of the oxidizer, or secondary air, may be injected in a number of ways with the particular method having an important effect on combustion efficiency and pollutant

formation. In fact, one of the NO_x control techniques discussed later in this chapter consists solely of controlling the secondary air injection. As the fuel particles enter the combustion chamber they absorb heat from the flame and the hot walls causing a very rapid temperature rise which initiates the devolatilization process.

An indepth explanation of devolatilization is beyond the scope of this investigation as evidenced by the number of papers concerning the subject. Nonetheless, a brief introduction to the process is imperative to the understanding of combustion. Those readers interested in delving into the matter are referred to detailed reviews such as those by Howard[4], Howard and Anthony[5], and Badzioch[6,63] or to an analysis of some of the more notable studies by Wegener[7].

Devolatilization may be explained as the natural coalification process accelerated to an appreciable rate. Coal originates as vegetable matter and is slowly pyrolyzed under conditions of great pressure to an eventual graphitic composition. The varied ranks of coal are attributable to different stages of this coalification which proceeds via the evolution of gases containing carbon, hydrogen, and oxygen leaving the coal progressively richer in carbon content. Coalification is discussed in detail by Essenhigh[8]. Heating of a coal sample causes the coalification to occur more rapidly and the resultant evolution of tars and gaseous species is termed devolatilization.

The commonly encountered gaseous products of devolatilization are CO, CO_2, H_2, H_2O, and hydrocarbons, but the relative yields of each as

well as the total volatile matter yield (as a weight percent of the original fuel) can vary extensively depending on conditions such as the heating rate, particle size, pressure, temperature, and sample properties. Due to variations in equipment and procedures in the numerous studies, there is still disagreement over the mechanisms of importance and the effects of altering the parameters mentioned above. Wegener[7] correlated the results of some of the more noteworthy recent experiments and arrived at several conclusions. Among his conclusions were:

1) The total yield of volatile matter increases as the maximum temperature is increased,

2) the effect of the heating rate is not fully established. Although most of the studies of this effect show that the yield of volatiles increases at higher heating rates, it has not been determined whether the higher heating rate or the measures taken to produce that heating rate are responsible for the increased yield,

3) there is disagreement as to whether the bulk of devolatilization occurs during the heat up process or after the particle has attained a steady temperature.

Returning to our simplified combustion model, we now have some mixture of solid particles and volatile species flowing in a high temperature region of the furnace. Ignition of one or both of the phases occurs next. The phase hosting ignition (and the early stages of combustion) is open to a great deal of controversy. Until about 1965, it was accepted that the Faraday mechanism, which holds that ignition occurs in the gas phase volatile species, was the correct view

of particle ignition. This supposition had broad support from the coal research community, including the United States Bureau of Mines, but only circumstantial experimental evidence. The strongest argument for gas phase ignition has been the success in correlating various measures of explosion severity with the fuel volatile content as determined from a standardized analysis. In 1965, Howard and Essenhigh[9,10] reported experimental results from which they inferred that ignition was occurring on the particle surface, and that significant devolatilization did not take place until after the particles had passed through the flame front. Data taken by Howard in support of heterogeneous combustion are shown in Fig. 1. These results have since been questioned by Badzioch and Hawksley[11] and Kimber and Gray[12] because Howard and Essenhigh based their findings on the lack of change in the ASTM volatile matter content between the coal and samples of particles taken near the flame; whereas subsequent studies have revealed that the volatile yield under combustion conditions may be twice the ASTM figure[7]. As an extension of their initial findings, Howard and Essenhigh[13,14] established a size criterion for particles above which the volatile flux was sufficient to shield the surface from the surrounding atmosphere and thus prevent reaction on the surface. Hence, ignition could be both homogeneous and heterogeneous or either mechanism could be dominant depending on the particle size distribution. The review of literature in the study by Seeker[15] details the experimental evidence supporting both theories.

Regardless of which ignition mechanism is accepted, it is experimentally observed that volatiles' combustion is completed long

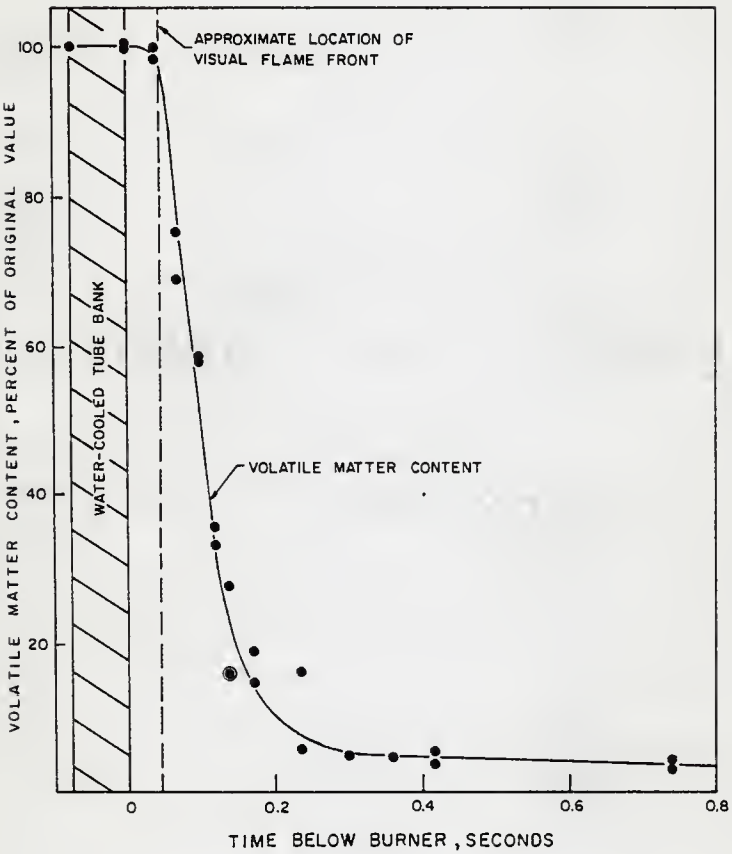

FIGURE 1 EXPERIMENTALLY OBSERVED ASTM VOLATILE MATTER LOSS IN PLUG FLOW FURNACE, AFTER (9)

before the finish of solid particle combustion, which is commonly termed char burnout. The char burnout regime in a well designed combustion chamber should conclude prior to the particle's entrance into the tube banks. Char burnout kinetics are intricately related to the structure of coal particles and particularly their porosity during the combustion. Pore volume measurement methods, several of which are detailed by Laurendeau[16] and by Orr and Dallavalle[17], have determined that the total surface area of various coals ranges from 100 to 400 m^2/gm, appreciably greater than the surface area of 1 μm diameter nonporous spheres which is 1.36 m^2/gm.[18] This porosity cannot be neglected when considering devolatilization, which may occur internally with subsequent removal of the volatile matter through the pores, or oxidation of the particle in which considerable reaction occurs within the pores.

Smith[19] has developed the following model for the sequence of events constituting a heterogeneous process, here applied to the char burnout mechanism:

1) transport of O_2 from the bulk fluid to the particle surface;
2) transport of O_2 from the surface to the interior of the particle;
3) absorption of O_2 at interior reaction sites of the coal particle;
4) chemical reaction of absorbed O_2 with carbon to form absorbed products (either CO or CO_2);
5) desorption of products;
6) transport of products from the interior to the surface of the coal particle;

7) transport of the products from the particle surface to the bulk fluid.

Modifying Seeker's[15] approach to a qualitative analysis of the process, it is possible to determine the rate controlling step based on properties of the coal and its surroundings. Utilizing the widely accepted nomenclature of Walerk, et al.[20] the conditions under which a certain mechanism proceeds so slowly as to control the rate of reaction are defined as zones. Figure 2 represents graphically the oxygen concentration gradient near a single coal particle for the different zones discussed below. Zone I comprises the regime wherein diffusion of oxygen first to the surface and ultimately to the interior of the particle is of such a speed that a chemical reaction, either adsorption or desorption, controls the reaction rate. According to Seeker[15] adsorption or desorption control can be established from the reaction order with respect to oxygen. A reaction of zero order, i.e., reaction independent of the bulk oxygen concentration, indicates desorption control while a first order oxygen dependence is expected when adsorption regulates the rate. In Zone II, oxygen penetrates into the particle, but the reaction is sufficiently fast that the oxygen is consumed prior to the diffusion of the oxygen to the center of the particle. In such a case, chemical reaction and pore diffusion both control the reaction rate. Mulcahy and Smith[21] have shown that determination of the measured order of reaction in this zone will again indicate whether adsorption (n=1) or desorption (n=1/2) is the rate

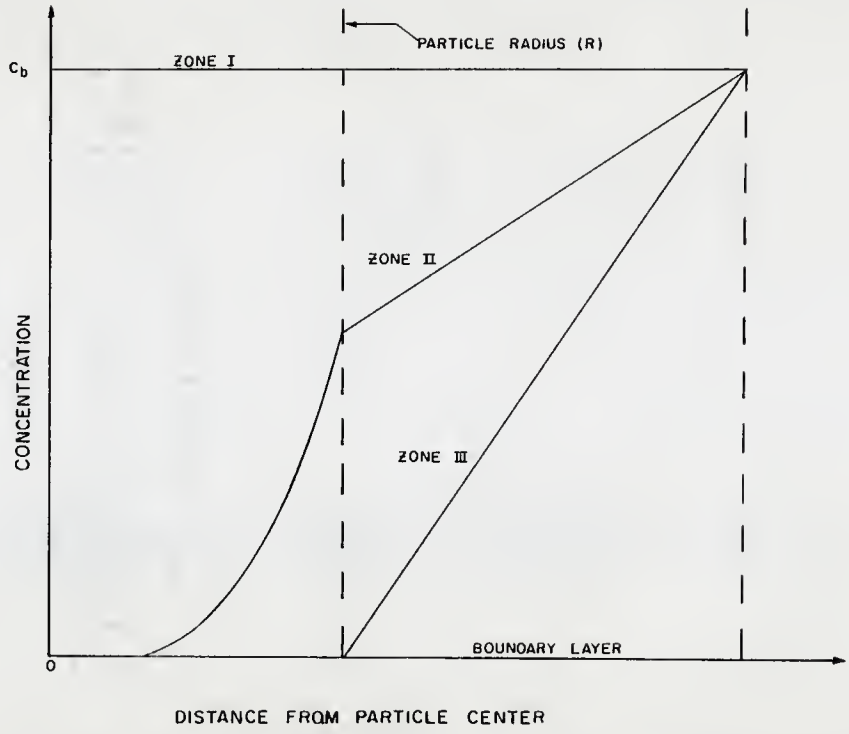

FIGURE 2 PREDICTED OXYGEN CONCENTRATION AS A FUNCTION OF DISTANCE FROM PARTICLE CENTER, AFTER (16)

controlling mechanism. Emphasis is placed on the qualifier "measured" because the true and measured reaction orders are not necessarily equal for Zone II, being related by the expression

$$n_m = (n_t+1)/2 \qquad (1)$$

where n_m is the measured and n_t the true order of reaction with respect to the bulk oxygen concentration. The final zone, Zone III, is controlled by transport of oxygen to the particle surface since the chemical reaction and product disposal mechanisms are rapid in comparison. In this instance, the porosity may be ignored since any oxygen reaching the particle external surface will find an abundance of reaction sites and will be consumed prior to being transported to the particle interior.

The concept of zone kinetics is useful in discussing one of the unresolved questions of char burnout, that being the burnout mode. When Zone I kinetics are observed, reaction occurs throughout the particle, and the particle may be expected to burn out at constant diameter with hollow spheres or cenospheres forming from the ash fraction. Lightman and Street[22] offer excellent pictorial evidence of this mode of burnout. Zone III kinetics, on the other hand, with the characteristic lack of oxygen at interior sites, necessarily result in combustion only at the particle surface, and give rise to a shrinking particle behavior. Zone II kinetics exhibit behavior intermediate between the shrinking particle and constant diameter modes.

The kinetics mode employed to explain combustion has a strong bearing on the expected particle burnout time. The constant diameter behavior of Zone I can be modeled by:

$$4\pi R^2 \omega = -\frac{4}{3}\pi R^3 \frac{d\rho}{dt} \qquad (2)$$

where R is the particle radius (cm), ω is the surface oxidation rate ($g/cm^2 \cdot s$), and ρ is the particle density (g/cm^3). Equation (2) may be rearranged and integrated to yield

$$3\omega(t_{bo}-t_o) = -R(\rho_{bo}-\rho_o) \; . \qquad (3)$$

The boundary conditions are defined by letting the combustion begin at time $t_o=0$ and considering burnout to be complete when the particle has essentially no mass remaining, i.e., $\rho_{bo} = 0$. This gives the burnout time for Zone I as

$$t_{bo} = \frac{\rho_o R}{3\omega} \; . \qquad (4)$$

For Zone III, the assumption is that the particle diameter shrinks during combustion, but the density remains constant. This condition is represented by

$$4\pi R^2 \omega = -\rho_o \; 4\pi R^2 \frac{dR}{dt} \; . \qquad (5)$$

Integration of this equation leaves the result

$$\omega(t_{bo}-t_o) = -\rho_o(R_{bo}-R_o) \; . \qquad (6)$$

For this mode, we assume the same initial condition, i.e., t_o=0, but the completion of the reaction is characterized by the particle radius going to zero or complete consumption of the particle (R_{bo}=0). Thus, the burnout time is given as

$$t_{bo} = \frac{\rho_o R_o}{\omega} \quad . \tag{7}$$

A prediction of burnout time vs. particle size for both diffusional control and chemical control is given in Fig. 3. Readers interested in studying the intricate details of char burnout kinetics are referred to any of the several excellent works concerning this subject[15,16,21,23].

It is clear that the above factors generic to the combustion of coal, make the modelling of the furnace behavior nearly intractable. It is also clear that the design of a combustion chamber must be based on some model, albeit crude. Pulverized fuel combustion system models have been developed and discussed by Field, et al.[24], Essenhigh[25], and Krazinski, et al.[26] to name a few. Presently there is no model that can be applied to simulate all the conditions within a conventional combustion chamber; the models in use require that simplifying assumptions be made concerning the flame zone. The simplest model is that known as the perfectly stirred reactor (PSR) model wherein the combustion chamber is assumed to contain a homogeneous mixture of fuel and products and any new fuel introduced is instantaneously distributed evenly throughout the chamber. The PSR is a zero dimensional model since there are no temperature or composition gradients in any direction within the furnace.

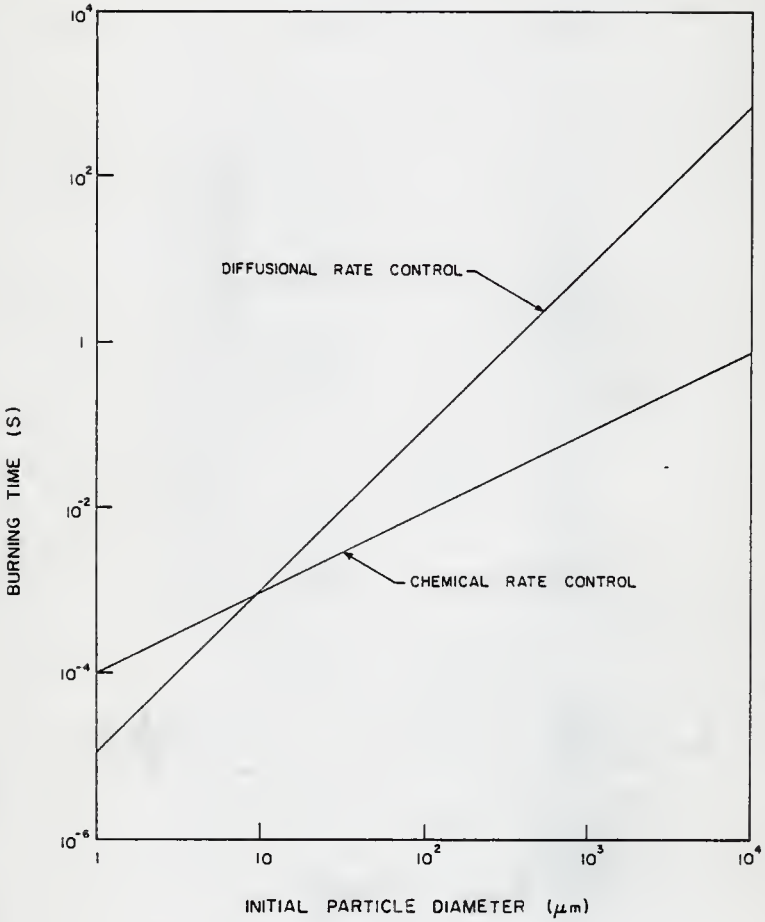

FIGURE 3 PREDICTIONS OF BURNOUT TIME vs. INITIAL PARTICLE DIAMETER, AFTER (16)

In some ways the PSR is too simple to be of use. For example, since all incoming particles are homogeneously mixed there is no unique residence time for a single particle within the furnace. The plug flow reactor (PFR) is a one dimensional model in which the fuel and oxidizer fill the entire cross section of the combustion chamber and flow as a plug through the furnace. In perfect plug flow it is a simple matter to calculate the residence time of a particle. The PFR is a widely used model and experimental furnaces such as those built by Beer, et al[27], Csaba[28], and Howard and Essenhigh[9,10,13,14] approximate plug flow to a greater extent than does the utility boiler. Application of the PFR model is therefore of considerable benefit. Two dimensional models that consider variations in composition and temperature both axially and perpendicular to the flame axis are non-existent in the analysis of an experimental furnace as far as this author can determine. The obvious difficulty of setting up and solving the necessary equations coupled with the adequate results of PFR models is undoubtedly responsible for this fact.

Appendix A discusses a chemical kinetics computer code developed by Bittker and Scullin[81] and employed in this study to formulate an estimate of the particle burnout distance for different initial particle sizes. As explained in the appendix, the simplifications of the plug flow model used by the code result in somewhat unrealistic burnout distances, but the velocity and, hence, the residence time of a gas slug in the furnace are estimated. The residence times can be compared with the predictions of Fig. 3 or with compilations of experimental and predicted burnout times

developed by Thring and Essenhigh[23] and by Field, et al.[24], which are represented in Fig. 4. In this way, an approximation of the particle size resulting in optimum operation was obtained for comparison with the sizing of the fuel used, which was sized such that 95% of the mass is in particles with diameter less than 75 μm.

1.3 Pollutant Formation

As previously mentioned, undesirable products such as NO_x, SO_2, particulate matter, and trace elements are formed or liberated during combustion of coal. The present investigation considers only the gaseous species since these are the focal point of the majority of recent EPA sponsored research. In order to facilitate a better understanding and appreciation of the problem, a limited explanation of the currently accepted formation mechanisms, reasons for concern, and current control technologies for NO_x and SO_2 emissions follows.

The body of literature relating to NO_x production and control is now so large that there are unavoidable differences of opinion; therefore, this review will attempt to present only those parts of the kinetics and mechanism that are not the subject of significant debate. Those readers wishing to examine other opinions or to study the intricacies of NO_x technology are referred especially to the series of International Combustion Symposia[29], the proceedings of the three Stationary Source Combustion Symposia[30,31,32] and the Proceedings of the NO_x Control Technology Seminar[33].

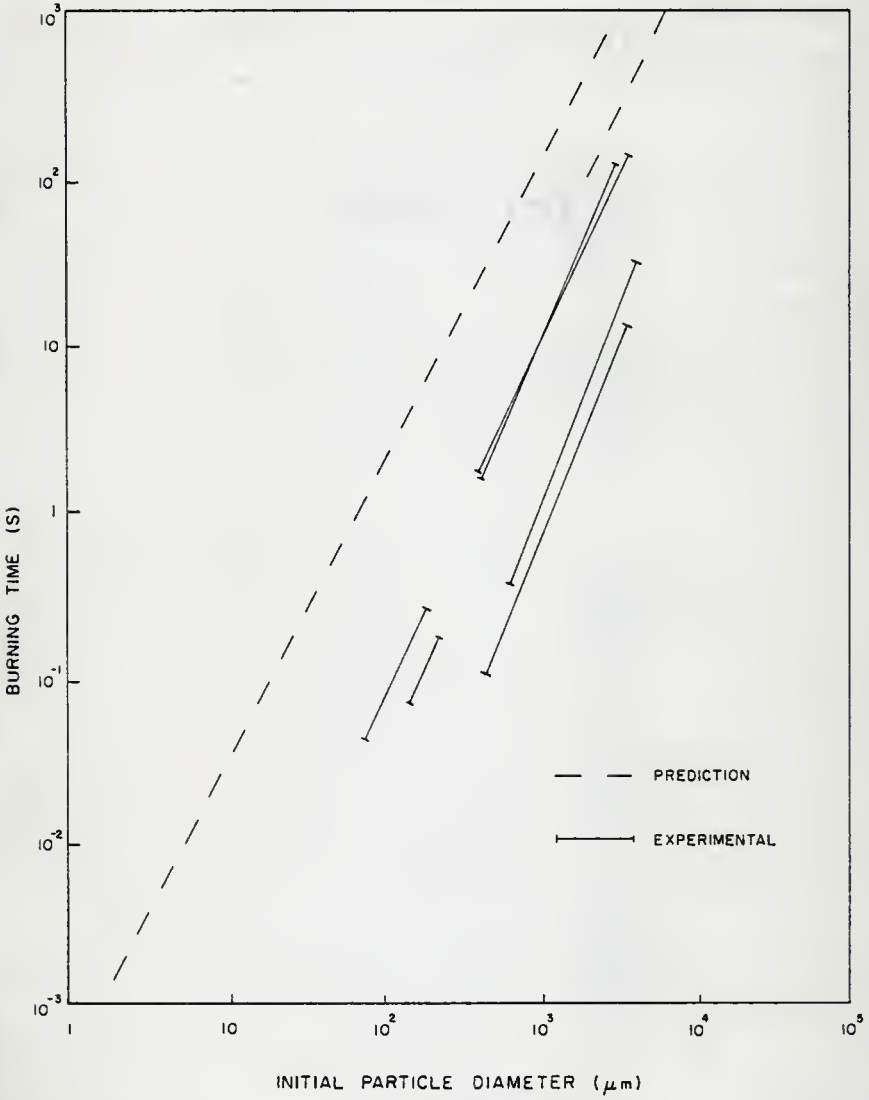

FIGURE 4 OBSERVATIONS OF BURNOUT TIME vs. INITIAL PARTICLE DIAMETER, AFTER (23)

The presence of NO_x is known to have serious consequences on health and is blamed for property damage as well. It can cause leaf damage and stunted growth in plants and may corrode metallic surfaces and speed the deterioration of rubber. In addition, it may irritate the eyes and nose membranes and it is a major constituent of photochemical smog[34]. For these reasons, the Clean Air Amendments of 1970[35] gave the EPA authority to regulate emissions of NO_x and any other hazardous species and broadened its power to sponsor research into the development of more effective emissions control methods.

The formation sequence of NO_x is now known in some detail[36]. During the combustion process oxides of nitrogen are formed by oxidation of both atmospheric nitrogen (thermal NO_x) and fuel bound nitrogen (fuel NO_x). The formation of thermal NO_x has been shown to follow the Zeldovich[37] mechanism through which formation depends exponentially on temperature and has a reaction order of 1/2 with respect to oxygen[38], i.e., is proportional to the square root of the oxygen concentration. The two reactions postulated by Zeldovich are

$$O + N_2 \rightarrow NO + N \qquad (8)$$

$$N + O_2 \rightarrow NO + O \qquad (9)$$

and Glassman[64] indicates that the chain is initiated either by the dissociation of O_2 or by H atom attack on O_2.

The fuel NO_x formation mechanism is not well understood, but some developments of fuel nitrogen conversion have been experimentally

observed. The fuel nitrogen is only partially converted with the degree of conversion strongly dependent on oxygen concentration but relatively insensitive to temperature[39]. Pershing et al.[40] utilized an artifical oxidizer containing no nitrogen to demonstrate that the predominant source of NO_x from pulverized coal combustion is fuel bound nitrogen which they found contributes approximately 80% of the total NO_x emissions. This differs from the findings of the same study for oil combustion wherein thermal and fuel NO_x were found to be roughly equivalent under normal firing conditions, and implies that control techniques that are successful in reducing NO_x emissions (predominantly the thermal NO_x) from oil burners may meet with only minimal effectiveness when applied to coal fired equipment.

The effects of flame temperature, coal composition, and burner configuration on NO_x formation, especially fuel NO_x, have been scrutinized by Pershing, et al.[40], Wendt and Pershing[41,42], and Heap, et al.[43,44]. These results coupled with the fuel NO_x formation observations have been correlated to set forth and verify the following conclusions:

1) NO_x control schemes aimed at lowering the flame temperature are effective in reducing thermal NO_x but relatively ineffective in combatting fuel NO_x;

2) Fuel NO_x is most effectively reduced by forcing the ignition and early stages of combustion to proceed in a fuel rich atmosphere;

3) Fuel nitrogen content comprises both that contained within the volatiles and char. Hence, total NO_x levels do not necessarily depend on total fuel nitrogen content.

The second conclusion listed above is the basis for the most widely used and most successful NO_x control technology available, that being staged combustion. Staging is accomplished by introducing insufficient combustion air in the initial section of the furnace causing the flame to exist in an underventilated state. It has been concluded that this increases the probability that devolatilized fuel nitrogen will collide and react with another nitrogen atom forming N_2 rather than oxidizing to NO. After the bulk of devolatilization has occurred, the remaining combustion air is introduced to allow char burnout to occur nearly stoichiometrically. Studies by Thompson, et al.[45], Friedrich and Pai[46], and Waterland, et al.[47] concur that staged combustion results in between 20 and 60 per cent reduction in NO_x levels in full scale field tests. However, Hollinden, et al.[48,49] have raised questions as to whether the reducing atmosphere essential to the staging mechanism is conducive to equipment longevity and performance by stating that corrosion problems have been noted in long term tests. Two other combustion modification control schemes merit a brief discussion, even though their overall effect is comparable to combustion staging. The use of burners out of service (BOOS), also known as bias firing, consists of shutting off the fuel flow to certain burners and using them only for introduction of air to the chamber. By operating the remaining burners in an underventilated state, the net effect of BOOS is a variation on combustion staging. In tangentially fired boilers, the use of overfire air (OFA) ports as explained by Selker[50] consists of

introducing air above the initial section of the combustion zone but in the path of the flame. Again, if combustion is initiated in a fuel rich state, combustion staging is the net result of OFA operation.

Post-combustion removal schemes for NO_x are not practiced, mainly because effective methods have not been available and those techniques recently proposed are not without problems. Friedrich and Pai[44] discuss a flue gas adsorption technique that claims a 30-50 percent reduction in NO_x levels with simultaneous removal of SO_2 and particulate matter. Since this is a proprietary technique, further details are sketchy, but the authors reported that full scale testing was planned at the time of publication. Another promising post-combustion technique was first noted by Wendt, et al.[51] with subsequent investigations by Lyon and Longwell[52] and Muzio, et al.[53]. This control method consists of injecting ammonia with the combustion products and either igniting the mixture[51] or allowing a non-catalytic gas phase reduction of the NO to occur[52,53]. Lab scale trials of the process have indicated that substantial reduction of NO_x can occur if the temperature is kept within a narrow range and the testing has determined that any effect of the technique on other pollutants is minimal if proper precautions are taken. However, Teixeira[54] challenged the applicability of the NH_3 method on the grounds of economics and the lack of full scale verification.

The literature regarding SO_2 emissions is not nearly as voluminous as that for NO_x; in fact, there are few references that detail the formation and emission of SO_2 from combustion chambers. The lack of

interest in SO_2 emissions is likely due to the adequate (though not ideal) control technologies already employed for emissions reduction coupled with the historical abundance of low sulfur fuels. Reviews of the field of sulfur oxidation by Levy, et al.[55], Cullis and Mulcahy[56], and Polavarapu[57] are recommended.

The importance of SO_2 as a pollutant is belied by the lack of emphasis in the literature. According to Nebergall et al.[34], known consequences of the presence of SO_2 are acute leaf damage, corrosion of metals, disintegration of book leather and pages, ruining of textiles, destruction of paint pigments, and erosion of statuary. Inhalation of SO_2 can cause irritation of the upper respiratory tract in humans and animals. Some staggering health effects of sulfur compounds in air taken from a report to the U.S. Senate[71] are given in Table 1. In addition, sulfur compounds can exhibit deleterious effects on combustion equipment. For example, fuel rich conditions favor the formation of hydrogen sulfide (H_2S), a strong reducing agent, which can attack boiler surfaces resulting in corrosion and loss of efficiency. The SO_2 may be converted to sulfur trioxide (SO_3) under oxidizing conditions which readily forms sulfuric acid when exposed to water. The corrosive properties of H_2SO_4 make it another undesirable agent in combustion systems.

Glassman[58] relates that the dominant product of sulfur oxidation reactions is SO_2, although one or two percent SO_3 may also be formed. Unlike fuel nitrogen, the fuel sulfur content and SO_2 emissions are

Table 1. Health Effects Associated with Sulfur Oxide Emissions*

	Remote Location	Urban Location
Cases of Chronic Respiratory Disease	25,600	75,000
Person-Days of Aggravated Heart-Lung Disease Symptoms	265,000	755,000
Asthma Attacks	53,000	156,000
Cases of Children's Respiratory Disease	6,200	18,400
Premature Deaths	14	42

*Source: (Reference 71, Ch. 13). Illustrative calculations based on distributive models, postulated conversions of SO_2 to SO_4, and EPA epidemiological data for representative power plants in the Northeast emitting 96.5×10^6 pounds of sulfur per year - equivalent to a 620-Megawatt (electric) plant.

well correlated in pulverized coal firing with usual fuel sulfur conversions of about 95 percent being noted.

One process often mentioned as an emissions control technique is the use of low sulfur coal or pre-combustion coal desulfurization. This has been an effective option in the past, but increasing demands for low sulfur coal along with depletion of supplies and the high costs attendant to desulfurization illustrate the need to apply other methods. Since sulfur is so readily evolved from the fuel and converted to an oxide, it appears impractical to attack the problem from a kinetics viewpoint. It is also difficult to foresee what sulfur compound, analogous to N_2, could be formed preferentially with respect to the oxides and still not have deleterious side effects on the combustion chamber materials. Therefore, the major technologies in use and under development operate by removal of the SO_2 after formation.

All of the notable techniques share a common basis of operation, that being the absorption of SO_2 by a sorbent of high mineral content. Differences in the schemes arise in the location where the sorbent is introduced and the phase of the sorbent, i.e., solid or liquid-slurry. One technique introduces the solid sorbent, either limestone or dolomite, to the combustion chamber with the fuel. The calcium in the sorbent chemically reacts with SO_2 and O_2 to form calcium sulfate which is easily removed with the particulate matter. This scheme is only effective in removing about 35 per cent of the total SO_2 emissions under normal firing conditions[65], but Zallen, et al.[59] have recently applied the technique to a low NO_x burner which produces conditions

more favorable for absorption of the SO_2. Other control technologies react the flue gas with the sorbent. Present methods employ a slurry sorbent and are termed scrubbers. Scrubbers are effective in removing up to 95 percent of the SO_2 from the flue gas, but handling and disposal problems with the slurry and the large capital required for initial installation limit its utility. Dry sorbent scrubbers are under development which should have comparable efficiency and eliminate the handling problems. Furthermore, anticipated regeneration processes will enhance the economics and produce elemental sulfur as a side product.

Besides economics and SO_2 removal efficiency, there are other factors to consider in developing an SO_2 emission control scheme. The effect of the method chosen on other pollutants must be taken into account. For instance, Wendt and Ekmann[60] have indicated that the presence of SO_2 in the combustion zone can hinder the production of NO_x. Though they did not offer substantial proof, they postulated that this effect was caused by the reduction of free radical species by the SO_2. This effect must be weighed before choosing coal desulfurization as a control technique because any savings gained in the desulfurization or use of low sulfur coal could conceivably be lost if otherwise unrequired NO_x control methods become necessary.

The pollutant formation mechanisms and control strategies outlined in this section are well enough documented that observation of these species is used as a performance gauge for the lab scale furnace employed in this investigation. For instance, when operating properly, a change

in the percentage of swirl air should affect the NO_x[17], but have no effect on SO_2 since fuel sulfur conversion has been observed to be nearly constant for a given fuel. Excess air should likewise affect NO_x without influencing SO_2 emissions. This procedure was invaluable during the initial stages of the investigation as an excessively high draft in the flue was causing excess air to be introduced through minute cracks in the furnace's outer wall. Use of the method throughout the study helped assure that the apparatus operated in a manner consistent with previous experimentation both from this project and others.

1.4 Fuel Properties

The previous sections have alluded to the influence of fuel properties on combustion efficiency and pollutant formation. The proximate and ultimate (elemental) analyses of the fuels burned in this investigation are given in Table 2. Several observations regarding the combustion process can be predicted from these analyses. The Kansas coal requires more combustion air than the western coal and the straw since it has a lower oxygen content. The air requirements for a given fuel can be estimated by the relation

$$\frac{\text{kg AIR}}{\text{kg FUEL}} = 11.53\ C + 34.34\ (H_2 - O_2/8) + 4.29S \qquad (10)$$

where C, H_2, O_2, and S represent the weight fractions of carbon, hydrogen, oxygen, and sulfur, respectively[66]. The extremely high volatile matter content of the wheat straw indicates that it may burn out more quickly,

Table 2. Proximate and Ultimate Analyses of Fuels on As-Received Basis.

	Ks Coal	Western Coal	Wheat Straw
Proximate Analysis*			
Moisture	1.74	5.26	4.75
Volatile Matter	26.55	35.99	70.51
Ash	37.68	16.89	6.77
Fixed Carbon	34.03	41.86	17.97
Sulfur, Total	5.38	0.73	0.11
Sulfur, Pyritic	3.34	0.19	--
Sulfur, Organic	1.41	0.54	--
Sulfur, Sulfate	0.63	<0.01	--
Heating Value (Btu/lb)	8228	9934	7383
Ultimate Analysis**			
Moisture	1.41	5.34	4.06
Ash	33.30	12.77	6.63
Carbon	49.86	60.26	43.21
Hydrogen	3.81	4.71	6.21
Nitrogen	0.84	1.17	0.55
Chlorine	0.06	<0.01	0.23
Sulfur	5.96	0.86	0.13
Oxygen (by difference)	4.76	14.89	38.98

*Analysis by Hazen Research, Inc., Golden, Co.

**Analysis by Galbraith Labs, Inc., Knoxville, Tn.

and since its heating value is comparable to that of the coals, boilers firing wheat straw might offer the advantage of being more compact. Note also that the Kansas coal has a high ash content. This will give rise to increased ash disposal requirements as well as an increase in particulate matter emissions.

The fuel analyses are also useful in predicting the pollutant characteristics of the fuels. As mentioned previously, NO_x emissions are not directly related to fuel nitrogen content, but to the classification (volatile or char) of that nitrogen. Since the Western coal has a relatively high nitrogen content and exhibits a high volatile matter content, it may be safe to assume that the NO_x levels from this coal will be higher than from the Kansas coal. The Kansas coal has a very high sulfur content which should give rise to excessive SO_2 emissions and may assist in reducing the NO_x emissions even further. Insofar as the wheat straw has such a low sulfur content, its SO_2 emissions should be negligible, but its NO_x emissions are difficult to predict because of its high ASTM volatile matter but low nitrogen content. Cofiring a mixture of Kansas coal and wheat straw is expected to reduce the SO_2 emissions by a fuel replacement action and may exhibit further reductions through a mechanism similar to the sorbent processes outlined previously. The predicted SO_2 emissions from Kansas coal-wheat straw mixtures as a function of the straw percentage (assuming only the replacement mechanism) is depicted in Fig. 5.

The effects discussed in this chapter were used in the design of the furnace and selection of materials. The burning time analysis in-

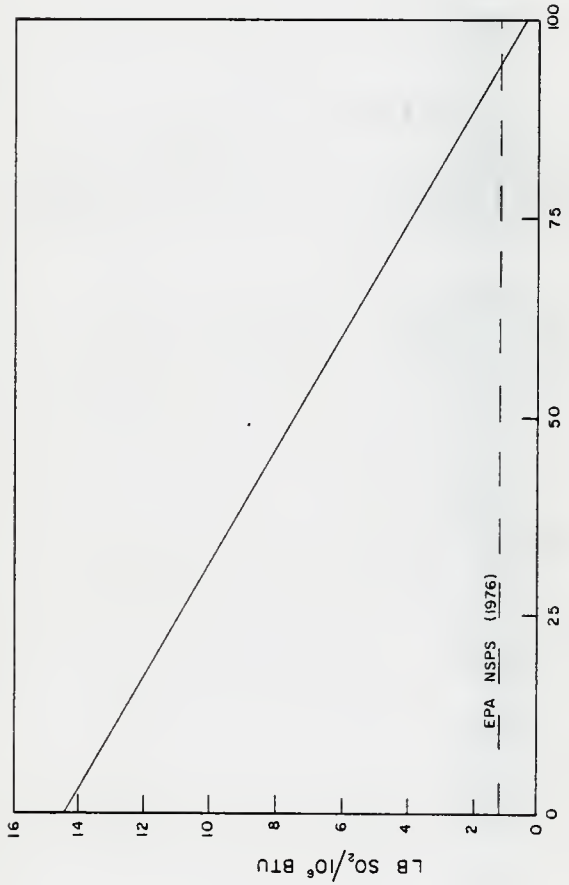

FIGURE 5 PREDICTED SO_2 EMISSIONS FOR MIXTURES OF KANSAS COAL AND WHEAT STRAW BASED ON 100 % CONVERSION OF FUEL SULFUR

fluenced the selection of the size distribution for the particles as well as the dimensions of the combustion chamber. Estimates of the flame and exterior wall temperatures were instrumental in deciding upon the proper materials for the inner walls and for sealing the exterior. As detailed in the section just completed, analysis of the pollutants was used to test the furnace performance. An elemental balance was employed to insure that the fuel-air ratio was correct and to check the degree of combustion. The final design arrived at and the construction procedure are covered in the next chapter.

2 APPARATUS DESIGN AND CONSTRUCTION

Small scale solid fuel combustion facilities are still uncommon in American universities. The design of this particular facility was patterned after two previous models, both of which can be traced back to a furnace constructed at the University of Sheffield, England in 1959. Beer, et al[27] designed that unit, comprising a combustion chamber, one-dimensional burner, and flue assembly measuring 610 cm in total length and having a circular cross section with 45.7 cm internal diameter. Its primary utilization was in the study of basic combustion mechanisms and coal properties. A successor to this furnace was structured in the early 1960s at Pennsylvania State University where it was employed by Howard and Essenhigh[9,10,13,14] in the development of several theories regarding the devolatilization and ignition processes of pulverized coal. About a decade later, Pershing[61], at the University of Arizona, designed and erected a furnace based on the Pennsylvania State model but possessing several new features. Most importantly, the combustion environment of utility boilers was simulated through the use of a concentric tube burner instead of a one-dimensional tube bank. The design has subsequently been duplicated at several facilities performing contractual studies for the EPA.

The furnace developed for the present investigation, pictured in Fig. 6, was designed to simulate as closely as possible conventional large scale facilities. It was constructed so that a wide range of experiments, demanding different instrumentation, could be easily

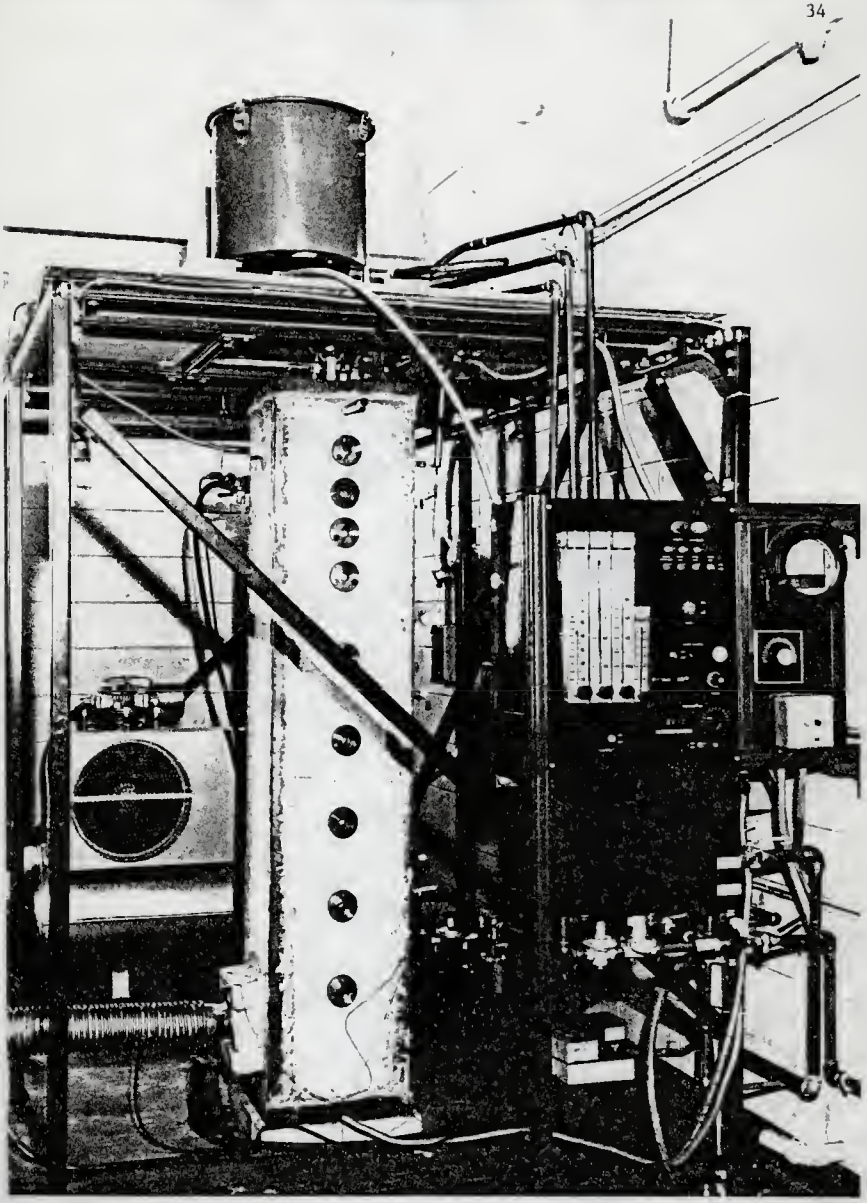

FIGURE 6 COMBUSTION FACILITY

accommodated. The construction of the basic system is detailed below, followed by a description of particular configurations used to satisfy different requirements. Examination of the equipment as represented in Fig. 7 reveals that the system can be separated into six components. These constituents, covered in the following six sections, are the combustion chamber, the natural gas supply system, the air supply network, the solid fuel feeding apparatus, the water supply, and the safety systems. The burners designed for use with the facility and the gas sampling system are explained in Sections 2.7 and 2.8.

2.1 Combustion Chamber

Figure 9 relates the orientation of the furnace and shows the distribution of the equipment described in this section.

The combustion chamber is approximately 183 cm in length and has a 16.5 cm square cross section. It is oriented vertically with the fuel being introduced at the top and the exhaust products exiting near the bottom. The downward burning pattern is utilized so that gravity does not interfere with feeding; this is especially important in the plug flow operation mode. Inasmuch as the flue exit is centered 22.9 cm above the chamber floor, a sump is provided which accommodates the removal of ash through an access port. Reference to Fig. 8 may assist in clarifying the ensuing discussion on the wall structure. The inner walls are constructed of a silica-alumina firebrick obtained from the J. B. Fine Company, and are rated to temperatures of 2025 K. The brick, also chosen for its reputed high resistance to slagging and oxidation,

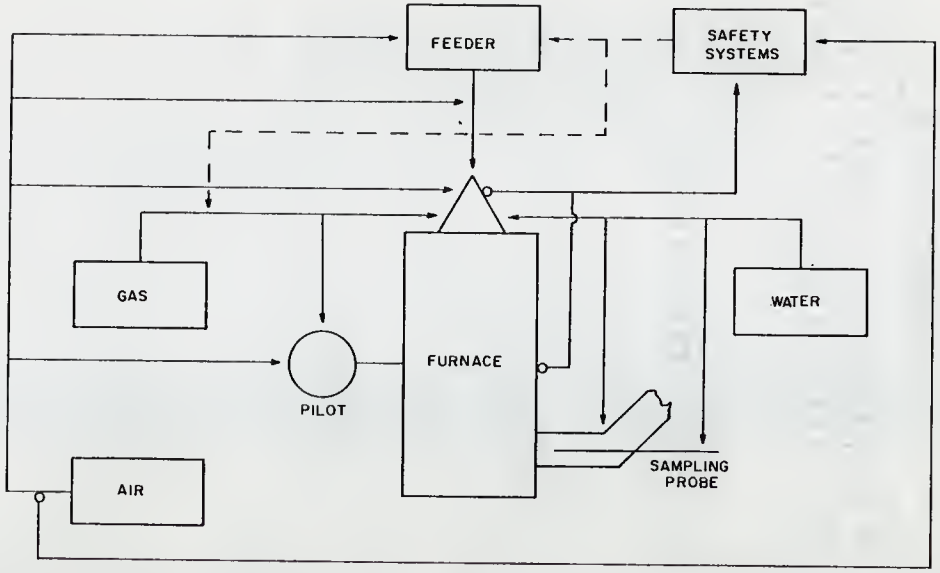

FIGURE 7 SCHEMATIC REPRESENTATION OF COMBUSTION FACILITY

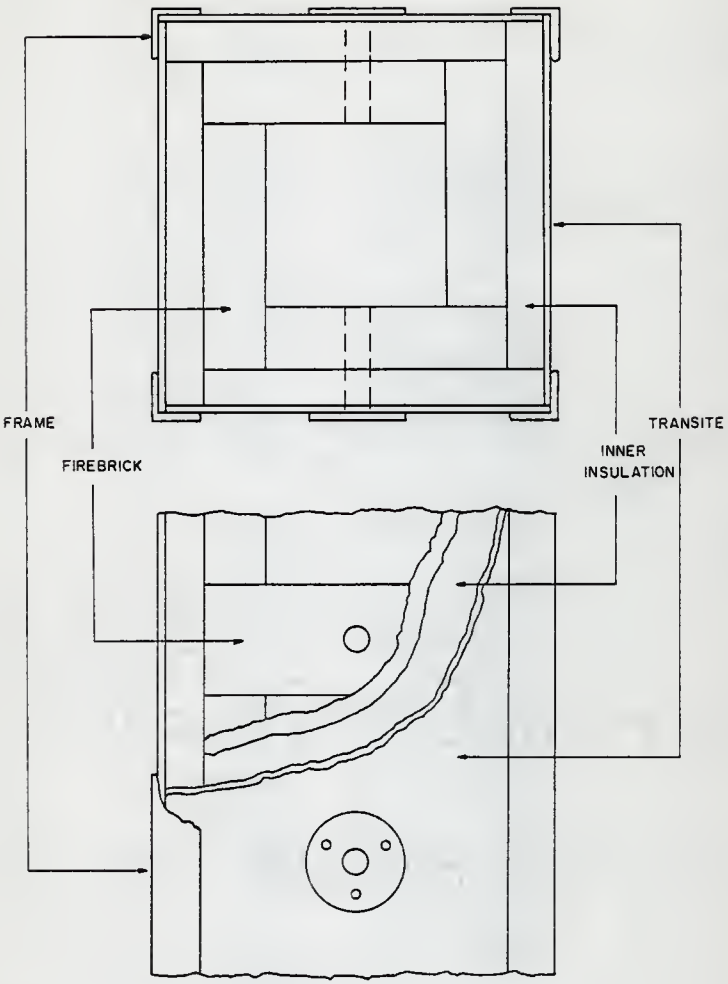

FIGURE 8 FURNACE WALL STRUCTURE

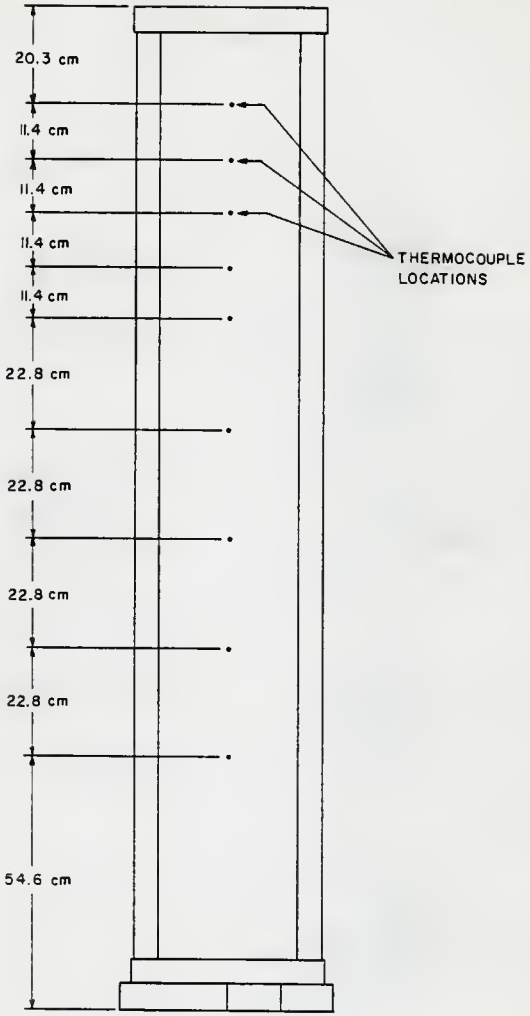

FIGURE 9

AXIAL THERMOCOUPLE POSITIONING

was dry laid, i.e., without mortar, in order to facilitate disassembly for replacement of parts and modifications in chamber geometry. The dry laying did not subject the final design to air leakage because the facility was carefully sealed on the exterior, a practice to be discussed shortly. The brick layer is surrounded by a 3.8 cm stratum of pressed insulating board of unverified composition. The best available information indicated that the material consists of pressed rock wool and asbestos. Insofar as the material had been obtained as surplus from the Boeing Company, little could be learned about its origin except that it was a very high temperature substance. The external skin of the furnace, a 0.65 cm thickness of transite pressed asbestos board covers the internal insulation layer. The walls are held rigidly by a frame of 0.65 cm x 5.08 cm angle iron. One piece of angle iron runs the length of each corner of the furnace and these are kept in place by welded caps of the same material. Thus, the external dimensions of the furnace are 40.6 x 40.6 x 205.7 cm (l x w x h). All seams, openings, and cracks are sealed with either General Electric high temperature silicone instant gasket material or Trowleze high temperature air setting bonding mortar to prevent air leakage. The silicone gasket material has a recommended maximum temperature of 590 K, but it is preferred to the much higher temperature mortar because of its pliant nature and durability. The mortar is susceptible to cracking during the repeated temperature cycling of the facility and must be repaired often.

The layers of the furnace walls do not contact snugly everywhere; therefore, heat transfer through the walls is reduced by dead air gaps.

An approximate numerical model of steady state heat loss from the furnace based on a heat generation rate of 23.4 kW determined that the outer wall temperature would reach approximately 465 K, and that the total heat transfer rate through the walls would be about 3.5 kW. Details of the model are contained in Appendix D. These values were used subsequently to determine specifications for auxiliary equipment that would interface with the furnace. Experimental measurements have shown the actual temperature of the external wall surface during tests to be much lower. The primary reason for disagreement is the difficulty in correctly accounting for the contact resistance between the wall strata, necessitating the use of conservative approximations.

There are numerous penetrations of the furnace walls. Two opposing walls each accommodate nine 2.54 cm diameter ports spaced along the flame axis. The highest is centered 17.2 cm below the top of the chamber and the next three are spaced at intervals of 11.4 cm center to center below the uppermost one. The remaining portals are spaced at 22.8 cm intervals. This spacing scheme was used in anticipation of probing, either optically or by mechanical means, of the flame near the top of the furnace. Currently, the ports are covered with Amersil optical grade quartz windows measuring 0.32 cm thick by 3.8 cm in diameter, held in place by stainless steel holders. The most common use of the ports throughout the experiment has been the visual observation of flame conditions within the chamber which assists in stabilizing the flame. The windows have also allowed the utilization

of an optical pyrometer to estimate the inside wall temperature. The uppermost portal on one wall accommodates the ignition pilot assembly which will be discussed within the context of the natural gas supply system.

The furnace is instrumented with thermocouples spaced along the centerline of one wall. The Pt vs. Pt-10% Rh thermocouples are spaced in a pattern similar to that of the viewing ports. The relative axial positions of the thermocouples are depicted in Fig. 10. Each axial location has two thermocouples, one of which penetrates into the brick to a point within about 0.65 cm of the inside wall while the second stops about 5.0 cm short of the chamber interior. Under steady state conditions the two temperatures can be used to extrapolate the temperature profile to the inside wall. The temperatures are displayed on an Omega Engineering model 2160A digital thermometer and the thermocouple selection is made via an Omega Engineering model OSW5-24 24 pole thermocouple selector switch, both located at the equipment control panel.

A flame detector is located 17.5 cm from the top of one of the furnace walls. The detector hole is angled slightly downward to help prevent accumulation of particulate matter. The flame detector, an integral part of the furnace safety system, will be discussed in more detail in Section 2.6. The exhaust flue exit is in the same wall as the detector, approximately 22.9 cm above the bottom of the furnace. The stainless steel flue has a flat metal flange at the furnace end which abuts against the brick layer of the chamber and is held in place

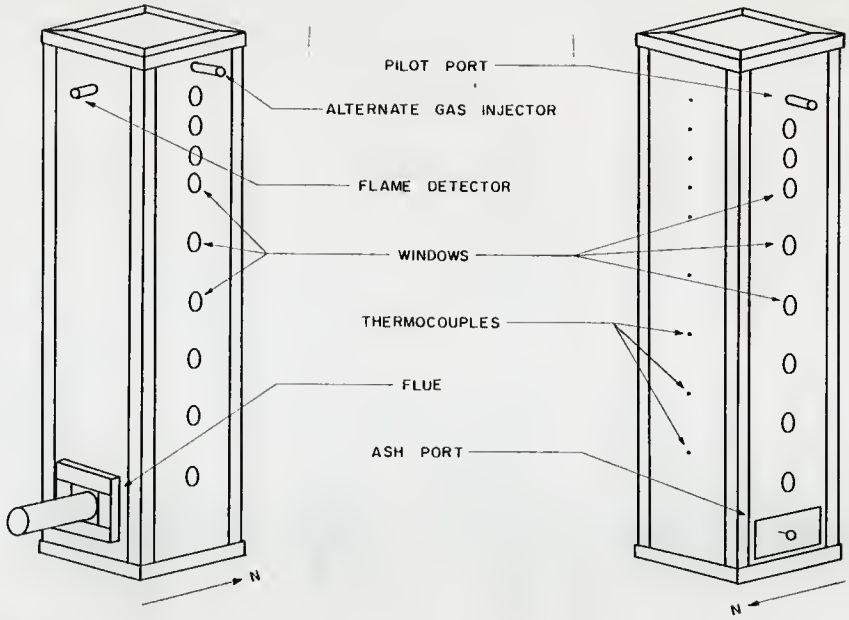

FIGURE 10 WALL PENETRATION GUIDE

by an extra framing of firebrick and sealed with a 1530 K ceramic fiber insulation material and high temperature mortar. The flue has a diameter of 11.4 cm and conveys the exhaust gases from the furnace through the roof of the building where an adjustable weather cap serves as a damper for regulating the draft within the furnace. The flue's initial section houses a water jacketed 0.48 cm i.d. stainless steel tube which protrudes from an offset portion and serves as a sampling probe for collecting flue gas samples.

There are two other openings in the furnace side walls. High on the wall opposite the pilot assembly, 5.72 cm below the top of the chamber is placed the main gas injector that will be used in future runs with the one-dimensional burner in place. The ash removal port is located at the bottom of the opposing wall. The port's door (11.4 cm x 16.5 cm) is fit tightly in the opening and air leakage is prevented by sealing with silicone gasket material.

2.2 Natural Gas Supply System

Natural gas service to the furnace is required for both a stabilizing pilot for the solid fuel and as a main flame for heating the combustion chamber in preparation for solid fuel firing. In addition, exhaust gas samples collected while firing natural gas were instrumental in the development of the gas sampling system. Natural gas service is taken from the building supply through a 1.6 cm i.d. steel pipe equipped with a manual ball valve at the equipment control panel. The piping schematic is shown in Fig. 11. In addition to the manual

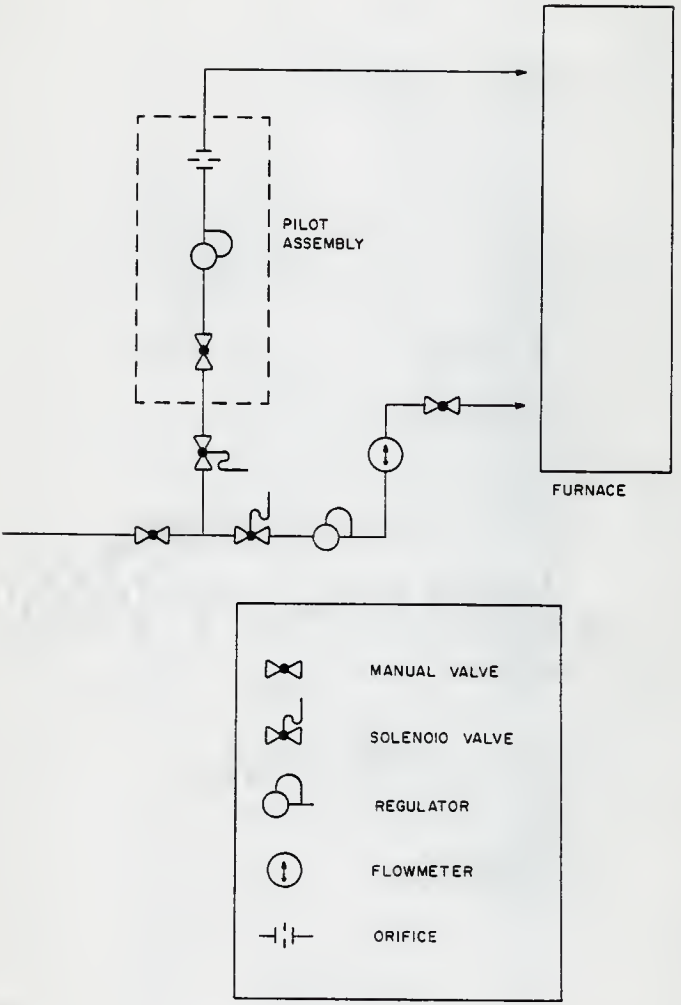

FIGURE II GAS PIPING SCHEMATIC

valve, both the pilot and main gas lines feature 110 V solenoid valves that are normally closed. The pilot burner, an Eclipse model 3EPA-12 pilot with Eclipse model 131PM pilot mixer, is portrayed in Fig. 12. An internal spark plug supplies the ignition source, and the total gas flow and flame stoichiometry are controlled by an adjustable gas regulator, a needle-seat metering orifice, and ball valves in the gas and air lines. The spark plug requires a dc voltage for proper operation, and this is provided by a Dongan model A06 5A6 6000 V ignition transformer.

The main gas supply is partly regulated by a Maxitrol model RV42 gas pressure regulator which controls the line pressure at 19.0 cm of water above atmospheric. The flow through the line is metered by a Dwyer RMC Ratemaster flowmeter calibrated up to 1,572 cm^3/sec of air. The gas is connected to the burner through a 1.3 cm i.d. automotive heater hose. Depending on the burner configuration utilized there are two main gas injectors that can be used. The injector used in this investigation is shown in Fig. 13. The alternative injector is used with the one-dimensional burner and introduces the gas below the tube bank to avoid destruction of the burner. Both of the burners mentioned are described in detail later in this chapter.

2.3 Air Supply Network

Pressurized air acts as the oxidizer in both the pilot and main flames and serves as a control for the speed of the solid fuel feeder. The air system piping schematic is shown in Fig. 14. The source of

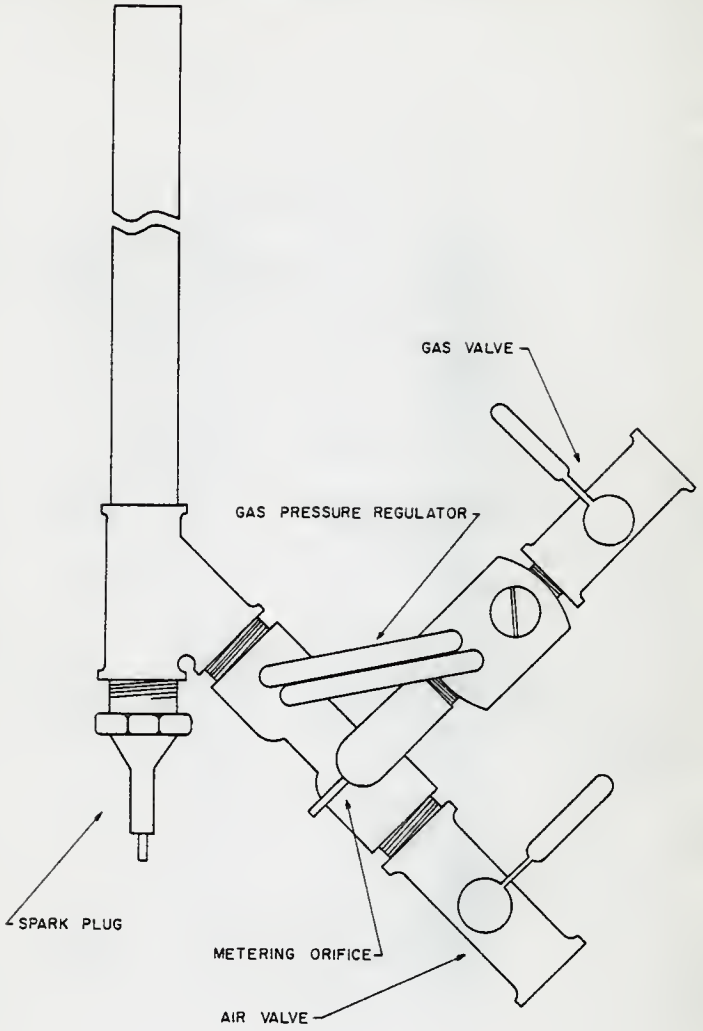

FIGURE 12 PILOT ASSEMBLY

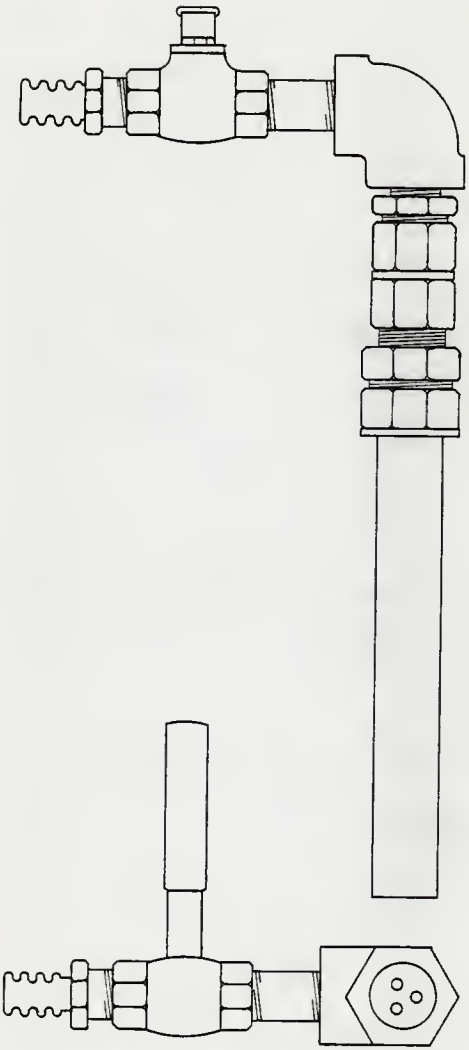

FIGURE 13 MAIN GAS INJECTOR

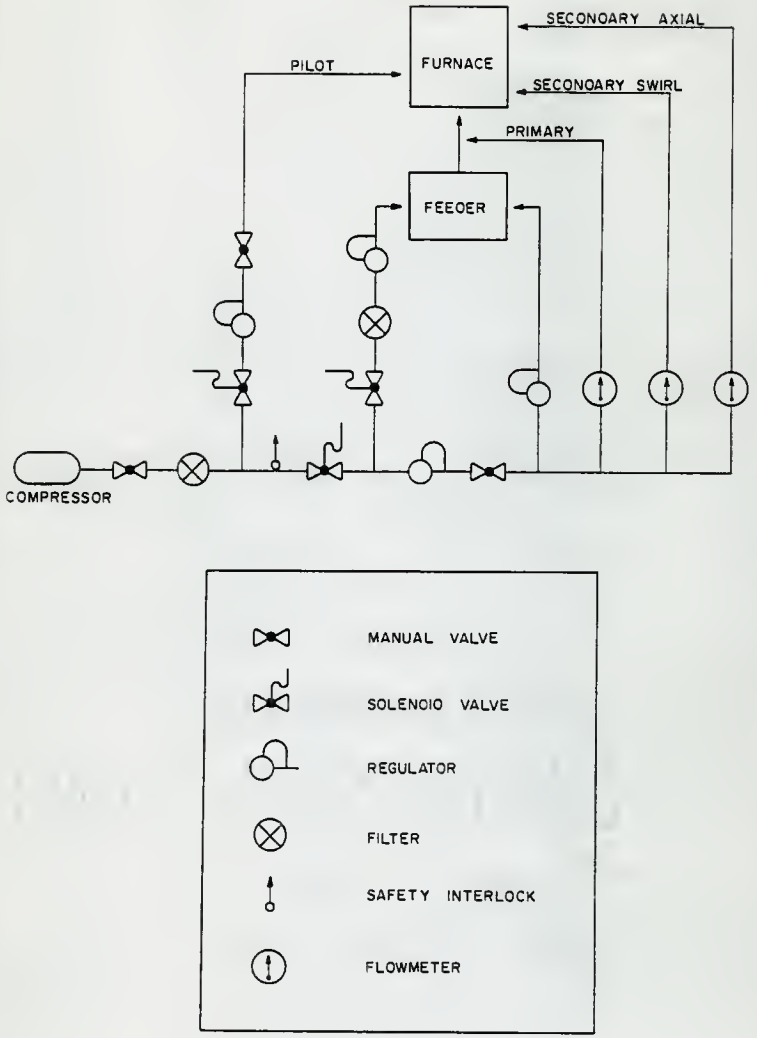

FIGURE 14 AIR PIPING SCHEMATIC

compressed air is a Kellogg model 340B air compressor rated to have a 1.37×10^4 cm^3/sec free air capacity at 652.6 kPa (80 psig). The compressor is equipped with an inlet valve unloader that allows the motor to run with no load whenever the pressure in the storage tank is above a predetermined level. This allows for cooler engine operation and a longer motor life than would be possible if the motor cycled with the tank at high pressures. The storage tank outlet is equipped with a manual ball valve at the entrance to the supply line. The air is filtered through a Schrader model 3536-1000 filter to remove compressor oil, moisture, and other impurities. After filtering, the pilot air line separates from the main air supply and passes through a normally closed 110 V solenoid valve and a Hoke model 5133F8A low pressure regulator, adjustable from 8.9 to 352 cm of H_2O above atmospheric, and subsequently to the pilot assembly.

A Ranco type 010 low pressure disconnect switch is located in the supply line immediately past the pilot air branch point. The operation of this device is explained in Section 2.6. Another branch separates downstream of the disconnect and passes through a normally closed solenoid valve to a Moore model 91F-60 adjustable air regulator and filter. Pressure of the line is maintained at 445.9 kPa (50 psig) and it serves as the reference air line for the solid fuel feeder's pneumatic speed control which will be explained in the next section.

The main air supply line pressure is reduced to 273.6 kPa (25 psig) by a Schrader model 3566-1100 variable air pressure regulator. The line

terminates with a manual ball valve at the equipment control panel, after which four separate air lines diverge. One passes through a Watts model 362-2 variable air regulator and gauge positioned on the control panel and proceeds to the solid fuel feeder where it serves as the control air line for the pneumatic speed regulator. The remaining three air lines supply combustion air to the furnace and pneumatically transport the solid fuel to the combustion chamber. The smallest of the three, termed the primary air, is metered by a Dwyer RMB Ratemaster flowmeter calibrated from 472 to 4,720 cm^3/sec of air. Flow through the two secondary air lines is metered by twin Dwyer RMC Ratemaster flowmeters calibrated from 944 to 9,440 cm^3/sec.

Routine maintenance of the air system is required to assure reliable operation. To this end, daily procedure calls for checking the compressor oil level, draining condensate from the air storage tank, testing the high pressure safety valve, and cleaning the main air supply line filter. The compressor oil is changed monthly and any other problems are corrected when noticed.

2.4 Solid Fuel Feeding Apparatus

The central feature of the solid fuel system is the screw feeder, a pre-assembled unit manufactured by the Vibra Screw Company and generously offered to this researcher on an indefinite loan basis. It includes an 8.5×10^4 cm^3 dust sealed live bin, so named because of the vibrating action designed to force all material to settle to the bottom of the bin, a 1.9 cm i.d. stainless steel pipe containing an auger of spring

steel to transfer the pulverized fuel to the furnace, and a pneumatic speed control mechanism. The latter comprises a valve positioner with an internal diaphragm separating two chambers of diverse pressure. On the reference side of the diaphragm a pressure of 445.9 kPa (50 psig) is maintained while the pressure on the control side may be varied from 122.0 to 204.7 kPa (3 to 15 psig). Adjustment of the control pressure causes the diaphragm and an attached piston to shift position. The piston causes the width of the groove of a variable width pulley to change which effectively varies the diameter of the pulley. The belt riding the pulley is forced to move either away from or toward the axis which varies the feeder speed.

The electrical requirements of the feeder are 220 V three phase which is provided through flexible conduit so that the vibratory motion does not damage the connection. The feeder also has an electrical tachometer mounted in an explosion proof case at the equipment control panel where the feeder start switch and reference air line solenoid valve control switch are located.

The feeder is mounted on a 224 cm high scaffolding constructed of Uni-strut structural steel material and sheeted with 1.91 cm thick plywood to which the feeder is bolted. The feeder is situated such that the end of its delivery tube is positioned above the burner. The tube feeds directly into a brass tee connection and is secured by Swagelok fittings. Opposite the feeder tube, the primary air line enters the

tee and the solid fuel injector emerges from the bottom. This arrangement is used regardless of the burner used, only the injector must be changed.

The output rate of the feeder was found to vary with the fuel used and with the fuel conditions, especially moisture content. Accurate feed rate calibrations were further hindered by the varying flow rates of primary air used to convey the fuel to the furnace and an unexpected dependence on the fuel level in the storage bin. Measurements were made in this study by blowing the primary air and fuel through a filter and weighing the fuel thus collected.

According to estimates by the manufacturer, a material with a density of about 1.12 g/cm^3 fed at a speed of 150 rpm should flow at about 3.9 cm^3/hr. Experimental flow rates with primary air were typically around 0.6 cm^3/hr at 100 rpm.

2.5 Water Supply

Contrary to the impression created by the brevity of this section, the water supply is vital to the facility operation. Water is used to cool the burners and gas sampling probe and shield personnel from the hot flue pipe. Inasmuch as temperatures within the combustion chamber commonly exceed 1600 K radiation to the exposed surfaces of the burners is appreciable, and their thermal destruction would quickly result if cooling were not provided. A water cooled copper coil which surrounds the initial section of the exhaust flue provides minimal cooling of the flue gases in addition to its protective function.

The gas sampling probe in the flue is enclosed by a water jacket. Calculations, shown in Appendix E, indicate that the gases entering the probe are cooled at approximately 10^5 K/sec. This cooling rate is sufficient to quench most reactions not involving radicals. Estimates of the conversion occurring in the probe of several species of interest are given in Appendix E. Rapid quenching is not as vital for collecting flue gas samples as it is for probes used to collect gas samples from the interior of the furnace where severe disequilibria still exist.

Water flow rates were not measured, but periodic checks of the hot legs of each line were made during operation to provide some assurance that all cooling requirements were being met. Originally, a safety interlock to furnace operations from the cooling water was planned, but the equipment received did not satisfy the specifications of the facility and it was deemed unnecessary after preliminary experimentation.

2.6 Safety Systems

The facilty is equipped with a number of safety interlocks that minimize the danger of a gas or dust explosion. A Honeywell model RA890G flame safeguard unit is used to monitor the gas and solid fuel flames and to control the distribution of power to all the solenoid valves in the gas lines, the solenoid valve in the feeder reference air supply line, the pilot air solenoid valve, the pilot assembly ignition circuit, and the feeder motor. The main air solenoid valves and compressor power are not controlled by the safeguard since a continuing

supply of air is used to purge the furnace in the event of an unanticipated shutdown. Furthermore, the flame safeguard unit automatically controls the initial startup process. Because of its importance to the overall system, this unit's operation is explained fully in Appendix C.

The interior of the combustion chamber is monitored by a Honeywell model C7027 Minipeeper ultraviolet flame detector, the position and orientation of which were covered in Section 2.1. When positioned properly, the detector's line of sight is aligned with the path of both the main and pilot flames. The detector provides a signal to the flame safeguard whenever there is a flame in its viewing range. If this signal is not present at the safeguard, fuel flow is halted to the furnace. Further details are explained in Appendix C. Thus, the flame detector insures that the fuel burns properly and prevents the dangerous accumulation of gas or solid fuel within the furnace.

Two additional safety systems are provided that open the circuit feeding line voltage to the flame safeguard. The first, a Ranco type 010 low pressure power disconnect, opens whenever the air pressure in the main air supply line drops below a preset level, usually maintained at 652.6 kPa (80 psig). Since, during normal operation, the compressor always keeps the pressure between 721.5 and 928.2 kPa (90 and 120 psig), this system effectively indicates either a compressor malfunction or a leak of serious proportions in the supply line. In either case, the flame is immediately extinguished before conditions allowing flashback into the fuel supply system can be realized.

The other safety monitor is a Penn series A19 temperature control featuring a copper sensing element at the end of a 100 cm copper line. This control opens the circuit whenever the temperature of the sensor exceeds a preset level between 311 and 389 K. The temperature is normally set at 355 K and the sensor placed above the burner. Under normal operating conditions, the cooling water in the burner maintains the temperature around 305 K, so the activation of this control would indicate either a flame above the furnace or the overheating of the burner assembly and would result in a loss of fuel to the furnace.

Throughout the operations of the facility, the low pressure and high temperature disconnects were never called upon except during simulated failures, e.g., turning the compressor off while burning. The flame detector functioned many times and occasionally malfunctioned (when soot or ash accumulated on it and blocked its line of vision). Though an operator was always present when a shutdown occurred, the greatest benefit of the safety systems was to allow the operator to leave the facility during operation without fear of serious consequences.

2.7 Burner Configurations

The combustion facility is designed in such a manner that it is easily modified to accommodate experiments with diverse instrumentation demands. The three configurations that were anticipated during the design phase of the project are the topic of this section. Two of these utilize the same burner but different injectors while the third employs a completely different burner. These burners have been

introduced by name previously in this report as the concentric firing burner and the one dimensional burner, but even the names are not truly descriptive as the following explains.

The concentric firing burner was developed to simulate the conventional burners used in utility boilers. The nomenclature stems from the method of fuel and oxidizer introduction to the furnace. The fuel and primary air are emitted from an injector in the center of the burner and the secondary air flows through an annular void surrounding the injector. The flame produced is primarily a diffusion flame since the fuel and the bulk of the oxidizer are introduced in separate streams, but, inasmuch as the primary air also serves as an oxidizer, the flame may show some characteristics of premixed flames. For this reason low air delivery pressures are considered to be dangerous since they may result in flashback into the delivery system.

A cutaway diagram of the concentric firing burner is shown in Fig. 15. The secondary air that enters the burner through the top inlets and flows straight down along the outside of the injector is termed the secondary axial air. The air entering near the bottom and passing through the curved vanes is denoted the secondary swirl air since the vanes impart a tangential velocity to it. The percent of the secondary air through the swirl vanes has a great bearing on the combustion conditions and emissions. This topic will be expanded upon in Chapter 3. The concentric burner can be used to simulate the firing patterns of two types of boilers, depending on the injector used. To simulate wall fired

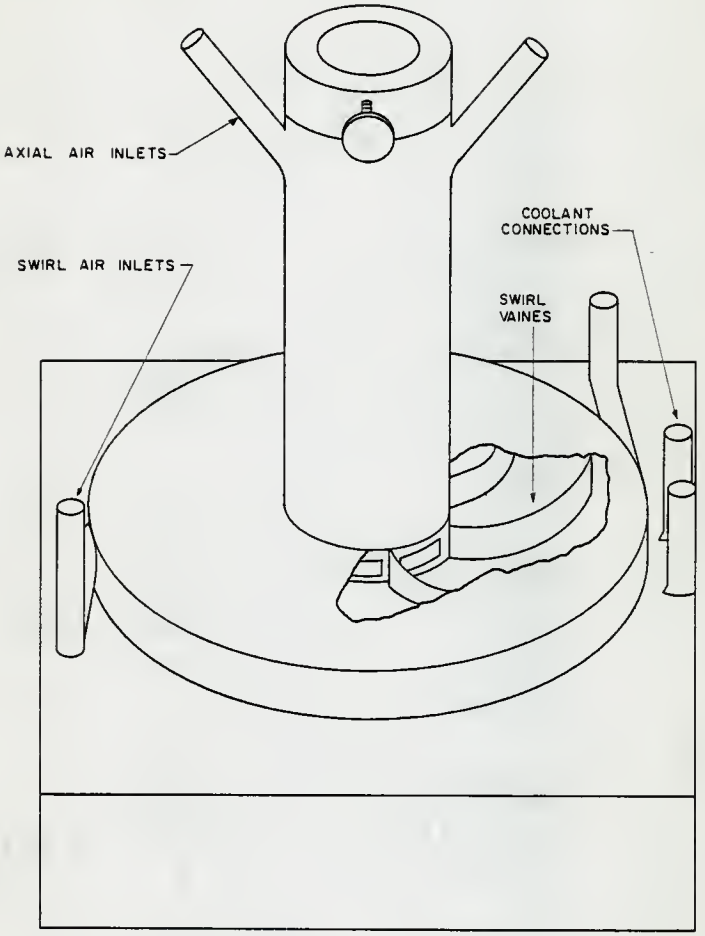

FIGURE 15 CONCENTRIC BURNER

boilers a divergent injector is employed, comprising a 17.8 cm length of 2.22 cm i.d. stainless steel pipe with a welded end plug containing three 0.36 cm holes that are angled away from the injector axis. The interior contains an inverted cone near the bottom to funnel fuel to the holes and prevent blockage. The divergent injector, shown in Fig. 16, promotes rapid mixing of the fuel and secondary air and is designed to produce a short, bulbous flame characteristic of wall fired boilers which feature several rows of these burners arranged on a single or opposing walls and firing horizontally into the combustion chamber. This is the configuration that was employed for the collection of data in this study.

The second injector utilizing the concentric firing burner is used to simulate tangentially fired boilers and is termed an axial injector. This injector, also depicted in Fig. 16, is identical to the divergent injector except for the holes in the endplug. Only one 0.62 cm hole is used to direct the fuel along the furnace axis. The flow area of this single hole is equivalent to that of the three holes in the divergent injector so that injection velocity does not vary between the two injectors. The axial injector produces a long, thin flame since the feeding pattern is not conducive to rapid mixing of the fuel and air. In tangentially fired boilers, similar burners are placed in the corners of the combustion chamber and directed toward a point slightly off center so that the flame assumes a toroidal shape when viewed from above.

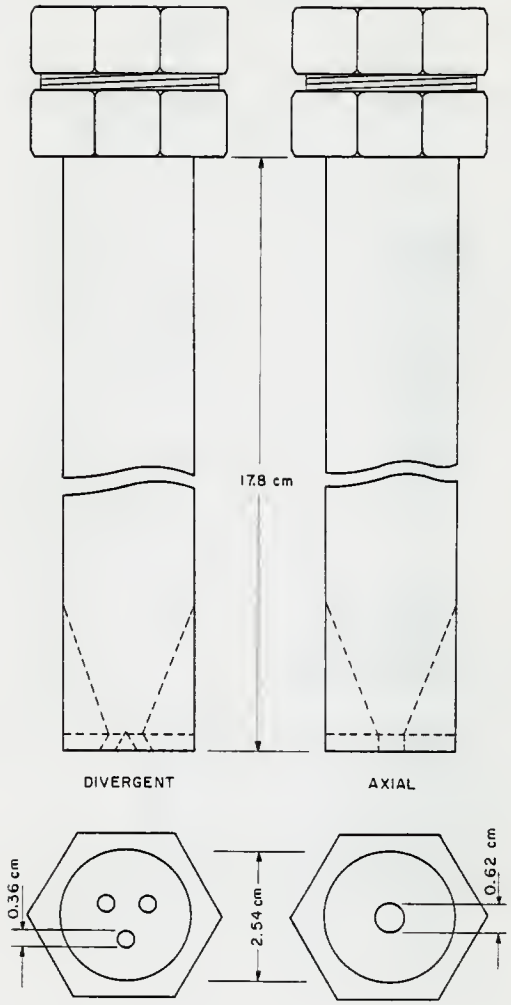

FIGURE 16 SOLID FUEL INJECTORS

The one dimensional burner is designed to produce plug flow conditions within the furnace. This burner, shown in Fig. 17, is pyramidal in shape. The fuel and primary air are inserted through the summit of the burner and the secondary air is directed upwards from a conduit penetrating one wall. This promotes complete mixing of the fuel and air which fills the cross section of the burner as it proceeds downward in plug flow. The bottom of the burner contains two horizontal rows of water cooled tubes. The tubes are separated by one tube diameter and the rows are staggered so that radiation from the combustion chamber is effectively prevented from causing ignition within the burner. Insofar as all the flow in the system is downward and the water cooled tubes also cool the burner walls, convection and conduction heat transfer to the burner mixture are also precluded. Hence, only after the fuel and air suspension passes through the tube bank does it begin to heat up. Ignition of the mixture occurs when sufficient heat is absorbed from the flame and the hot chamber walls and results in the formation of an identifiable flame front about 6 cm below the tube bank[9]. The location of the flame front below the tube bank is in some ways comparable to the ignition delay time used to describe the ignition process in shock tubes. All physical properties remaining invariant, the ignition distance has been interpreted as a measure of fuel reactivity by Cogoli, et al.[62].

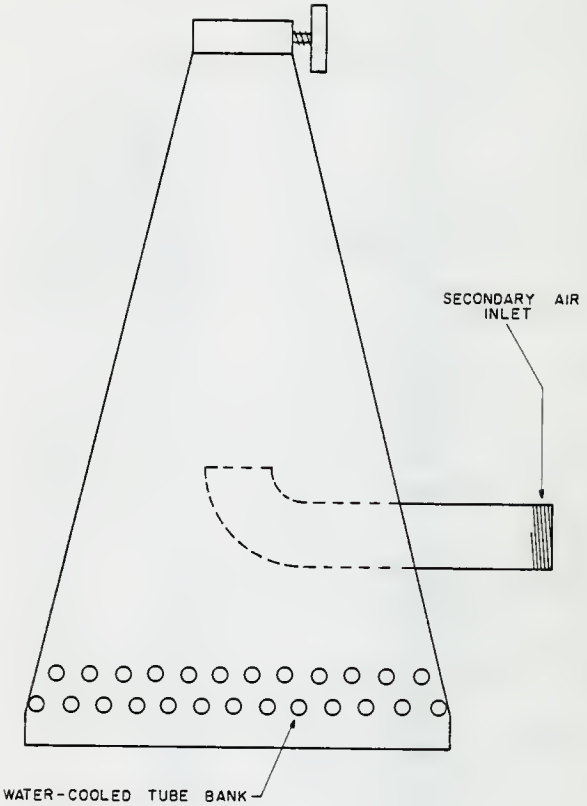

FIGURE 17 ONE DIMENSIONAL BURNER

2.8 Gas Sampling System

Much of the scope of this investigation involved the collection, identification, and quantification of gaseous species from the flue. Figure 18 is a representation of the gas sampling probe enclosed within the flue. An approximation of the gas cooling rate in the probe may be found in Appendix E, in addition to an estimate of the probe's quenching effectiveness. Separation of the samples from the main gas stream and quenching them is only a portion of the collection procedure. The schematic of Fig. 19 depicts the collection apparatus. The gas is transferred via 0.48 cm stainless steel tubing through a glass wool filter, a refrigerated dryer, and two dryers containing anhydrous calcium chloride in preparation for collection. Inasmuch as Saltzman reported that anhydrous calcium chloride could absorb up to 20% of the NO_x in a flow system, samples were taken both with and without the dessicant to investigate this effect. The flow of gas then proceeds through a three-way valve and a compression volume to a 500 ml steel bottle equipped with valves at both ends. The vacuum source, a water aspirator, is located just past the steel sampling bottle. The sampling procedure, depicted in Fig. 20, consists of allowing gas flow through the system until it has been fully flushed. Then the valve between the sample bottle and the vacuum is closed and the gases in the system are allowed a few seconds to reach atmospheric pressure. The three-way valve is then closed to gas flow and the line toward the sampling bottle is opened to a saturated salt water line. The salt water reservoir is

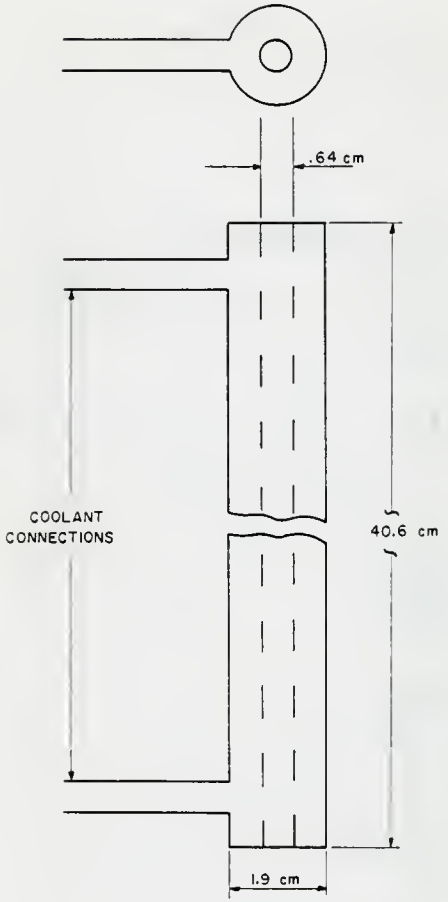

FIGURE 18 GAS SAMPLING PROBE

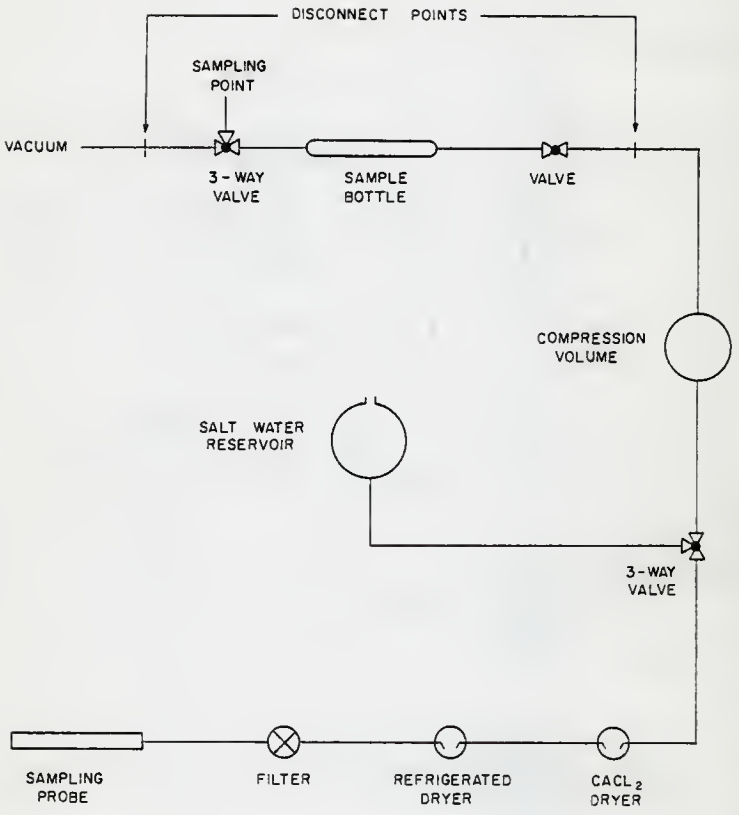

FIGURE 19 GAS SAMPLING SYSTEM

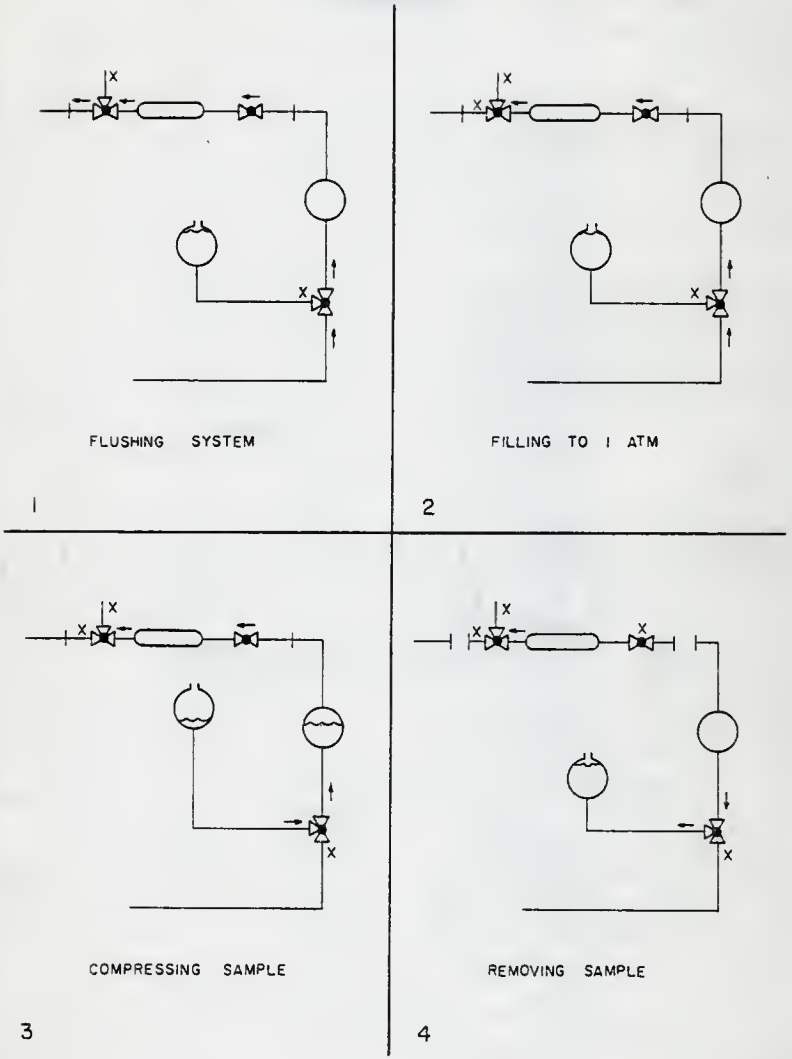

FIGURE 20 GAS SAMPLING PROCEDURE

lifted causing the fluid to flow into the compression volume and produce a positive gage pressure on the gas in the sampling bottle. Saturated salt water is used to prevent the absorption of the gases in the water. The pressures produced by this method have been about 120 cm of salt water above atmospheric. When the sample has been compressed, the valve between the compression volume and sampling bottle is closed and the bottle may be removed by opening a Swagelok quick-disconnect fitting located between the sampling bottle and vacuum source.

Analysis of the gases is performed in two diverse manners. NO_x and SO_2 levels are determined by wet chemical detection techniques while O_2, N_2 CO, CO_2, and CH_4 levels are found using gas chromatography. Both of the detection methods are detailed in Appendix B.

The facility described in this chapter was the result of an evolutionary process. Careful planning and consultations with the builders of similar furnaces allowed the initial design to meet many requirements, and preliminary testing provided information on necessary modifications. The procedures developed for use of the facility and the experimental results are described in the next chapter.

3 EXPERIMENTAL PROCEDURES AND RESULTS

The purpose of this chapter is to detail the experimental methods conceived and the difficulties encountered in the attainment of the goals set forth in Chapter 1 and to report the results of the experimentation.

3.1 Experimental Approach

The first aim of the study was to demonstrate the comparability of data from the facility to those obtained from utility boilers. Inasmuch as flame conditions and emissions can vary greatly, depending upon the equipment and fuel properties, this study attempted to simulate the behavior of furnaces employed in previous studies, particularly the research documented by Pershing, et al.[40]. Their results had already been compared at length with utility boiler emissions and it was concluded that the combustion facility they used was suitably representative of utility boilers. The problems of comparing the furnace in this work to that chamber was further simplified by striving to reproduce only the general trends observed in the earlier work rather than matching the results precisely. For instance, absolute levels of NO_x are not comparable to those measured previously inasmuch as most workers have used air preheat to help stabilize the flame; whereas, this research was performed without air preheat. Since nitric oxide emissions can vary with the reaction zone temperatures, NO_x levels here should be less than those measured previously if the flame geometry remains unaltered. This will be discussed further in Section 3.4. The relative variation of NO_x

levels with percent swirl and excess air levels should be unaffected by air preheat and these parameters served as the basis of comparison. Even so, it is not possible to state unequivocally that the observed results are functions of the excess air and percent swirl only and not of a still misunderstood function of a combination of burner parameters and aerodynamics. Thus, it is extremely difficult to determine whether the results obtained from a study of this type are applicable to full scale equipment. This, however, has not kept researchers from testing firing techniques found to be promising in small scale facilities in larger burners. Though there is no guarantee of applicability, experience dictates that the results obtained from small scale furnaces are valuable in design revisions for full scale equipment. Hence, the approach of evaluating the applicability of the present facility by comparison to previous lab scale combustion chambers was held as a reasonable method.

The tests performed to demonstrate the similarity mentioned above consisted mainly of varying the fraction of secondary air introduced as swirl and the percent of excess air used. Results of the tests and details of the comparison are documented in Sections 3.3 and 3.4.

The second objective of the investigation was to study the effects of cofiring wheat straw and coal mixtures in the furnace. The approach to this problem was straightforward, requiring only the repetition of a set procedure while firing the various mixtures. The results of these tests are also contained in Sections 3.3 and 3.4.

3.2 Experimental Techniques

The procedures for normal starting and operation of the furnace are given in Appendix F and are valid regardless of the solid fuel fired. The experimental method employed for data collection enabled a full set of samples to be collected in as short a time as possible, thus conserving fuel and allowing the full complement of runs to be accomplished in a few weeks. One set of data comprised collection of gas samples at four different values of swirl input and three different excess air settings. The procedure was adjusted when necessary because of properties of the individual fuel being fired. There were six sets of samples collected, each corresponding to either a coal, a blend of coals, or a mixture of coal and straw. The composition of the fuel for each run and the test conditions are given in Table 3.

The furnace was started and allowed to reach operating temperature ($\sim$ 1325 K) in accordance with the procedures set forth in Appendix F. When starting with cold walls, about six hours was required to attain this temperature. The warm up time was used to place absorbing reagent samples in the sample vials, check out the vacuum system, fill the feeder hopper with fuel, and perform maintenance on any equipment requiring it. When the operating temperature was reached, the switch from natural gas to solid fuel was made. An estimate of the feeding rate, made possible by information from feed tests, provided enough information to estimate the air requirements and stabilize the flame near stoichiometric. A stable flame was assumed present when a change of less than 1 K/min was recorded at the thermocouple position near the chamber's inner wall and 88.7 cm from the top of the furnace. Once the temperature stabilized, a gas

Table 3. Test Conditions

FUELS FIRED
1) Kansas coal
2) Kansas coal with 25% wheat straw
3) Kansas coal with 50% wheat straw
4) Kansas coal with 50% Western coal
5) Western coal
6) Western coal with 25% wheat straw

AIR INPUT PARAMETERS	
At 5% Excess Air:	
	20% swirl
	40% swirl
	60% swirl
	80% swirl
At 60% Swirl:	
	15% excess air
	30% excess air

sample was collected and analyzed by gas chromatography to determine the O_2 and CO contents. At stoichiometric conditions, the O_2 content of the flue gases was assumed to be approximately 3% and the CO content was less than 1%. A higher CO content implied the flame was fuel rich while the lack of CO and higher O_2 levels indicated fuel lean conditions. The air input settings were varied and additional samples taken until near stoichiometric conditions were obtained.

The primary air level was held constant for each fuel at about 15% of stoichiometric. This was done to nullify any change in feed rate caused by a difference in primary air supply. The percent swirl parameter was defined as

$$\% \text{ Swirl} = \frac{FR_s}{FR_s + FR_a} (100) , \qquad (11)$$

where FR_s and FR_a represent the swirl and axial secondary air flow rates, respectively.

For each sample condition, two complete sets of gas samples were collected so that a check could be made of the steady state flame approximation. One set of samples consisted of a NO_x sample, an SO_2 sample, and sampling for permanent gases. Immediately after collecting the second set of samples at a given set of conditions, the gas chromatographic analysis was begun while the air input parameters were altered to the next desired states. In this manner the time required for the flame to approach steady state coincided with the time needed to perform the GC analysis. When the analysis was complete, the sample bottles were returned to the sampling line and the procedure repeated for the next

set of conditions. Barring complications, the chromatographic analysis could be accomplished in about 45 minutes; thus, a minimum of 6 hours was required for each full run after warm-up and the location of stoichiometric conditions.

After collection and quantitative analysis of the gas samples were completed, the results were plotted as ppm NO_x or ppm SO_2 vs. percent swirl at a given level of excess air or as ppm NO_x or ppm SO_2 vs. percent excess air at a given level of swirl. The levels were adjusted to account for dilution by the oxygen through the use of the relation

$$C_c = \left(\frac{21}{21 - C_{O2}}\right) C_m \,, \qquad (12)$$

where C_c and C_m denote the corrected and measured concentrations of the pollutant, respectively, and C_{O2} represents the concentration (in percent) of oxygen. This relation is widely used among authors to correct for dilution in order to aid comparison of data, and C_c is reported as the pollutant concentration reduced to stoichiometric conditions[72].

3.3 Experimental Observations

The fuel mixtures all burned at about the same temperature, as indicated by wall thermocouple readings. However, the thermocouple results are not comprehensive enough to present as conclusive evidence, since, due to slagging on the inside walls, the temperature measured by the thermocouples was difficult to correlate with the inner wall temperature and thermal destruction of the thermocouples at certain positions

occurred so often that it was difficult to collect readings at these points consistently. The Kansas coal produced the worst slagging, and the problem was reduced by co-firing the coal with straw. This is not surprising since the ash content of the Kansas coal was nearly 40% by weight while the straw contained only about 7% ash. The slag was burned from the furnace walls by firing natural gas between data collection runs in order to prevent emissions from slag oxidation interfering with the analysis of emissions in subsequent runs. During this cleaning procedure, a definite odor of H_2S could be detected in the furnace room indicating that either the slag never lost the sulfur it contained when introduced or that it absorbed SO_2 during combustion of coal. This possibility will be discussed later in this section.

The wheat straw appeared visually to burn with a luminosity approximately equal to that of coal. In addition, it was observed to burn out sooner than the coal as evidenced by the lack of unburned straw residue in the flue. Because of its high volatile content, the straw should burn more rapidly. These two factors are germane to the utilization of straw as a boiler fuel since the luminosity affects the radiative heat transfer to the boiler tubes and the rapid burning could allow the construction of more compact boilers. Feeding of the straw to the furnace presented a problem in that the straw exhibited a tendency to pack or "bridge" in the feeder. This prevented the burning of mixtures containing more than 50% of straw and necessitated a manual agitation procedure to complete the Kansas coal/50% straw data collection run. However, by examining alternative methods of reducing the straw size, a procedure should be found that will allow easier feeding of the straw.

It was found that ash and unburned coal (possibly caused by lack of air preheat) collected in the exhaust flue's long horizontal section and necessitated cleaning of the section after every other run to prevent blockage. This does not affect the conversion percentages discussed later in this section since conversion is computed on the basis of the fuel feed rate calculated from gas chromatographic analysis of the exhaust gases. Hence, the assumed feed rate does not include that fuel which does not burn and generate exhaust products.

3.4 Gas Analysis

The emissions data from the experimentation are shown graphically in Figs. 21 through 27. The NO_x dependence on percent swirl at 5% excess air is shown in Fig. 21. Most of the runs yielded qualitatively similar results with the minimum NO_x concentration occurring at 50 to 60 percent swirl. This does not agree with the behavior noted by Pershing, et al.[40], but Pershing[72] has stated that, due to the complexity of the entire mechanism, the trends noted in that study should be accepted with caution. Percent swirl is, in fact, a particularly troublesome factor to reproduce inasmuch as it may be a function of the angle of the swirl vanes and the size of the opening through which it is introduced. Also, insofar as furnace aerodynamics can radically affect emissions, it is not surprising that conflicting trends are observed. The consistent nature of the data throughout the runs reduces the probability that the trend noted herein is an anomalous effect, however, the ability to predict the effect of swirl on NO_x emissions remains an elusive goal.

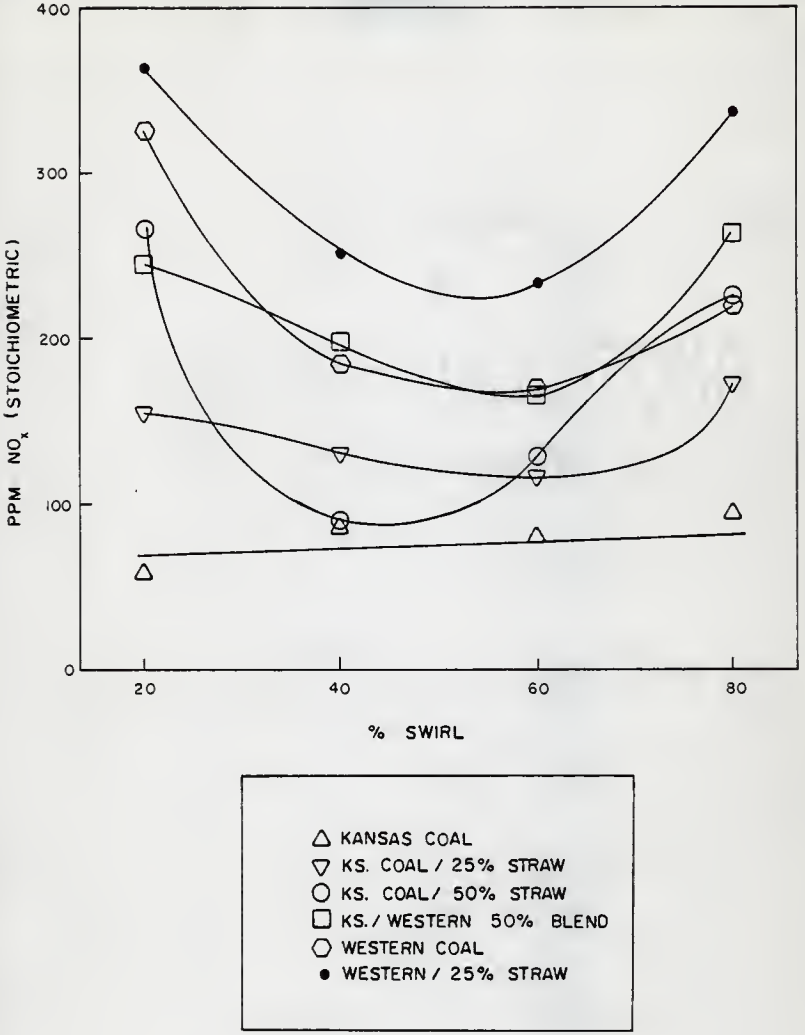

FIGURE 21 NO_x EMISSIONS vs. % SWIRL AT 5 % EXCESS AIR

From a conceptual point of view, the influence of swirl on NO_x emissions is unsatisfying. If intimate contact between nitrogen and oxidizer early in the flame is directly responsible for enhanced NO_x production from fuel bound nitrogen, then increasing swirl, and thereby the turbulence level, of the primary zone should promote NO_x formation; however, in the present experimentation, an increase in swirl at low swirl levels produces a reduction in NO_x emissions as indicated in Fig. 21. This inexplicable phenomenon is not unique to the current study, but also appears as a reduction in NO_x emissions with increase of percent swirl over 80% in the results of Pershing et al.[40] Study of the dependence of NO_x emissions on aerodynamic conditions is an area in which significant contributions can still be made. Even though the effects of varying excess and swirl air levels on NO_x has been probed, the results cannot be explained from a fundamental basis.

The magnitude of the NO_x emissions in this study is significantly lower than that seen in some previous investigations, but this may be explained by the use of air preheat in those studies. Pershing, et al.[40] indicate that NO_x emissions are reduced under low air preheat conditions, despite their contention that fuel NO_x levels are nearly independent of temperature. This indicates that the dependence of fuel NO_x on the flame zone temperature is another mechanism that is not well understood. Until recently, it was believed that fuel nitrogen conversion, unlike thermal fixation, was insensitive to temperature. This was based on the

relative ineffectiveness of temperature reduction schemes in reducing NO_x emissions from fuel bound nitrogen. Also, Pohl and Sarofim[78] contend that any increase in nitrogen emitted with the volatiles at higher temperatures is offset by an increase in the fuel equivalence ratio caused by the increased devolatilization kinetics. There is some support for a slight temperature dependence. Figure 22 shows the effect of temperature that Pershing, et al[40] noted on fuel NO_x emissions. Pershing[72] stated that without using air preheat, the NO_x emissions increased to about 800 ppm, contradicting the trend observed in Fig. 23. He attributed the increase to a detached flame produced when air preheat was not utilized. However, since a pilot flame is used in the present study to stabilize the flame, the system approximated a flame attached to the burner so the trend exhibited in Fig. 22 may be expected to continue. The lower levels in this study may also be a result of interferences by SO_2 on the detection of NO_x in the chemical indicator, though this is supposedly eliminated by addition of acetone to the absorbing reagent.

The qualitative behaviors of the NO_x emissions from each fuel are consistent with the predictions made in Section 1.4, based on the fuel nitrogen and volatile matter contents. The data presented in Fig. 23 lend credence to the contention that the fraction of nitrogen released with the volatile species has more bearing on the NO_x emissions than the total nitrogen content[44], as illustrated by the rise in NO_x emissions from wheat straw mixtures even though the straw has a lower nitrogen (but higher volatile matter) content than either of the coals. In the

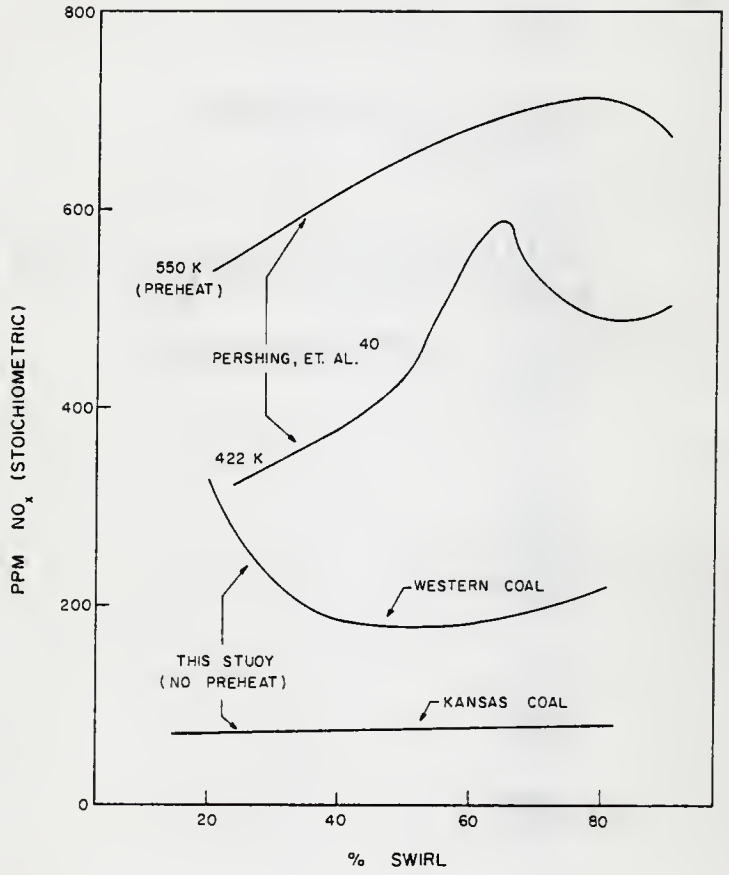

FIGURE 22 DEPENDENCE OF NO_x EMISSIONS ON TEMPERATURE

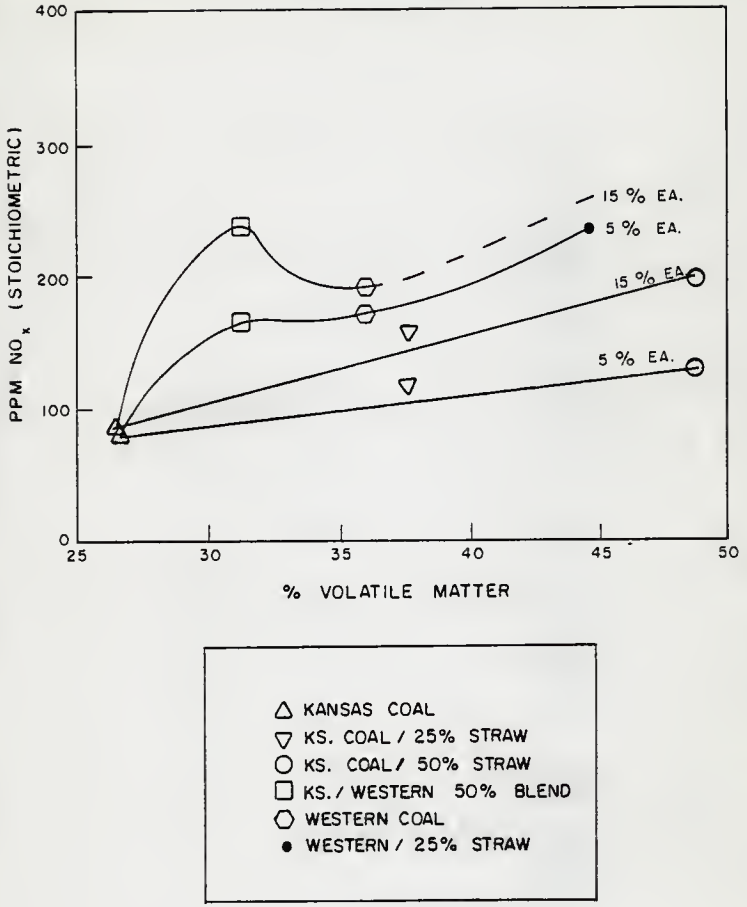

FIGURE 23 NO_x EMISSIONS vs. % VOLATILE MATTER AT 60 % SWIRL

figure, the two upper curves demonstrate the effect of increasing the fraction of Western coal in a Kansas/Western coal blend until 100% Western coal is reached, at which point the same curves continue by showing the effect of increasing straw content in Western coal/straw mixtures. The lower two curves depict the effect of increasing the straw fraction in Kansas coal/straw mixtures. The high NO_x levels attendant with wheat straw are expected since much of the nitrogen is contained in protein groups which may release amines during devolatilization. The amine group is subsequently oxidized to form NO_x. The nitrogen in coal molecules may be bound in aliphatic groups which are decomposed relatively easily during devolatilization or in various aromatic forms which exhibit a higher thermal stability[79]. This is the underlying basis of the observation that NO_x is not strictly dependent on fuel nitrogen content, but has a volatile matter dependence as well. Calculations show that only 3.5% conversion of the nitrogen in Kansas coal occurs while 7.3 to 11% of the Western coal's nitrogen forms NO_x. These values may be contrasted with conversions of 28% noted by Pershing and Wendt[42] and 10-50% reported by Pohl and Sarofim[75]. Part of the difference may be attributable to the mechanisms noted by Wendt and Ekmann[60] wherein the presence of SO_2 in the flame region inhibits the formation of NO_x, but more likely the absence of air preheat had a dominant effect.

The data of Fig. 24 show the effect of increasing excess air on the NO_x emissions. The lack of data for the firing of Kansas coal/50% straw and the Kansas/Western coal blend was caused by difficulties in feeding those fuels to the furnace; whereas the Western coal data are incomplete

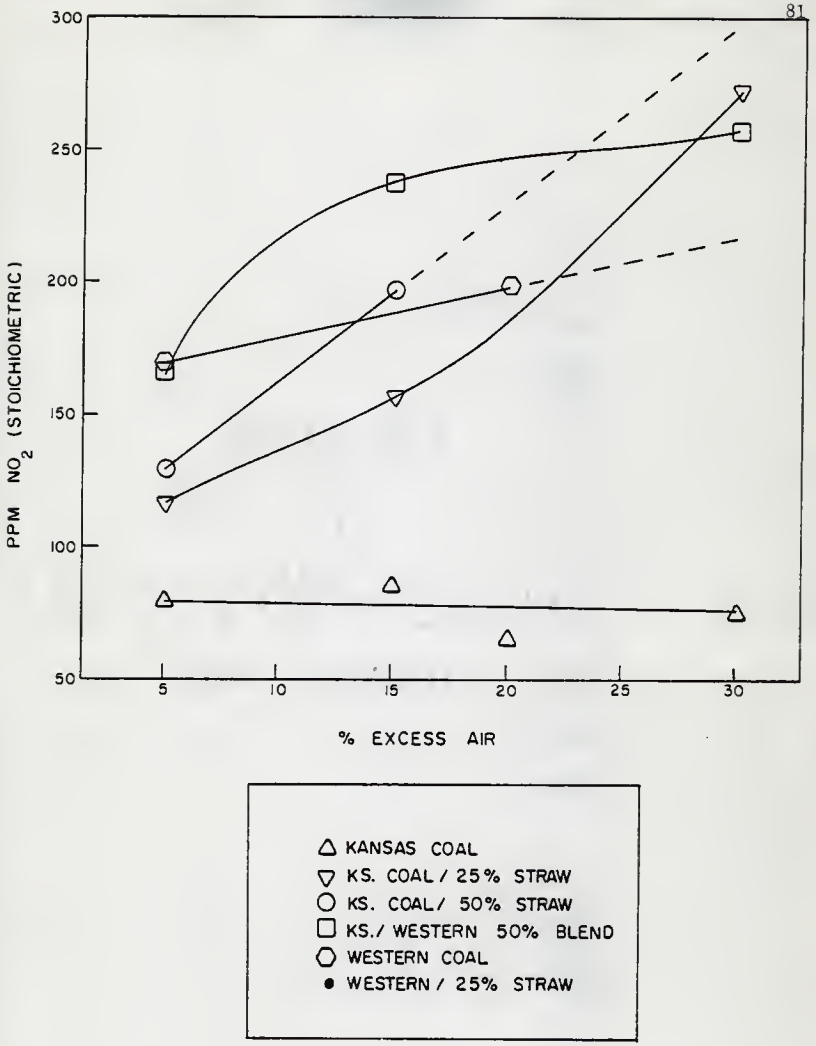

FIGURE 24 NO_x EMISSIONS vs. % EXCESS AIR AT 60% SWIRL

because the experimental procedure was altered slightly for that run. For this coal the effect of swirl was tested again at a higher excess air level. The general trend exhibited by the data approximates the behavior presented in the literature, i.e., a rise in NO_x levels with increasing excess air[40-42]. The nearly constant emissions noted when firing the Kansas coal may be caused by the SO_2 inhibition reaction since the SO_2 emissions increase with excess air, as will be seen shortly.

Comparisons of the excess air dependence of NO_x emissions from this study with that from previous investigations is shown in Fig. 25. The plot, with NO_x emissions normalized to 20% excess air, show that the furnace combustion behavior is similar in at least one aspect to the furnaces employed by other workers.

Fig. 26 portrays the dependence of SO_2 emissions on the percent swirl. As stated earlier, it is generally agreed that the levels of SO_2 in the flue gas are relatively independent of air input conditions and are normally proportional to the fuel sulfur content. All of the fuels fired in this study, with the exception of the Kansas coal, exhibited that behavior. The variation in SO_2 emissions noted with the Kansas coal may be due to absorption of SO_2 by the ash and slag in the furnace. Although this effect is not reported in the literature, there is some support for the idea and investigation into the mechanism is likely[72]. Note that SO_2 data are not presented for the Western coal/25% straw mixture. In analyzing the gas samples it was found that the levels of SO_2 for that fuel mixture were so low as to be undetectable.

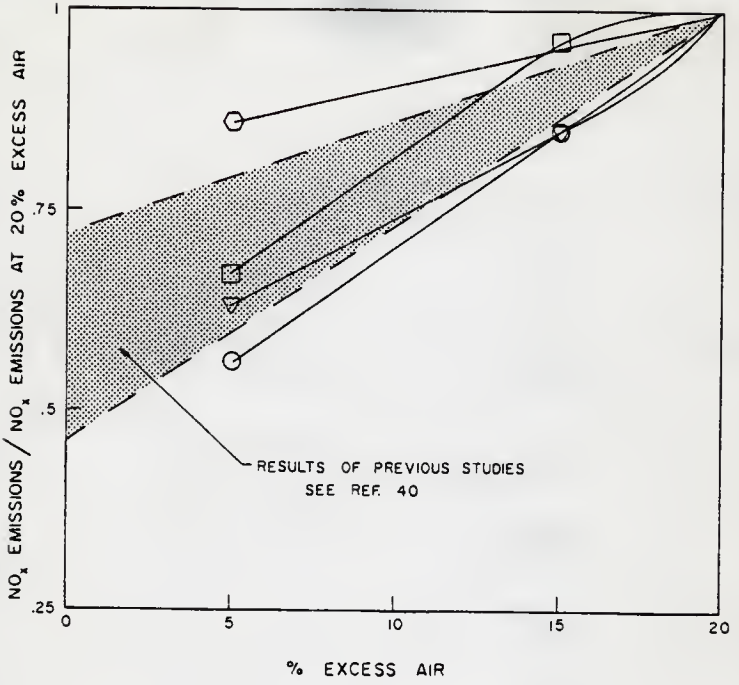

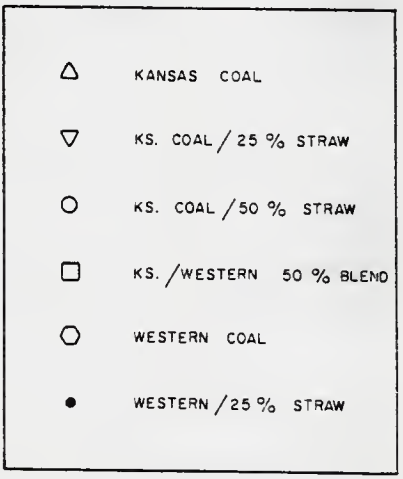

FIGURE 25 COMPARISON OF NO_x EMISSIONS vs. % EXCESS AIR WITH PREVIOUS STUDIES

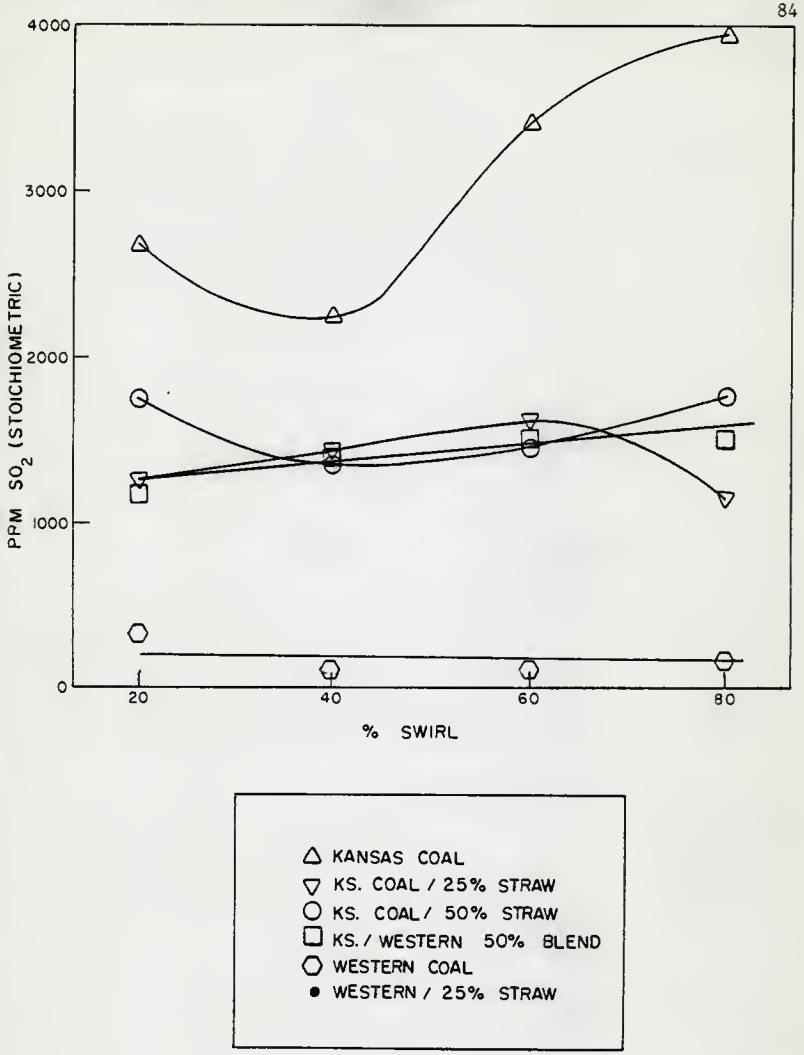

FIGURE 26 SO_2 EMISSIONS vs. % SWIRL AT 5% EXCESS AIR

The SO_2 conversion percentages noted in this study are shown in Table 4. These conversions may be compared with values of about 85-95% reported by Ely and Barnhart[76] and Zallen[77]. The reduced conversions observed herein are most likely due to the lower flame temperatures attendant with the absence of air preheat. At the flame temperatures (estimated from wall temperatures, heat loss, and adiabatic flame temperature) seen in this study, Polavarapu[57] noted similar conversions of SO_2. He examined the contributions to the total emissions from the different forms of sulfur through the use of model compounds, and found that between 55 and 75% conversion of organic sulfur and about 40% conversion of pyritic sulfur occurred. On the basis of 40% pyritic and 65% organic sulfur conversion, calculations show that SO_2 emission levels from Kansas coal should be around 3080 ppm while Western coal should emit about 600 ppm SO_2 during combustion. These levels compare very well with observed values for Kansas coal, but the experimentally noted emissions from Western coal were well below the calculated values.

It is interesting to note that the SO_2 emissions from the Kansas coal/25% straw mixture are roughly equivalent to the levels given off when firing Kansas coal/50% straw. Table 4 shows that the 25% mixture reduces the conversion appreciably below the conversion for the Kansas coal. Although further investigation is required, this may indicate that the mineral matter of the straw is absorbing SO_2 and converting it to a sulfate, much the same as a dry sorbent mechanism. However, the fact that the conversion increases with the addition of more straw (up to 50%) cannot be explained by that mechanism. It is possible that the reduced slagging attendant with the firing of the 50% mixture resulted

Table 4. Conversion of Fuel Sulfur to SO_2 At Excess Air And 60% Swirl

FUEL	PPM SO_2	100% CONVERSION*	% CONVERSION
KS Coal	3406	6490	52.5
KS coal/25% straw	1619	5025	32.2
KS coal/50% straw	1442	3570	40.4
Western coal	94	1030	9.1
KS/Western coal blend	1499	3121	48.0

*100% Conversion is Based on The Fuel Sulfur Content With The Sulfates Omitted.

in less absorption of SO_2 by the slag.

The effects of varying excess air levels on the SO_2 emissions are illustrated in Fig. 27. This figure bears a strong similarity to the results plotted in Fig. 26. Note that the plots for the Kansas coal/50% straw and the Western coal runs are extrapolated since experimental difficulties prevented collection of sufficient data. The extrapolated behavior for the Kansas coal/50% straw mixture is based on its behavior in Fig. 26 and on the plots of the Kansas coal/25% straw mixture and Kansas/Western coal blend. As for the excess air figure, it is generally agreed that conversion of sulfur to SO_2 is independent of excess air, provided the conditions are not fuel rich. These conclusions have, however, been drawn from work in which air preheat yielded high enough flame temperatures that virtually all the sulfur should have been converted to SO_2.

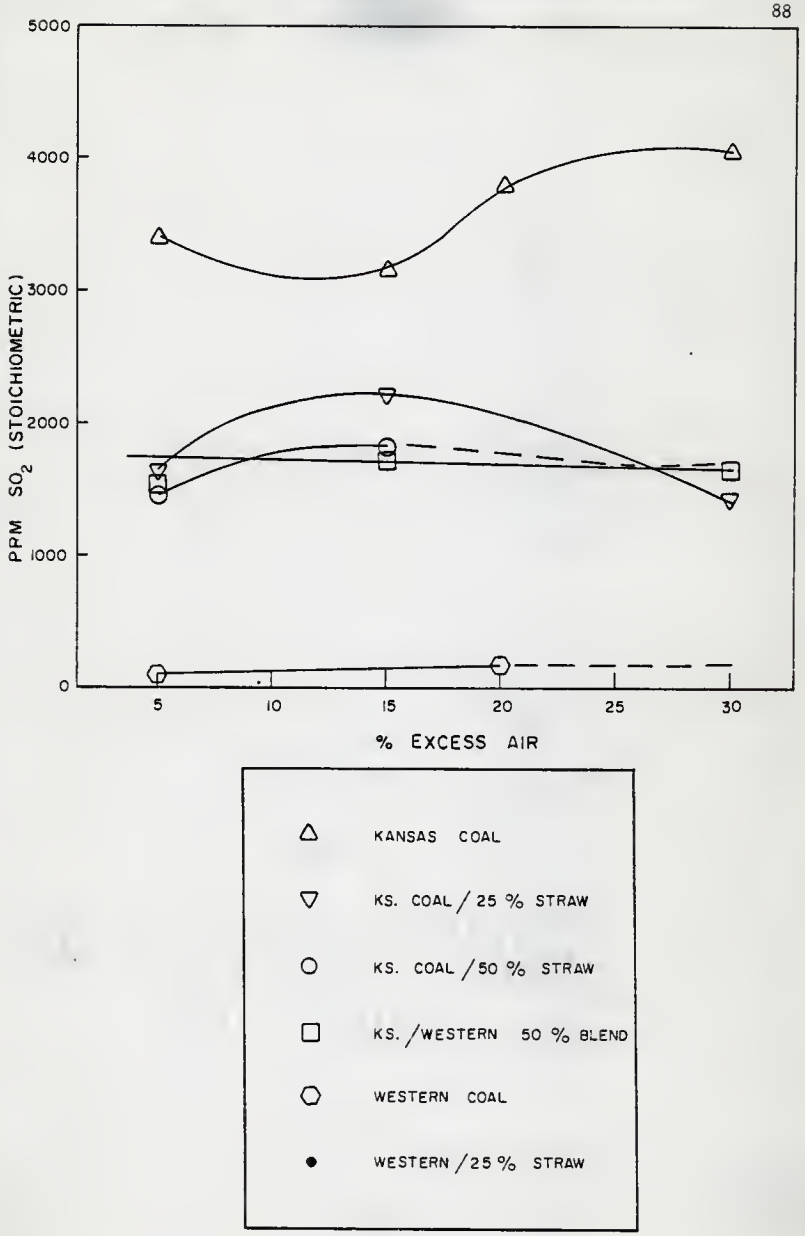

FIGURE 27 SO_2 EMISSIONS vs. % EXCESS AIR AT 60 % SWIRL

4. CONCLUSIONS AND RECOMMENDATIONS

4.1 Combustion Facility

As noted repeatedly in Chapter 3, the major factor differentiating this facility from similar models is the lack of air preheat. All of the discrepancies between the data of this report and those of previous investigations could be at least partially attributed to this factor. This leads to the conclusion that the combustion chamber and associated equipment operate satisfactorily and produce the expected trends in emissions where sufficient understanding exists that predictions can be made. It also indicates that any improvements in hardware should incorporate air preheating apparatus in the secondary air supply lines.

Another suggestion for upgrading the utility of the system is the acquisition of on-line, continuous monitoring gas sampling equipment. The present sampling and analysis methods performed adequately, but were time and labor intensive and were vulnerable to error due to momentary oscillations in emissions levels.

Implementation of solid and gas sampling in the flame region is a third recommendation. In the plug flow configuration, the solid sampling option yields information particularly germane regarding the combustion mechanism. In two-dimensional flow, the solid material collected at a given point is not as uniform as in plug flow, but can still reveal many facts concerning the combustion.

The three suggestions discussed above should be considered seriously to bring the system to a condition wherein results more readily comparable to those of other studies could be obtained. The primary reason

they were not implemented during the initial construction stage was the large capital expenditure required.

Further modifications to the facility are possible that would allow simulation of more advanced technology. Foremost among these is the implementation of a combustion staging system. With this revision, the facility would have the capability of modeling some of the advanced NO_x control techniques mentioned in the previous chapters. A system allowing for the introduction of an alternative oxidizer containing no nitrogen would allow for discrimination between the fuel and atmospheric nitrogen contributions to NO_x emissions. These modifications are desireable, but have a lower priority than those mentioned before.

4.2 Combustion of Coal/Straw Mixtures

This study represents the first systematic attempt to monitor the gaseous pollutants of agricultural residues when fired under conditions comparable to utility boilers. Wheat straw exhibits characteristics desirable in boiler fuels in that its high volatile matter content promotes rapid combustion which may allow for more compact boilers. Furthermore, the low ash content of the straw produces less slag on boiler sufaces and, possibly, less fly ash in the flue gases. Visual observations and thermocouple readings indicate that the luminosity and temperature of the flame are comparable to a coal flame. Therefore, the radiative heat transfer characteristics should simulate those of coal, although this observation is merely qualitative and more detailed study is certainly required. The straw apparently had more than just a

sulfur replacement effect on the SO_2 emissions when co-fired with high sulfur coal, although this too is preliminary and may be patently untrue when the combustion temperature is increased to such a level that complete sulfur evolution from the coal is assured. All of these factors enhance the attractiveness of straw as a boiler fuel.

Further study of the effects of co-firing wheat straw with coal are required in order to allow more authoritative statements to be made. Combustion staging techniques should be applied to assess the effectiveness of current control technologies on the NO_x emissions. The results of the present study indicate that a substantial fraction of the nitrogen in the straw is evolved readily. Hence, combustion staging, which promotes rapid evolution of fuel nitrogen in a fuel rich atmosphere to enhance the production of N_2, should exhibit marked success in reducing the NO_x levels. Measurements of the flame temperature and luminosity should be made so that a quantitative assessment of these characteristics can be reported. Combustion in plug flow with concurrent probing of the solid particles and gases at various locations in the flame should be attempted in order to delineate the devolatilization and combustion behavior of the straw on a more fundamental level.

References

1. P. Averitt, Coal Resources of the United States, January 1, 1974, USGS Bulletin 1412.

2. H. H. Lowry (ed.), Chemistry of Coal Utilization (Wiley and Sons, New York, 1963) Suppl. Vol.

3. Babcock and Wilcox, Steam/Its Generation and Use, (Babcock and Wilcox, New York, 1975), 39th ed.

4. H. C. Howard, Chemistry of Coal Utilization (Wiley and Sons, New York, 1963) Suppl. Vol., p. 340.

5. D. B. Anthony and J. B. Howard, AIChE Journal, 22, 625 (1976).

6. S. Badzioch, BCURA Monthly Bulletin, 31, 193 (1967).

7. D. C. Wegener, The Production of Lower Molecular Weight Hydrocarbons During the Thermal Decomposition of Pulverized Coal in Air and Nitrogen, Master's Thesis, Kansas State University (1978).

8. R. H. Essenhigh, Sixteenth Symposium (International) on Combustion, p. 353, The Combustion Institute (1977).

9. J. B. Howard, Mechanisms of Ignition and Combustion in Flames of Pulverized Bituminous Coal, Ph.D. Dissertation, Pennsylvania State University (1965).

10. J. B. Howard and R. H. Essenhigh, Combustion Flame, 10, 92 (1966).

11. S. Badzioch and P. G. W. Hawksley, Ind. Eng. Chem. Process Design and Devel., 9, 521 (1970).

12. G. M. Kimber and M. D. Gray, Combustion Flame, 11, 360 (1967).

13. J. B. Howard and R. H. Essenhigh, Eleventh Symposium (International) on Combustion, p. 399, The Combustion Institute (1967).

14. J. B. Howard and R. H. Essenhigh, Ind. Eng. Chem. Process Design and Devel., 6, 74 (1967).

15. W. R. Seeker, The Kinetics of Ignition and Particle Burnout of Coal Dust Suspensions Under Rapid Heating Conditions, Ph.D. Dissertation, Kansas State University (1978).

16. N. M. Laurendeau, Prog. Energy Combust. Sci., 4, 221 (1978).

17. C. Orr and J. M. Dallavalle, Fine Particle Measurement (MacMillan Company, New York, 1959).

18. Short Course on Coal Characteristics and Coal Utilization, Pennsylvania State University, October 24-28, 1977 (P.H. Given, Course Chairman).

19. J. M. Smith, Chemical Engineering Kinetics (McGraw-Hill Company, New York, 1970), 2nd ed.

20. P. L. Walerk, F. Russinko, and L. G. Austin, Advances in Catalysis, 11, 133 (1959).

21. M. F. R. Mulcahy and I. W. Smith, Rev. Pure and Appl. Chem., 19, 81 (1969).

22. P. Lightman and P. J. Street, Fuel, 47, 7 (1968).

23. M. W. Thring and R. H. Essenhigh, Chemistry of Coal Utilization (Wiley and Sons, New York, 1963) Suppl. Vol., p. 754.

24. M. A. Field, D. W. Gill, B. B. Morgan, and P. G. W. Hawksley, Combustion of Pulverized Coal (BCURA, Leatherhead, England, 1967).

25. R. H. Essenhigh, Combustion Technology: Some Modern Developments (Academic Press, New York, 1974) p. 374.

26. J. L. Krazinski, R. O. Buckius, H. Krier, Journal of Heat Transfer, 100, 105 (1978).

27. J. M. Beer, and M. W. Thring, and R. H. Essenhigh, Combustion Flame, 3, 557 (1959).

28. J. Csaba, Flame Propagation in a Fully Dispersed Coal Dust Suspension, Ph.D. Dissertation, University of Sheffield, Sheffield, England (1963).

29. Symposia (International) on Combustion, 16 vols., The Combustion Institute.

30. Proceedings of the Stationary Source Combustion Symposium, EPA-600/2-76-152, 3 vols. (1976).

31. Proceedings of the Second Stationary Source Combustion Symposium, EPA-600/7-77-073 (1977).

32. Proceedings of the Third Stationary Source Combustion Symposium, EPA-600/7-79-050, 5 vols. (1979).

33. Proceedings of the NO_x Control Technology Seminar, EPRI-SR-39 (1976).

34. W. H. Nebergall, F. C. Schmidt, and H. F. Holtzclaw, College Chemistry with Qualitative Analysis (D. C. Heath and Company, Lexington, Massachusetts, 1972).

35. Clean Air Amendments of 1970 (Public Law 91-604).

36. W. W. Habet and B. M. Howell, Proceedings of the NO_x Control Technology Seminar, EPRI-SR.39, Session I, Paper D (1976).

37. Ya. B. Zeldovich, P. Ya. Sadovnikov, and D. A. Frank-Kamenetskii, Academy of Sciences of the USSR, Institute of Chemical Physics, Moscow-Leningrad, Translated by M. Shelef, 1947, Scientific Research Staff, Ford Motor Co.

38. K. A. Bueters, W. W. Habelt, C. E. Blakeslee, and H. E. Burbach, 66th Annual AIChE Meeting (1973).

39. C. P. Fenimore, Combustion Flame, 19, 289 (1972).

40. D. W. Pershing, G. B. Martin, and E. E. Berkau, AIChE Symposium Series, 71, no. 148, 19 (1975).

41. J. O. L. Wendt and D. W. Pershing, Combustion Science and Technology, 16, 111 (1977).

42. D. W. Pershing and J. O. L. Wendt, Sixteenth Symposium (International) on Combustion, p. 389, The Combustion Institute (1976).

43. M. P. Heap, T. J. Tyson, T. M. Lowes, 68th Annual AIChE Meeting (1975).

44. M. P. Heap, D. W. Pershing, G. C. England, J. W. Lee, and S. L. Chen, Proceedings of the Third Stationary Source Combustion Symposium, EPA-600/7-79-050b, Volume II, p. 3 (1979).

45. R. E. Thompson, M. W. McElroy, and R. C. Carr, Proceedings of the NO_x Control Technology Seminar, EPRI-SR-39, Session I, paper B (1976).

46. J. L. Friedrich and R. H. Pai, Proceedings of the NO_x Control Technology Seminar, EPRI-SR-39, Session I, paper E (1976).

47. L. W. Waterland, K. J. Lim, and R. J. Schreiber, Proceedings of the Third Stationary Source Combustion Symposium, EPA-600/7-79-050a, Volume I, p. 119 (1979).

48. G. A. Hollinden, N. D. Moore, and R. L. Zielke, Proceedings of the NO_x Control Technology Seminar EPRI-SR-39, Session I, paper G (1976).

49. G. A. Hollinden, J. R. Crooks, N. D. Moore, R. L. Zielke, and C. Gottschalk, Proceedings of the Stationary Source Combustion Symposium, EPA-600/2-76-152b, Volume II, p. III-31 (1976).

50. A. P. Selker, Proceedings of the Stationary Source Combustion Symposium, EPA-600/2-76-152b, Volume II, p. III-3 (1976).

51. J. O. L. Wendt, C. V. Sternling, and M. H. Matovich, Fourteenth Symposium (International) on Combustion, p. 897. The Combustion Institute (1973).

52. R. K. Lyon and J. P. Longwell, Proceedings of the NO_x Control Technology Seminar, EPRI-SR-39, Session II, paper B (1976).

53. L. J. Muzio, J. K. Arand, and D. P. Teixeira, Proceedings of the NO_x Control Technology Seminar, EPRI-SR-39, Session II, paper C (1976).

54. D. P. Teixeira, Proceedings of the NO_x Control Technology Seminar, EPRI-SR-39, Session II, paper D (1976).

55. A. Levy, E. L. Merryman, and W. T. Reid, Environ. Sci. Technol. 4, 653 (1970).

56. C. R. Cullis and M. F. R. Mulcahy, Combustion Flame, 18, 222 (1972).

57. J. Polavarapu, Evolution of H_2S and SO_2 During Rapid Heating of Pulverized Coal and Sulfur Containing Model Compounds, Master's Thesis, Kansas State University (1979).

58. I. Glassman, Combustion (Academic Press, New York, 1977).

59. D. M. Zallen, R. Gershman, M. P. Heap, and W. H. Nurick, Proceedings of the Third Stationary Source Combustion Symposium, EPA-600/7-79-0506, Volume II, p. 73 (1979).

60. J. O. L. Wendt and J. M. Ekmann, Proceedings of the Stationary Source Combustion Symposium, EPA-600/2-76-152a, Volume I, p. I-35 (1976).

61. D. W. Pershing, Nitrogen Oxide Formation in Pulverized Coal Flames, Ph.D. Dissertation, University of Arizona (1976).

62. J. G. Cogoli, D. Gray, and R. H. Essenhigh, Combustion Science and Technology, 16, 165 (1977).

63. S. Badzioch, Combustion of Pulverized Coal (BCURA, Leatherhead, England, 1967), Ch 4.

64. I. Glassman, Combustion (Academic Press, New York, 1977), p. 213.

65. Babcock and Wilcox, Steam/Its Generation and Use (Babcock and Wilcox, New York, 1975), 38th ed., p. 18-3.

66. Babcock and Wilcox, Steam/Its Generation and Use (Babcock and Wilcox, New York, 1975), 38th ed., p. 6-7.

67. Annual Book of ASTM Standards, Volume 26, procedure D1607-76 (1974).

68. B. E. Saltzman, Analytical Chemistry, 26, 1949 (1954).

69. P. W. West and G. C. Gaeke, Analytical Chemistry, 28, 1816 (1956).

70. Intersociety Committee, Methods of Air Sampling and Analysis (American Health Assoc. Publg., Washington, DC, 1968) p. 447.

71. National Academy of Sciences/National Academy of Engineering/National Research Council, Commission on Natural Resources. Report prepared for Committee on Public Works, U.S. Senate, Serial No. 94-4 (1975).

72. D. W. Pershing, Personal Communication, April 1979.

73. J. G. Knudsen and D. L. Katz, Fluid Dynamics and Heat Transfer (McGraw-Hill Company, New York, 1958), p. 366.

74. E. Tschuikow-Roux, Phys. Fluids, 8, 821 (1965).

75. J. H. Pohl and A. F. Sarofim, Proceedings of the Stationary Source Combustion Symposium, EPA-600/2-76-152a, Volume I, p. 1-125 (1976).

76. F. G. Ely and D. H. Barnhart, Chemistry of Coal Utilization (Wiley and Sons, New York, 1963) Suppl. Volume, p. 857.

77. D. M. Zallen, Personal Communication, May 1979.

78. J. H. Pohl and A. F. Sarofim, Sixteenth Symposium (International) on Combustion, p. 491, The Combustion Institute (1976).

79. R. A. Vogt and N. M. Laurendeau, Nitric Oxide Formation in Pulverized Coal Flames, Report No. PURDU-CL-76-8, The Combustion Laboratory, Purdue University, October, 1976.

80. D. R. Pitts and L. E. Sissom, Heat Transfer, Schaum's Outline Series (McGraw-Hill Company, New York, 1977).

81. D. A. Bittker and V. J. Scullin, General Chemical Kinetics Computer Program for Static and Flow Reactions, with Application to Combustion and Shock Tube Kinetics, NASA TN D-6586 (1972).

82. F. L. Dryer and I. Glassman, Alternative Hydrocarbon Fuels: Combustion and Chemical Kinetics, Project SQUID, Progress in Astronautics and Aeronautics, Vol. 62, p. 295 (1977).

83. R. B. Edelman and O. F. Fortune, AIAA Paper 69-86, New York (1969).

84. E. M. Suuberg, W. A. Peters, and J. B. Howard, Seventeenth Symposium (International) on Combustion, The Combustion Institute (1979).

ACKNOWLEDGEMENT

The author would like to express his gratitude to everyone who had a hand in this project; if any participant has been inadvertently omitted, his contribution was nonetheless appreciated. For their assistance in various stages of the design and construction of the combustion chamber, recognition is due Dr. Piyawat Boon-Long and Messrs. Kyle Garrett and Steve Vaughn. The help of Messrs. Dave Rencher, Marc Elkins, and Gary Bultman in collecting the data and Jayaram Polavarapu and Galen King in analyzing the gas samples was greatly appreciated. Mr. Kou-John Hong provided aid in using the NASA-Lewis code. The contribution of Mr. Bill Starr, who maintained the equipment and provided troubleshooting support cannot be neglected.

Superb technical assistance, suggestions, and discussions provided by Professors Tom Lester and Fred Merklin were of particular value throughout the project. The guidance and support offered by Dr. Lester, the author's major professor, was instrumental in the success of the endeavor.

Special thanks are extended to Vibra-Screw Inc. for providing the feeder. The inconspicuous but vital contributions of Shelly Kemnitz and Merna Brisbin, who typed the manuscripts, and Greg Lancellotti, who performed the drafting work, are gratefully acknowledged.

The author wishes to express his gratitude for the consistent support of his parents, Mr. and Mrs. Robert L. Nelson. Finally, an inestimable amount of credit is due the author's wife, Kathy, for her love, encouragement, and uncanny ability to occupy herself with various diversions during the long hours the author was engaged with the project.

APPENDIX A

Application of NASA-Lewis Chemical Kinetics Code to Combustion Conditions in the Furnace

As mentioned in Section 1.2, the calculation of furnace parameters in a coal flame is most difficult. In a departure from the standard approach, an available general chemical kinetics code was employed to estimate the particle burnout time and, most importantly, the residence time of a slug of gas in the furnace.

A.1 NASA-Lewis Chemical Kinetics Code

The chemical kinetics code employed to simulate the combustion reactions in the furnace was developed by Bittker and Scullin[81]. A complete description of the program is beyond the scope of this work, but the following paragraphs provide an adequate explanation for the purposes of this study.

The program mentioned above is designed to compute the conditions in a wide range of reactor configurations including reaction behind a shock wave, ignition and combustion reactions in a static or flowing system, combustion and nozzle expansion, and general reaction in a static system or one dimensional frictionless flow. The user provides a list of the desired reactions along with the corresponding pre-exponential factor, temperature dependence, and activation energy for each reaction. The input concentration of each component, initial temperature, velocity, flow area, and pressure are also specified by

the user. (As an alternative to pressure, the programmer may specify either mass flow rate or density.) Other input options are listed in detail in the program user's manual[81].

After reading the input, the program establishes a set of differential equations characterizing the specified equations. Integration over the desired variable (either time or distance) is accomplished by using an implicit integration scheme. A compilation of all species present and their concentrations and net formation rates along with the physical characteristics of the system is printed at each of the print stations specified by the programmer. By comparing the output at successive steps, the reaction's progress can be followed.

A.2 Input Specifications

A quasi-global modelling approach was taken in this study. The term "quasi-global" is that employed by Edelman and Fortune[83] and implies an initiation step from the parent hydrocarbon generally to CO and a series of elementary reactions always including the "wet" carbon monoxide and hydrogen/oxygen reaction shcemes. The elementary reactions employed are taken from Dryer and Glassman[82] and Mulchay and Smith[21], and are listed in Table A1 as reactions (A-1) through (A-13).

The first reaction, the oxidation of solid carbon to CO and O is a most complicated step and can be approximated in only the most crude fashion by reaction (A-1). Insofar as rate data for carbon and coal reactions are given usually in a form incompatible with the program input, a transformation was required.

Table A-1. Elementary Reaction Rate Data for Combustion Reactions Employed in This Study. ($k_f = AT^n \exp(-E/RT)$).

Eq. #	Reaction	A*	n	E/R*	Source
A-1	$C(S) + O_2 \rightarrow CO + O$	$3.89 - 7.793 \times 10^{11}$	0	1.797×10^4	21
A-2	$CO + OH \rightarrow H + CO_2$	5.6×10^{11}	0	$.543 \times 10^3$	82
A-3	$CO + O_2 \rightarrow CO_2 + O$	3.0×10^{12}	0	25.0×10^3	82
A-4	$H_2 + O_2 \rightarrow OH + OH$	1.7×10^{13}	0	24.7×10^3	82
A-5	$OH + H_2 \rightarrow H_2O + H$	2.19×10^{13}	0	2.59×10^3	82
A-6	$OH + OH \rightarrow O + H_2O$	5.75×10^{12}	0	$.393 \times 10^3$	82
A-7	$O + H_2 \rightarrow H + OH$	1.74×10^{13}	0	4.75×10^3	82
A-8	$H + O_2 \rightarrow O + OH$	2.24×10^{14}	0	8.45×10^3	82
A-9	$CO + O + M \rightarrow CO_2 + M$	1.8×10^{19}	-1	2×10^3	82
A-10	$O + H + M \rightarrow OH + M$	1.0×10^{16}	0	0	82
A-11	$O + O + M \rightarrow O_2 + M$	9.38×10^{14}	0	0	82
A-12	$H + H + M \rightarrow H_2 + M$	5.0×10^{15}	0	0	82
A-13	$H + OH + M \rightarrow H_2O + M$	1.0×10^{17}	0	0	82

* Units: cm, mole, sec for A and cal, mole, K for E.

Mulcahy and Smith[21] give the following expression for the rate constant under conditions of chemical control;

$$R = 8.71 \times 10^3 \, p_{O_2} \exp(-35,700/RT) \qquad \text{(A-14)}$$

where p_{O_2} is the partial pressure of oxygen in atmospheres and the units on R are $g/cm^2 \cdot sec \cdot atm\ O_2$. The units for the rate constants given by Dryer and Glassman[82] are in cm, mole, sec, the exact form dependent upon the order of the reaction. It it is assumed that oxygen can be characterized as an ideal gas, then the ideal gas equation of state yields the conversion factor

$$\frac{n}{PV} = \frac{1}{RT} = 9.58 \times 10^{-6} \quad \frac{mol}{cm^3 \cdot atm\ O_2} \quad , \qquad \text{(A-15)}$$

the inverse of which can be multiplied by Eq. (A-14) to give

$$R = 9.092 \times 10^8 \, p_{O_2} \exp(-35,700/RT). \qquad \text{(A-16)}$$

In order to convert from the units of Eq. (A-16) which are $g \cdot cm/mol \cdot sec$ to $cm^3/mol \cdot sec$, a quantity with the units cm^2/g, the area to mass ratio of a particle, must be multiplied by Eq. (A-16). That ratio is given by

$$\frac{A}{m} = \frac{4\pi R^2}{4\pi R^3 \rho/3} = \frac{3}{\rho R} \quad , \qquad \text{(A-17)}$$

where R is the initial particle radius, and the density of coal particles is taken to be about $1.4\ g/cm^3$ [15]. If we assume that burnout is chemically controlled, then it follows that diffusion of oxygen into the coal particle may occur, and we can safely assume that burnout occurs at constant diameter with reducing density. The density during

combustion will vary from 1.4 to 0 g/cm^3, with the average density being 0.7 g/cm^3. Note that the same results would be given by Eq. (A-17) if constant density and reducing diameter were assumed. In order to eliminate the partial pressure of oxygen found in Eq. (A-16), and insofar as Eq.(A-14) fits most experimental observations only to within a factor of 2, the pre-exponential factor of Eq. (A-17) was reduced by a factor of two, giving

$$\frac{A}{m} = \frac{3}{\rho 2R} = \frac{3}{\rho D} \qquad \text{(A-18)}$$

where D is the initial particle diameter. For particles with diameters of 50 and 100 μm, Eq. (A-18) gives area to mass ratios of 857.14 and 428.57 cm^2/g, respectively. Multiplying these values by Eq. (A-16), the pre-exponential factors for the two particle sizes are found to be 7.793×10^{11} and 3.89×10^{11} cm^3/mol·sec, which have the desired units for use in the program. These values are comparable in magnitude to the pre-exponential factors for most second order equations, and were thus judged acceptable for input to the code.

The runs for this study used the code's distance-area version and the area was set equal to a constant value of 272.6 cm^2 which is the flow area of the furnace. The input compositions corresponded to a stoichiometric cloud of coal dust in air with pressure equal to 1 atm, temperature equal to 1000K, and flow velocity of 59.4 cm/sec. These were the calculated conditions when feeding 4.93 g/sec of Kansas coal to the furnace. The mole fractions of each input species were given by: C = 0.1339, O_2 = 0.1726, H_2 = 0.0609, H_2O = 0.0026, N_2 = 0.6300.

The nitrogen was assumed to be an inert species and all third body efficiencies were set equal to 1. The initial temperature corresponded to the temperature, as observed by Suuberg, et al[84] at which significant devolatilization occurs for several bituminous coals.

The parameters guiding the integration scheme were not specified; hence, the default values provided by the program were employed. These allowed for a minimum step size of 1×10^{-4} cm, a maximum step size of 0.1 cm, an initial step size of 1×10^{-4} cm, and a maximum relative error of 1×10^{-4}. The error criterion utilizes information from the two previous iterations to estimate the optimum step size possible without exceeding the specified error limit. This is reportedly a more efficient process than the standard doubling and halving method of estimating the optimum step size.

A.3 Results

For particle sizes of 50 and 100 μm, the profiles of O_2 and CO_2 concentration, temperature, carbon mass fraction, and coal particle diameter are depicted in Figs. A-1 and A-2. From Fig. A-1, it is seen that burnout (arbitrarily defined as the position where the particle diameter is reduced to 2.5% of the original diameter) occurs about 20cm into the furnace when 50 μm particles are introduced and about 40 cm for 100 μm particles. These predictions were found to be inconsistent with experimental observations from this study, but comparison with the results of Howard[9] showed good agreement. The coal used by Howard was sized such that about 90% by weight was contained in particles with diameters of 100 μm or less. He observed particle burnout times of

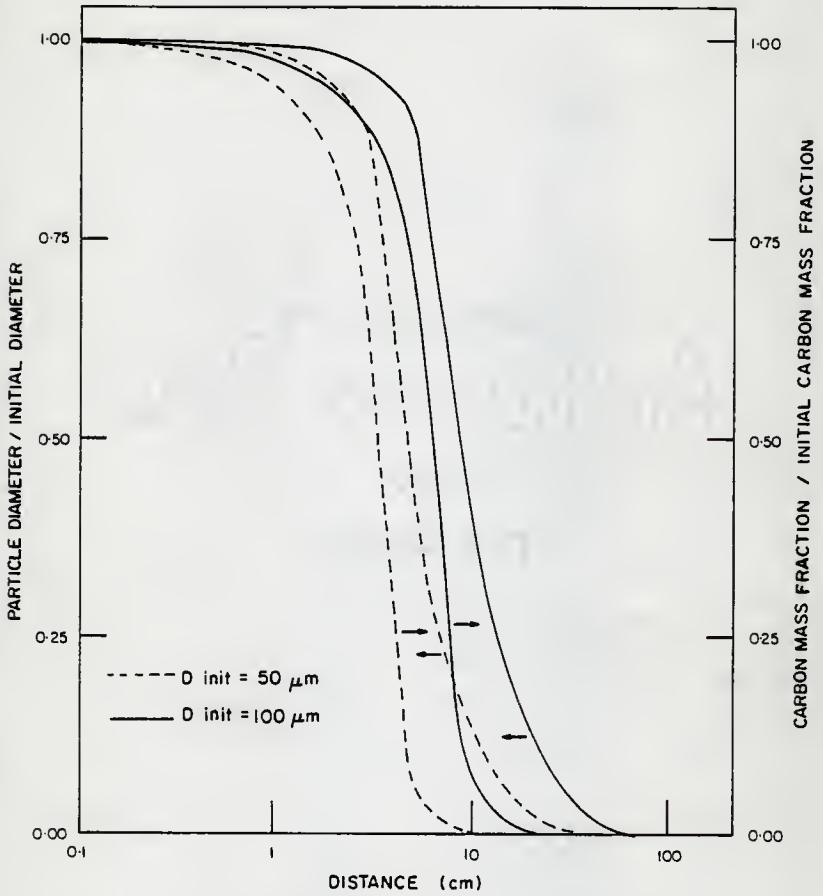

FIGURE A-1 EFFECT OF INITIAL PARTICLE SIZE ON CARBON MASS FRACTION AND PARTICLE DIAMETER

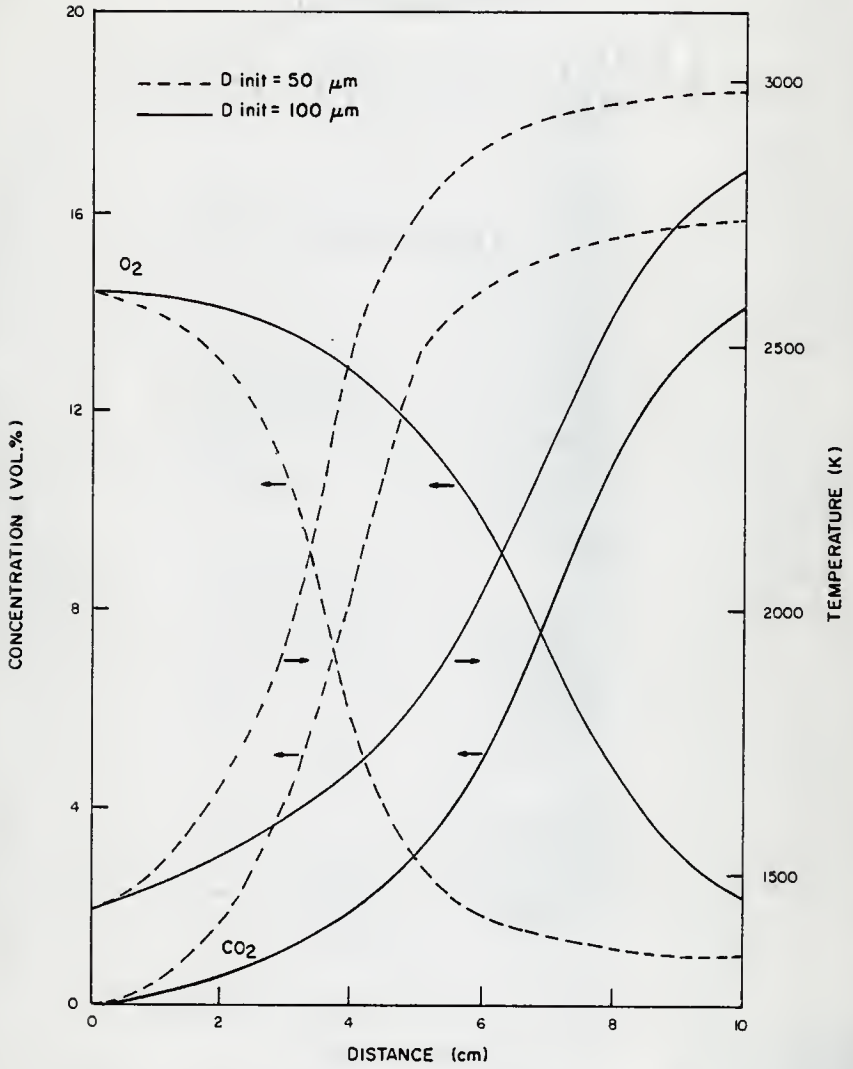

FIGURE A-2 EFFECT OF INITIAL PARTICLE SIZE ON TEMPERATURE AND O_2 AND CO_2 CONCENTRATIONS

between .5 and .8 sec. The model employed in this study predicted burnout times of about .3 to .5 sec. Since the model did not account for heat loss to the furnace walls and assumed that the reactants were introduced at elevated temperature (1000 K), the model is seen to be a surprisingly good approximation of plug flow reactors.

Inasmuch as probing of the solid matter from the flame region was not attempted in this study, comparison of experimental burnout times with the results of Howard[9] is difficult. However, visual observations showed that luminous particles were still present at the bottom of the combustion chamber, about 200 cm below the burner. This observation can be explained in two ways. First, at the temperatures encountered in the combustion chamber, the chemical reaction rate is so high that the reaction becomes diffusionally controlled; hence, the reaction proceeds at a rate slower than that predicted by the model, which assumes chemical control. Second, the luminous particles may not be coal particles undergoing oxidation, but may be high temperature ash particles.

Howard also showed burnout concentrations of O_2 and CO_2 of about 3% and 14%, respectively. These are in excellent agreement with the experimentally observed values of 1-2% and 15%, and with the predicted values of 1% and 16%.

Although the burnout time predictions were unrealistic for this study, the model was still very useful in that it produced an estimate of the velocity profile vs. distance, from which an approximation of the particle residence time in the furnace was obtained. The two cases previously mentioned yielded an estimated residence time of about 1.3 s.

According to Fig. 3, this time would be adequate for complete burnout of initial particle sizes of between 100 and 10,000 μm. However, this is based on reaction at 1500 C[16]. Thus, the heat up time of the particles must be accounted for. One of the predictions shown in Fig. 4 estimates a 1 s burnout for particles of about 100 μm, which is more in line with the results of this investigation.

APPENDIX B

Gas Analysis

Analysis of the gaseous combustion products was accomplished in three ways. The NO_x concentration was determined by employing the wet chemical Saltzman method, SO_2 by a second wet chemical detection technique, and the remaining gases (O_2, CO, and CO_2) via gas chromatography. Details of the three schemes are set forth in the following three sections.

B.1 Saltzman Method

The technique used in this investigation for the quantitative determination of NO_x emissions is the Broering modification of the Greiss-Saltzman procedure[67], which was derived from the method developed by Saltzman[68] for the detection of small amounts of NO_2 in air. The modification provides for the measurement of higher concentrations and the detection of NO; whereas the original procedure was designed for only NO_2 detection. The principle of the technique involves the absorption of the sample gas by a liquid phase reagent which turns from a transparent state to a red color upon the absorption of NO_2. The degree of the color change is proportional to the NO_2 concentration and can be accurately determined through the use of a spectrophotometer or colorimeter. Detection of NO is accomplished by allowing sufficient time for the oxygen in the sample gas to oxidize the NO to NO_2.

The reagents employed in the determination must be made from analytical grade chemicals in nitrite-free water prepared by redistilling distilled water in an all-glass still after adding a crystal each of

potassium permanganate and barium hydroxide. They are stable for a few weeks if stored at room temperature, but their life may be extended by storing them in dark bottles and refrigerating them. The absorbing reagent is produced by dissolving 5 g. sulfanilic acid in 945 ml of distilled water and 5 ml of glacial acetic acid. After the sulfanilic acid has dissolved, 50 ml of the dye stock solution is added and the reagent is diluted to 1 l. with distilled water. The reducing effect of SO_2, which prevents oxidiation of the NO to NO_2 in the samples, may be nullified by the addition of 1% of acetone to the absorbing reagent. The dye stock solution is prepared by dissolving 0.1 g. of N-(1-Naphthyl)-ethylenediamine dihydrochloride in 100 ml of distilled water. The standardizing reagent is made by dissolving .0218 g of sodium nitrite in 1 l. of distilled water.

Two calibration techniques are widely used; the one utilized in this study was the indirect calibration with sodium nitrite solution. The calibration curve was obtained by diluting various amounts of the standardizing reagent to 25 ml with absorbing reagent. For instance, 1 ml of the sodium nitrite solution in 24 ml of the absorbing reagent is equivalent to an NO_2 concentration of 0.4 µl NO_2 per ml of absorbing reagent. A plot of absorbance vs. 1 NO_2 per ml of absorbing reagent is made using the calibration samples and employed in determination of the amount of NO_x in the gas samples. A new calibration curve was produced for each set of samples to account for any absorption efficiency loss of the reagent. The other popular calibration technique consists

of reacting the absorbing reagent with known amounts of NO and constructing a calibration curve from these results.

The Saltzman method of determination is amenable to either the sampling of gas over a long period of time such as with an impinger or a batch sampling procedure. In this case, batch sampling was executed with either 5 or 10 cc gas samples being injected into 25 ml vials containing 10 ml of the absorbing reagent. The vials were stored for several hours to allow oxidation of NO to NO_2 and subsequent absorption of the NO_2.

The actual measurement of the color change was accomplished by comparing the absorbance at 550 nm of an exposed portion of the absorbing reagent to a fresh sample. A Cary model 14 recording spectrophotometer was employed for the measurements and construction of the calibration curves. Using the calibration curve as a guide, each sample was correlated to the NO_x concentration, M, with units of µl NO per ml absorbing reagent. Conversion to ppm NO_x was then effected via the relation

$$\text{ppm } NO_x = \frac{V_r M}{V_s} (1000) \frac{T}{294} \frac{76.0}{P} \qquad \text{(B-1)}$$

where,

V_r = volume of absorbing reagent, ml,

V_s = volume of sample, ml,

T = temperature at syringe when pulling sample, K,

P = barometric pressure, cm of Hg.

B.2 SO_2 Wet Chemical Analysis

The wet chemical technique exercised for the determination of SO_2 levels was developed by West and Gaeke[69]. The particular procedure used accounts for the interference of oxidants in the gas sample through the introduction of additional chemicals and by allowing time before detection for some oxidants to decay[70]. The principle behind this method consists of the formation of a dichlorosulfitomercurate complex by bringing the gas sample into contact with a solution of potassium tetrachloromercurate (TCM). The concentration of SO_2 in the gas directly affects the pH of the final solution and a pH indicator added to the solution provides the color which is measured by a spectrophotometer.

The reagents for the SO_2 wet chemical method must be ACS analytical reagent grade and the distilled water must be free from oxidants and preferably double distilled. The absorbing reagent is formed by dissolving 10.86 g of mercuric chloride (CAUTION: highly poisonous), 5.96 g of potassium chloride, and 0.066 g of ethylene diaminetetraacetic acid disodium salt (EDTA) in distilled water and diluting to 1 l. The EDTA is added to complex heavy metals that may interfere by oxidation of the SO_2 before formation of the dichlorosulfitomercurate. An absorbing reagent pH of less than 5.2 may result in poor collection efficiency and is usually caused by one of two problems. If the ratio of $HgCl_2$ to KCl is incorrect, the pH can be adjusted by addition of a dilute solution of KCl. If the EDTA is not the disodium salt, the dropwise addition of dilute alkali will raise the pH. The absorbing reagent is stable for

six months, but should be discarded if a precipitate forms. A solution of 0.6% sulfamic acid is prepared by dissolving 0.6 g of sulfamic acid in 100 ml of distilled water. This solution is used to destroy the nitrite anion during detection and may be kept for several days if protected from air.

Pararosaniline reagent is prepared by adding 20 ml of purified stock pararosaniline reagent (and an additional 0.2 ml of stock for each percent the stock assays below 100 percent) to 25 ml of 3M H_3PO_4 and diluting to 250 ml with distilled water. The assay procedure for the stock as well as a source of purified stock are covered in Ref. 70. The pararosaniline reagent is stable for at least 9 months. A 0.2% solution of formaldehyde must be made daily by diluting 5 ml of 40% formaldehyde to 1 l. with distilled water. Pararosaniline, formaldehyde, and the bisulfite anion react to form the intensely colored pararosaniline methyl sulfonic acid.

A 0.01N iodine solution is prepared by dissolving 0.0127 g of iodine and 0.04 g of potassium iodide in distilled water and diluting to 1 l. Trituration of 0.4 g of soluble starch and 0.002 g of mercuric iodide with a little water and slow addition of the paste to 200 ml of boiling water forms a starch indicator solution. The boiling is continued until clear and the solution is transferred to a glass-stoppered bottle after cooling. The iodine and starch indicator solutions are used in the preparation of the standardizing solutions.

A standard 0.1 N sodium thiosulfate solution is produced by dissolving 25 g of sodium thiosulfate ($Na_2S_2O_3 \cdot 5H_2O$) in 1 l. of

deaerated double distilled water and adding 0.1 g of sodium carbonate. The solution is allowed to stand for one day before standardizing. To standardize, 1.5 g of potassium iodate is dissolved and diluted to 500 ml. To 50 ml of the iodate is added 2 g of potassium iodide and 10 ml of a 1:10 dilution of concentrated hydrochloric acid. The flask is stoppered for five minutes, then titrated with thiosulfate to a pale yellow color. After the addition of 5 ml of starch indicator solution, the titration is completed. The normality of the thiosulfate solution (N) is then given by

$$N = \frac{W}{V_t} \frac{10^3 \cdot 0.1}{35.67} \qquad \text{(B-2)}$$

where W is the weight of the KIO_3 (g) and V_t is the volume of titer used in the titration (ml).

The standard sulfite solution is prepared by dissolving 0.300 g of sodium metabisulfite in 500 ml of deaerated double distilled water. The concentration of SO_2 in this solution is determined by titrating against the sodium thiosulfate solution. Into each of two 500 ml flasks, 50 ml of the 0.01 N iodine solution is placed. To flask A (blank) 25 ml of distilled water is added and to flask B (sample) is added 25 ml of the standard sulfite solution. The flasks are stoppered for five minutes and then titrated to a pale yellow color with the thiosulfate solution. The titration is completed after addition of 5 ml of starch solution to each flask. The concentration of sulfur dioxide in the standard sulfite solution is calculated by

$$SO_2 \left(\frac{\mu g}{ml}\right) = \frac{(A-B)\ NK}{V}\ , \qquad (B-3)$$

where

A = ml of titer required for blank,

B = ml of titer required for sample,

N = normality of thiosulfate solution,

K = micro equivalent weight (32,000 μg for SO_2)

V = sample volume taken (ml).

The standard sulfite solution is unstable. Immediately after titration, 2 ml of the standard solution is diluted to 100 ml with 0.04 M TCM. The dilute sulfite solution is stable for 30 days at 278 K.

Collection of the gas samples for SO_2 analysis was identical to the collection of NO_x samples, with 5 cc portions being injected into vials containing 10 ml of the 0.04 M TCM absorbing reagent. The reagent was protected from sunlight to prevent deterioration and analysis was performed after several hours to coincide with the NO_x measurements.

The exposed samples were transferred to 25 ml volumetric flasks for analysis using about 5 ml of distilled water for rinsing. A reagent blank was prepared by adding 10 ml of unexposed absorbing reagent to a 25 ml volumetric flask. To each of the flasks, 1 ml of 0.6 percent sulfamic acid was added and 40 minutes was allowed for destruction of the nitrite from NO_x. The original method called for a wait of 10 minutes, but Polavarapu[57] discovered that a 40 minute allowance eliminated the oxidizing effect of NO_x on the SO_2. Then 2 ml of the 0.2 percent formaldehyde and 5 ml of the pararosaniline reagent was added to each

flask. All flasks were brought to volume with deaerated distilled water and left for 30 minutes. After the 30 minutes, the absorbance of each sample against the reagent blank was determined at 548 nm using the Cary model 14 recording spectrophotometer.

The calibration procedure comprised diluting graduated amounts of the dilute sulfite solution to about 10 ml with fresh absorbing reagent. The additional reagents mentioned in the analysis procedure were added and the absorbance was measured. A plot of absorbance against total micrograms of SO_2 was produced and employed in relating the absorbance of the samples to the SO_2 content. For SO_2, only one calibration curve was required for each batch of absorbing reagent.

The concentration of SO_2 in the sample gas was determined by calculating a calibration factor (B, g/absorbance unit) equal to the reciprocal of the slope of the calibration curve. The concentration was then given by

$$\text{ppm } SO_2 = \frac{AB}{V}\, 0.382, \qquad \text{(B-4)}$$

where

A = the sample absorbance,

0.382 = the volume (µl) of 1 µg SO_2 at 278 K, 76 cm Hg (STP),

V = sample volume (l) corrected to STP by PV = nRT.

B.3 Analysis of Permanent Gases

Analysis of other gases was required to make a check on the combustion process and to provide for an oxygen dilution correction factor. An F&M model 700 gas chromatograph with a thermal conductivity

detector was used to determine the levels of O_2, CO, and CO_2. A Carbosieve S column was employed with a helium carrier gas maintained at a pressure of 445.9 kPa (50 psig). Determination of the concentrations was aided by comparison with a canned sample gas containing 5.13% O_2, 7.23% CO, and 15.0% CO_2 in N_2. The detection of the gases was obtained in two steps. At a column temperature of 45°C, the output was useful for analyzing the O_2 and CO contents, but the retention time for CO_2 was too great to allow its detection. A sample chromatogram at 45°C is shown in Fig. B-1. At a column temperature of about 160°C the CO_2 was detected, but there was no resolution between N_2 and O_2, and very little between N_2 and CO. A sample chromatogram at 160°C is depicted in Fig. B-2. Running each sample at both temperatures allowed quantitative determination of all three gases.

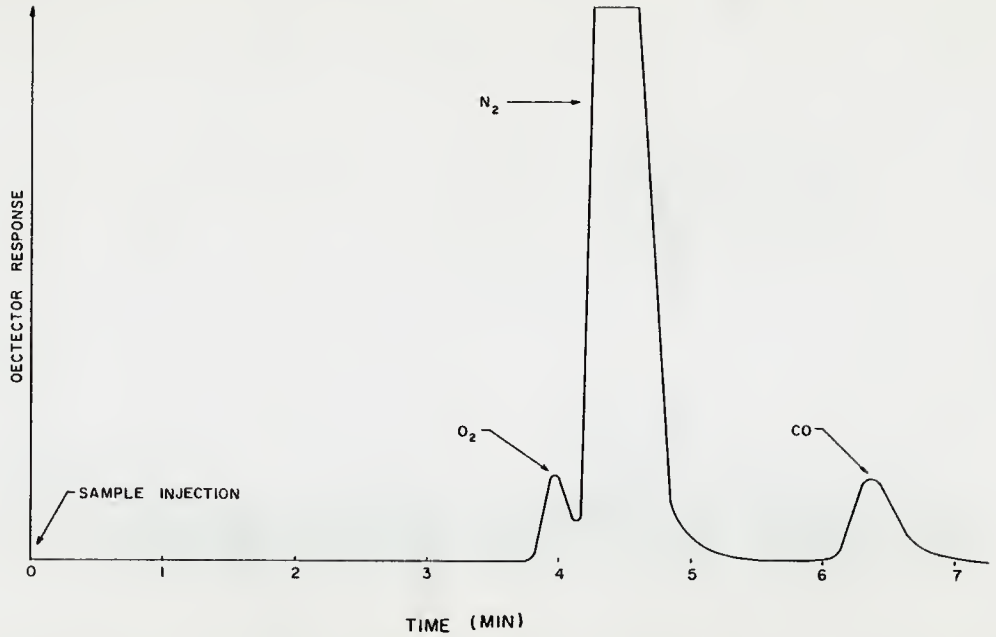

FIGURE B-1 GC SAMPLE OUTPUT AT 45°C

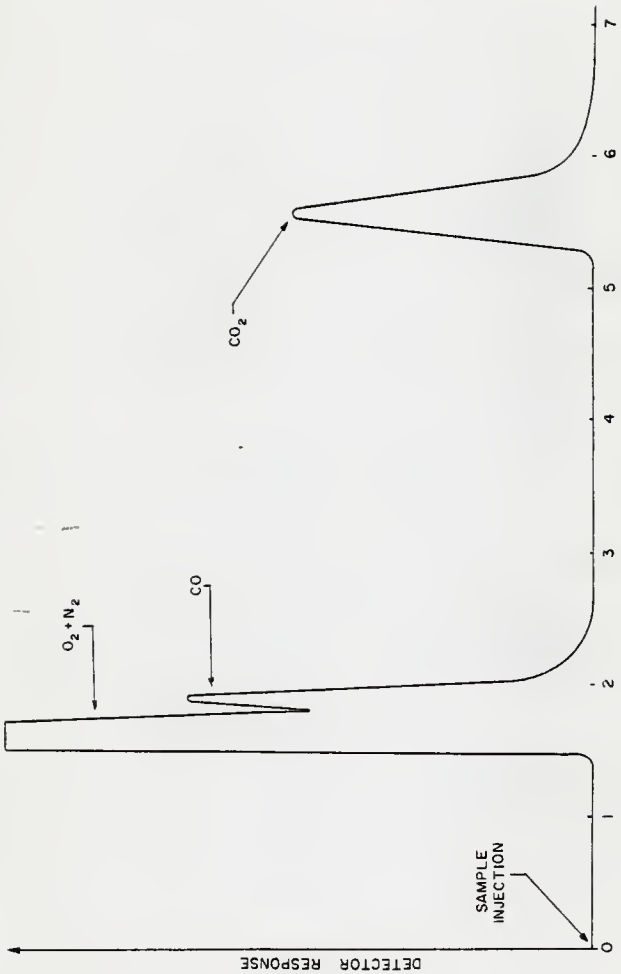

FIGURE B-2 GC SAMPLE OUTPUT AT 160° C

APPENDIX C

Flame Safeguard Unit

The flame safeguard unit diagrammed in Fig. C-1 acts as a breaker in the power supply to the systems supplying fuel to the furnace. Line voltage is applied initially through the POWER switch on the control panel, through two other safety cutoffs, through the FLAME SAFEGUARD switch on the control panel, and to terminals 1 and 6 of the unit. The unit has a total of 10 terminals. Terminal 2 grounds the unit, while 1 and 6 provide the power for the safeguard. The two terminals marked T are connected to each other and F and G accommodate the leads from the ultraviolet flame detector. These can be denoted signal terminals, and they enable other terminals whenever T and T are connected and the proper signal (corresponding to a flame in the detector's line of sight) is fed to F and G. The remaining terminals, 3, 4, and 5, are output terminals, but the signal timing at each is not identical.

Terminal 3 accommodates the leads for the pilot gas and pilot air solenoid valves and is at ground except when the unit is enabled or in the startup mode. Terminal 4 is attached only to the pilot assembly ignition transformer and is held at ground except during startup. Terminal 5 supplies line voltage to the main gas supply line solenoid valve and to a solenoid actuated relay that controls the application of the 220 V., three phase power for the feeder. This terminal is closed to line voltage only when the flame safeguard is enabled. Each of the circuits mentioned has a separate switch on the control panel so that in addition to the flame safeguard, manual control is also required.

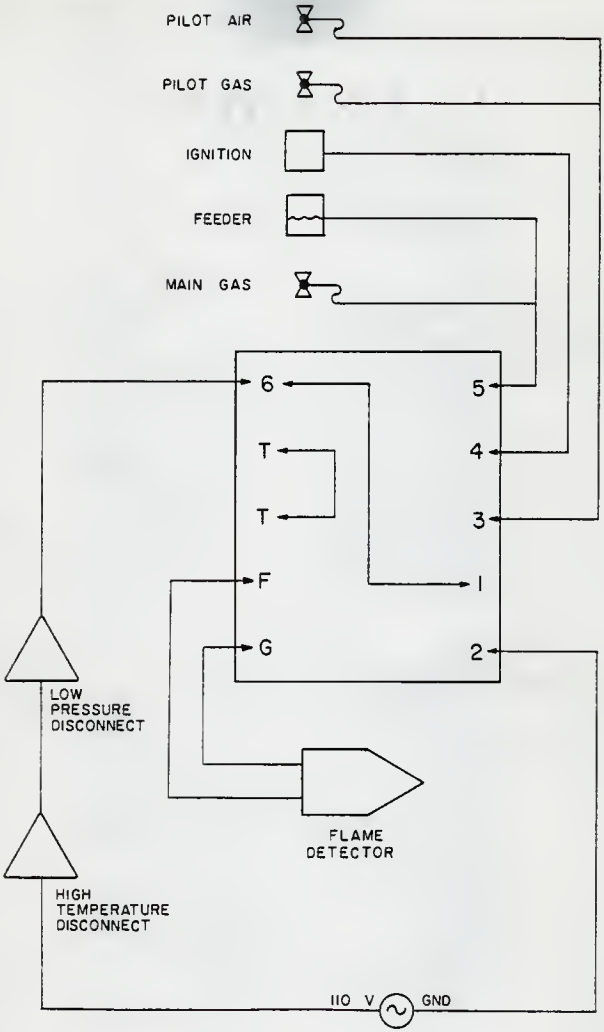

FIGURE C-1 FLAME SAFEGUARD SYSTEM

As indicated above, there are two operational modes for the flame safeguard unit. When the proper signals appear at the input terminals and power is applied at terminals 1 and 6, the unit is in the enabled mode. If no flame is present, but a manual signal is received, (either by turning on the power to the unit or operating the unit's RESET button) the unit is in the startup mode. The enable state is a steady state which remains until some external impetus is received, i.e., either the power to the unit is disconnected or a required signal is lost. The startup mode is finite and lasts only as long as a self contained thermistor's resistance is below a certain level or a signal is received at terminals F and G. If the thermistor's resistance exceeds the limit, the RESET button pops out and breaks the connection of line voltage to terminals 1 and 6. If a flame is achieved, i.e., a signal is received at F and G, the unit automatically enters the enabled mode.

During startup, power is applied to the pilot gas, the pilot air, and the ignition transformer. As soon as the pilot flame lights, the flame detector signals the flame safeguard which shuts down the ignition transformer and applies line voltage to the main gas line and feeder. Under normal operation, the manual switches for these two systems are kept open until the pilot is lit. Then, the main gas switch is closed to light the gas flame or the feeder is started to ignite the solid fuel flame. Since these are activated in the enable mode, this continues until either the flame is extinguished or the system is manually shut down.

APPENDIX D

Numerical Approximation of Heat Flux Through The Furnace Walls

In order to estimate the heat loss from the furnace during operation, a computer code was developed from which determinations could be made of the heat flux and temperature profile in the wall, based on the inside and outside wall temperatures. Originally, it was intended that the bulk gas temperatures inside and outside the furnace would be specified as boundary conditions in order that convection heat transfer could also be included. However, the difficulty of determining the convective heat transfer coefficients at the respective solid-gas interfaces provided the impetus for using experimentally observed wall temperatures as the boundary values.

The initial step taken in developing the code was to determine the thermal conductivities of the wall strata. The firebrick thermal conductivity was set equal to 1.21 W/m^2k since this figure is intermediate between the values listed for various types of firebrick by Pitts and Sissom[80]. The firebrick thermal conductivity and two experimentally observed temperatures (at two separate points in the firebrick) were used to yield the heat flux through the brick using the finite difference approximation to Fourier's law,

$$q'' = k \frac{\Delta T}{\Delta x} \quad , \qquad \text{(D-1)}$$

where

q'' = heat flux, W/m^2 ;

k = thermal conductivity, W/mK ;

ΔT = temperature difference across Δx, K ;

Δx = distance between points of analysis, m.

The thermocouple readings, taken during a steady state run firing natural gas, showed a temperature difference of 194 K over a distance of .048 m in the firebrick. From Eq. (D-1), the heat flux was found to be 4906 W/m^2 at the inside wall.

Inasmuch as the thermal conductivities of the insulation layers were not known and air gaps of various sizes were present in the walls, the outer strata of the wall were consolidated and considered as a single layer for the purpose of the program. The inside boundary temperature was found by extrapolating the firebrick temperature profile to the interface and the outside temperature was experimentally observed. The law of conservation of energy at steady state required that the heat flux through the consolidated layer was equal to

$$q'' = q_1'' \frac{A_1}{A_2} \qquad \text{(D-2)}$$

where

q_2'' = heat flux through consolidated layer, W/m^2;

q_1'' = heat flux through firebrick, W/m^2 ;

A_1 = average heat transfer area of firebrick layer, m^2 ;

A_2 = average heat transfer area of consolidated layer, m^2.

Since the thickness of the outer layer was known, the temperature difference, heat flux, and thickness were inserted in Eq. (D-1) to yield a consolidated layer thermal conductivity of $k = 0.233\ W/m^2K$.

The second step in the development consisted of setting up the proper finite difference equations and dividing the furnace wall into a network of control zones, each characterized by a node at the center

of the zone. The problem was taken to be two-dimensional by neglecting heat transfer in the direction parallel to the furnace axis. The system was further simplified by considering only a symmetrical section of the furnace. Insofar as the furnace had two axes of symmetry (the corner line and the wall centerline), the section was taken as one eighth of the furnace comprising that region from one corner to the centerline of one wall. The actual dimensions of the section were 0.197m x 0.083m x 0.114m, denoting the outside wall length, inside wall length, and wall thickness, respectively. In order to fit a reasonably sized grid spacing of 0.0127m, it was necessary to subtract 0.0064m from the wall length dimensions. This allowed the establishment of a grid system containing 92 nodes. The nodes were classified in several cases, as follows:

1) node in material interior,
2) node on furnace centerline,
3) node on cornerline,
4) node on interface of brick and consolidated layer,
5) centrline node at interface, and
6) cornerline node at interface.

The firebrick and consolidated layer thermal conductivities were denoted k_2 and k_1, respectively.

A double subscript notation was adopted to distinguish between nodes with the first subscript specifying distance normal to the inside wall and the second denoting distance parallel to the wall. A separate heat balance was performed for each of the six cases defined above. The analysis for the first case is outlined below and only the results for cases 2 through 6 are given.

Considering a unit length in the direction normal to the plane of the grid, Fourier's law was employed to give the heat transferred in to node i,j from the nodes surrounding it as

$$q_{i+1,j\to i,j} = k(T_{i+1,j} - T_{i,j})/\Delta \quad , \tag{D-3}$$

$$q_{i-1,j\to i,j} = k(T_{i-1,j} - T_{i,j})/\Delta \quad , \tag{D-4}$$

$$q_{i,j+1\to i,j} = k(T_{i,j+1} - T_{i,j})/\Delta \quad , \tag{D-5}$$

$$q_{i,j-1\to i,j} = k(T_{i,j-1} - T_{i,j})/\Delta \quad , \tag{D-6}$$

where Δ is the spacing between nodes. At steady state, the sum of Eqs. (D-3) through (D-6) must be equal to zero; hence,

$$T_{i+1,j} + T_{i-1,j} + T_{i,j+1} + T_{i,j-1} - 4T_{i,j} = 0. \tag{D-7}$$

Eq. (D-7) characterizes nodes satisfying the conditions for case 1. Cases 2 through 6 are handled by Eqs. (D-8) through (D-12).

$$T_{i+1,j} + T_{i-1,j} + 2T_{i,j+1} - 4T_{i,j} = 0 \tag{D-8}$$

$$T_{i+1,j} + T_{i,j-1} - 2T_{i,j} = 0 \tag{D-9}$$

$$\frac{2k_1}{k_1 + k_2} T_{i+1,j} + \frac{2k_2}{k_1 + k_2} T_{i-1,j} + T_{i,j+1} + T_{i,j-1} - 4T_{i,j} = 0 \tag{D-10}$$

$$\frac{k_1}{k_1 + k_2} T_{i+1,j} + \frac{k_2}{k_1 + k_2} T_{i-1,j} + T_{i,j+1} - 2T_{i,j} = 0 \tag{D-11}$$

$$\frac{2k_1}{3k_1 + k_2} T_{i+1,j} + \frac{k_1 + k_2}{3k_1 + k_2} T_{i,-1,j} - T_{i,j} = 0 \quad . \qquad \text{(D-12)}$$

The system of equations formed by using the proper equation at each of the 92 nodes developed a problem comprising 92 equations in 92 unknowns. The main program performed the task of setting up the array representing the system of equations. The actual solution was effected by subroutine SIMQ, which may be found in the IBM Scientific Subroutine Package. The main program then directed the output of the temperature profile.

Subroutine SIMQ solves the system of equations by employing a method of elimination using the largest pivotal divisor. Application of this scheme replaces the matrix of coefficients with a triangular matrix. The triangular matrix is easily solved since the last equation specifies a value for one variable and each previous equation adds only one variable.

Applying Eq. (D-1) to each node adjacent to either wall, estimates of the heat transferred into the wall from the combustion chamber and out of the wall to the room environment were obtained. These estimates showed that the heat transfer values in and out through the respective walls were equal to within about 1.5%. The furnace wall temperature profile for a run with inside wall temperature of 1200 C and outside wall temperature of 120 C is shown in Fig. D-1. The pages following the figure contain a listing of the main program described herein.

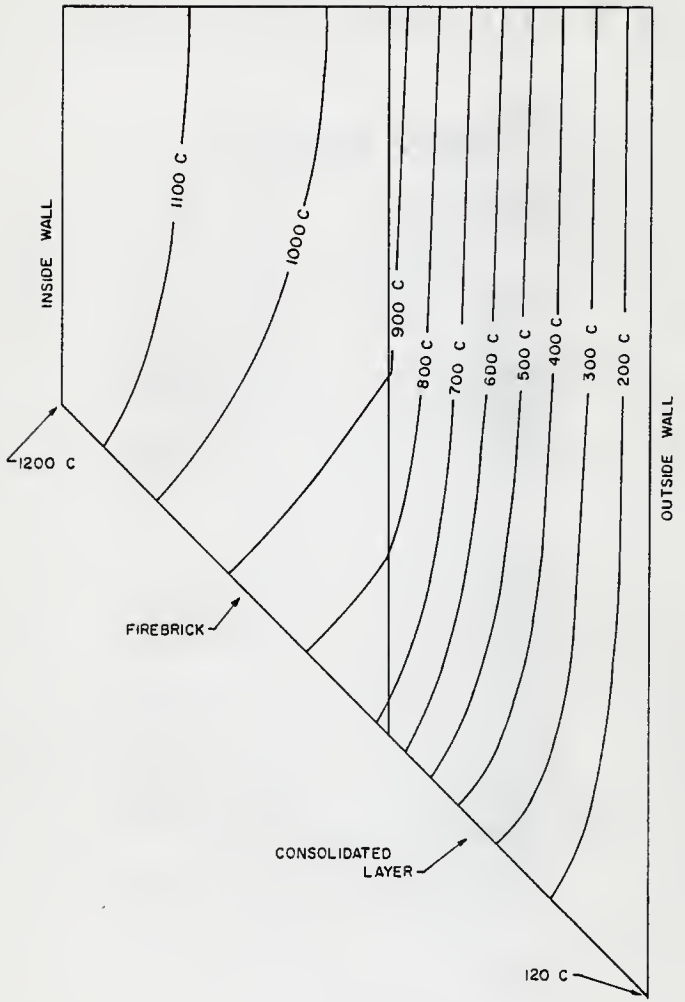

FIGURE D-1 COMPUTED ISOTHERMS IN FURNACE WALL

```
C
C           CALCULATION OF FURNACE WALL TEMPERATURE AND HEAT FLUX
C
C       THE MAIN PROGRAM SETS UP THE EQUATIONS AND HANDLES I/O.
C       SOLUTION OF THE SYSTEM OF EQUATIONS IS ACCOMPLISHED BY SIMQ.
C
C       SUBPROGRAMS REQUIRED:                    SIMQ
C
C       VARIABLES USED:
C            A = MATRIX OF COEFFICIENTS STORED IN COLUMN FORM
C            B = VECTOR OF CONSTANTS COMPRISING BOUNDARY VALUES
C
      REAL A(8464)/8464*0./,B(92)/92*0./
      N = 92
      TI = 1200.
      TO = 120.
      RK1 = .233
      RK2 = 1.21
      DEL = .0127
      DO 50 I=1,92
      A(92*(I-1)+I) = 1.
   50 CONTINUE
      A(737) = -.25
      A(93) = -.5
      B(1) = TI/4.
      DO 100 I=2,7
      A(93*I) = -.25
      A(92*(I-2)+I) = -.25
      A(92*(I+7)+I) = -.25
      B(I) = TI/4.
  100 CONTINUE
      A(560) = -.5
      A(1388) = -.5
      A(9) = -.25
      A(837) = -.5
      A(1573) = -.25
      DO 150 I=10,16
      A(93*I) = -.25
      A(92*(I-2)+I) = -.25
      A(92*(I+8)+I) = -.25
      A(92*(I-9)+I) = -.25
  150 CONTINUE
      A(1397) = -.5
      A(2317) = -.5
      A(2502) = -.25
      A(1674) = -.5
      A(754) = -.25
      DO 200 I=19,26
      A(93*I) = -.25
      A(92*(I-2)+I) = -.25
      A(92*(I+9)+I) = -.25
      A(92*(I-10)+I) = -.25
  200 CONTINUE
      A(3339) = -.5
      A(2327) = -.5
```

```
      A(3524) = -.25
      A(2604) = -.5
      A(1592) = -.25
      DO 250 I=29,37
      A(93*I) = -.25
      A(92*(I-2)+I) = -.25
      A(92*(I+10)+I) = -.25
      A(92*(I-11)+I) = -.25
  250 CONTINUE
      A(4434) = -.5
      A(3350) = -.5
      D1 = 2.*(RK1+RK2)
      A(4639) = -RK1/D1
      A(3627) = -.5
      A(2523) = -RK2/D1
      DO 300 I=40,49
      A(93*I) = -.25
      A(92*(I-2)+I) = -.25
      A(92*(I+11)+I) = -RK1/D1
      A(92*(I-12)+I) = -RK2/D1
  300 CONTINUE
      D2 = 3. *RK1+RK2
      A(3662) = -2.*RK1/D2
      A(4488) = -(RK1+RK2)/D2
      A(5847) = -.25
      A(4743) = -.5
      A(3547) = -.25
      DO 350 I=52,62
      A(93*I) = -.25
      A(92*(I-2)+I) = -.25
      A(92*(I+12)+I) = -.25
      A(92*(I-13)+I) = -.25
  350 CONTINUE
      A(6963) = -.5
      A(5875) = -.5
      A(7148) = -.25
      A(5952) = -.5
      A(4664) = -.25
      DO 400 I=65,76
      A(93*I) = -.25
      A(92*(I-2)+I) = -.25
      A(92*(I+13)+I) = -.25
      A(92*(I-14)+I) = -.25
  400 CONTINUE
      A(8337) = -.5
      A(6977) = -.5
      A(7254) = -.5
      A(5874) = -.25
      B(78) = TC/4.
      DO 450 I=79,91
      A(93*I) = -.25
      A(92*(I-2)+I) = -.25
      A(92*(I-15)+I) = -.25
      B(I) = TC/4.
  450 CONTINUE
      A(8372) = -.5
      B(92) = TC/2.
      CALL SIMQ(A,B,N,KS)
```

```
      IF(KS.EQ.0) GO TO 500
      WRITE(6,900)
      CALL EXIT
  500 WRITE(6,905)
      DO 550 I=1,7
      WRITE(6,901) TC,B(I+77),B(I+63),B(I+50),B(I+38),B(I+27),B(I+17),
     1     B(I+8),B(1),TI
  550 CONTINUE
      WRITE(6,901) TC,B(85),B(71),B(58),B(46),B(35),B(25),B(16),B(8)
      WRITE(6,901) TC,B(84),B(72),B(59),B(47),B(36),B(26),B(17)
      WRITE(6,901) TC,B(87),B(73),B(60),B(48),B(37),B(27)
      WRITE(6,901) TC,B(88),B(74),B(61),B(49),B(38)
      WRITE(6,901) TC,B(89),B(75),B(62),B(50)
      WRITE(6,901) TC,B(90),B(76),B(63)
      WRITE(6,901) TC,B(91),B(77)
      WRITE(6,901) TC,B(92)
      WRITE(6,901) TC
      HFI = 0.
      HFO = 0.
      DO 600 I=1,6
      HFI = HFI+RK2*(TI-B(1))/DEL
  600 CONTINUE
      HFIA = HFI/6.
      DO 650 I=78,91
      HFO = HFO+RK1*(B(I)-TC)/DEL
  650 CONTINUE
      HFOA = HFO/14.
      WRITE(6,902) HFIA,HFOA
      STOP
  900 FORMAT('1   SINGULAR SOLUTION')
  901 FORMAT(' ',10(F7.1,5X))
  902 FORMAT('-   AVG INSIDE HEAT FLUX, W/M**2 = ',E14.7,'AVG OUTSIDE HE
     1AT FLUX = ',E14.7)
  905 FORMAT('1')
      END
```

APPENDIX E

Quenching of Samples in the Gas Sampling Probe

To help the reader appreciate the extent to which probe cooling can affect the observed results, a sample calculation is presented in this Appendix. To identify certain initial and boundary conditions, the following assumptions will be made:

1) Complete combustion at stoichiometric conditions firing 2.27 m^3/hr of methane as measured at 300 K and 1 atm;
2) product gases enter the probe at 1533 K;
3) entrance to the probe is isokinetic, i.e., the velocity of the gases entering the probe is equal to the bulk gas velocity in the flue;
4) the product gases behave as an ideal gas mixture and their properties can be approximated by the properties of air at the same temperature;
5) the probe temperature remains constant at 283 K;
6) energy release by exothermic reactions in the probe does not affect the thermal or velocity profiles.

The complete combustion of 2.27 m^3/hr of methane generates 121.76 m^3/hr of products at 1533 K and atmospheric pressure. Since the flue's cross sectional area is 0.01 m^2, the flue gas velocity is found to be 3.32 m/s which, by assumption 3, is also the initial velocity in the cooling probe. The Reynolds number for the flow is thus given by

$$Re_D = \frac{VD}{\nu} = \frac{(3.32 \text{ m/s})(4.75 \times 10^{-3} \text{ m})}{(2.304 \times 10^{-4} \text{ m}^2/\text{s})} = 68.6 , \qquad \text{(E-1)}$$

where

V = gas velocity in the probe;

D = probe inside diameter;

ν = kinematic viscosity of the fluid,

which indicates that flow in the probe is laminar.

The enthalpy change of the gas must be equaled by the heat loss to the probe, or

$$mC_p \frac{dT}{dt} = hA\ (T_w - T)\ , \qquad \text{(E-2)}$$

where

m = mass of the fluid;

C_p = specific heat of the gas;

T = temperature of the gas;

T_w = temperature of the probe;

t = time;

h = convection heat transfer coefficient;

A = area through which heat is transferred.

Defining the variable θ as

$$\theta \equiv T - T_\infty\ , \qquad \text{(E-3)}$$

where T_∞ is the entrance temperature of the gas, Eq. (E-2) can be rewritten in the form

$$mC_p \frac{d\theta}{dt} = -hA\ (\theta - \theta_w)\ . \qquad \text{(E-4)}$$

Equation (E-4) can be rearranged and integrated to yield

$$\ln (\theta-\theta_w) = \frac{hAt}{mC_p} + C \ , \qquad \text{(E-5)}$$

where C is a constant of integration. At t=0 (the entrance to the probe) it must also be noted that $\theta=0$. Then Eq. (E-5) can be expressed as

$$\frac{\theta-\theta_w}{-\theta_w} = \exp\left(-\frac{hAt}{mC_p}\right) . \qquad \text{(E-6)}$$

Substituting Eq. (E-5) into (E-6), it is found that

$$T = T_w + (T_\infty - T_w) \exp\left(-\frac{hAt}{mC_p}\right) . \qquad \text{(E-7)}$$

The only unknown quantity in Eq. (E-7) is the convective heat transfer coefficient. In order to obtain a solution for the temperature behavior in the probe, h must be determined. The solution is best approached in two parts, one representing the entrance region of the probe where the velocity profile is developing, and the other covering the fully developed flow region.

The problem of heat transfer from a fluid in laminar flow through a tube with constant wall temperature was first solved in 1929 by Leveque. The procedure is detailed by Knudsen and Katz[73], from whom this development is taken. The Leveque solution is applicable in the range

$$100 < Pe\left(\frac{D}{X}\right) < 5000, \qquad \text{(E-8)}$$

where

Pe = Peclet number = $Pr \cdot Re_D$;

Pr = Prandtl number;

X = distance from the tube entrance.

The method yields a solution for h at any position in the tube with the result being given by

$$h = \frac{K}{0.893} \left(\frac{8\ V}{9D\alpha x}\right)^{1/3} \qquad \text{(E-9)}$$

where

k = thermal conductivity of the gas;

α = thermal diffusivity of the gas = $k/\rho C_p$;

ρ = gas density.

An average value for h over the region in which the solution is valid is obtained by integrating over the axial length; that is

$$\bar{h} = \frac{1}{L} \int_o^L h dx. \qquad \text{(E-10)}$$

Inserting Eq. (E-9) into (E-10) and integrating (assuming constant velocity) yields

$$\bar{h} = 1.62\ K \left(\frac{V}{D\alpha L}\right)^{1/3} . \qquad \text{(E-11)}$$

If an average temperature over the region is estimated and used to calculate an average velocity, Eqs. (E-11) and (E-7) may be employed to find the final temperature. The estimate of average temperature may then be updated and the procedure continued until the computed and estimated average temperatures coincide. Here it is estimated that at the end of the entrance region, the temperature of the fluid will be 1210 K. The average temperature is thus found to be 1372 K. At this temperature the gas velocity in the probe is

$$V_{1372} = \frac{1372}{1533} V_{1533} = 2.97 \text{ m/s} . \qquad \text{(E-12)}$$

Inasmuch as the Peclet number is required to determine the length of the entrance region, the Reynolds number must also be computed. The Reynolds number is found to be 72.7 which yields a Peclet number of 52.6. From Eq. (E-8) it is seen that the Leveque solution is valid from the entrance to x = 0.0025 m. Inserting this value for L into Eq. (E-11) gives a value of 127.5 W/m^2K for $\bar{h}$, which can be used in Eq. (E-7) to give

$$T = 283 + 1250 \exp(-346.8t) \qquad \text{(E-13)}$$

At the assumed average velocity, the time required for a particle to flow through the entrance region to x=L is found to be 8.4×10^{-4}s. Inserting this time into Eq. (E-13) yields the temperature at the end of the entrance region as 1217 K which is very close to the estimated value of 1210 K. Hence, a second iteration is not required.

The cooling rate in the entrance region of the sampling probe is then found by differentiating Eq. (E-13) with respect to time to yield

$$\frac{dT}{dt} = -4.34 \times 10^5 \exp(-346.8t) \text{ K/s.} \qquad \text{(E-14)}$$

The problem of heat transfer accompanying fully developed laminar flow in tubes is classified as the classical Graetz problem which is also detailed by Knudsen and Katz[13]. The boundary conditions are different since cooling occurred in the entrance region. The gases enter the fully developed flow region at a temperature 1217 K, and it is estimated that the gas temperature will approach the probe temperature long before reaching the end of the probe. Thus, the average temperature in the

range where cooling occurs is well defined, but the length of the cooling region must be determined via an iterative procedure.

From the classical Graetz solution, the mean Nusselt number (Nu_m) over a given range can be expressed as

$$Nu_m = 3.66 + \frac{0.0668\ [(x/D)/Pe]^{-1}}{1 + 0.04\ [(x/D)/Pe]^{-2/3}} \quad . \qquad \text{(E-15)}$$

Solution for the cooling rate in the fully developed region involves finding the length of the region by an iterative process mentioned above and solving Eq. (E-15) for Nu_m which can be used to find $\bar{h}$. Equation (E-7) is then differentiated to yield the cooling rate.

The average temperature in the fully developed flow region is found to be 750 K, which indicates an average velocity of 1.62 m/s. An estimate for the cooling length is taken as 0.16 m, and Eq. (E-15) then gives $Nu_m = 3.79$. The average value for the convection heat transfer coefficient is thus found to be $\bar{h} = 43.88\ W/m^2 \cdot K$. Inserting this value into Eq. (E-7) yields

$$T = 283 + 934 \exp(-72.3\ t)\ K/s \quad . \qquad \text{(E-16)}$$

Inasmuch as the cooling distance is assumed to be 0.16 m and the average velocity is taken as 1.62 m/s, the time for a particle to pass through the region is found to be t = 0.099 s. Using this value in Eq. (E-16) gives the temperature at the end of the cooling region as T = 283.7 K, which is very close to the probe wall temperature. Hence, an incrementation of the cooling region length is not required.

Differentiating Eq. (E-16) with respect to t yields an expression for the cooling rate in the fully developed flow regions, as follows.

$$\frac{dT}{dt} = -6.75 \times 10^4 \exp(-72.3\ T)\ K/s\ . \qquad \text{(E-17)}$$

Although developed for a shock tube analysis, the results of Tschuikow-Roux[74], who related the cooling rate in a shock tube to the amount of reaction that would occur during the cooling process, is of value in the present case. This relation is given by

$$\ln\left(\frac{N_i}{N_f}\right) = -A \exp(-E/Rt_\infty) \frac{RT_\infty^2}{E_m} \left[1-\exp\left(-\frac{E\Delta T}{RT_\infty^2}\right)\right] \qquad \text{(E-18)}$$

where

N_i = number of moles of reactant initially;

N_f = number of moles of reactant after cooling;

A = pre-exponential or frequency factor;

E = activation energy of reaction;

R = universal gas constant, 1.985 cal/mol·K;

m = initial cooling rate;

ΔT = amount of cooling.

Typical values of A for first order reactions of interest in the probe are about $10^{10}\ s^{-1}$. Inserting this value into Eq. (E-18) and varying the activation energy, it is found that negligible loss of reactants occurs for reactions in which E is above about 50 kcal/mol while loss of approximately one fourth of the reactants is noted for an activation energy of 40 kcal/mol.

APPENDIX F

Furnace Operating Procedures

Any person who works closely with or operates the plug flow furnace should be familiar with the procedures outlined below. Figure F-1 contains a sketch of the equipment control panel which should aid in clarifying the ensuing instructions.

1 Emergency Procedures

1.1 In case of an emergency, the entire system may be shut down immediately by:

1.1.1 Turning off the POWER switch on the control panel, and

1.1.2 pushing the compressor STOP switch (on the wall, adjacent to the control panel). The POWER switch will terminate the supply of air, gas, and solid fuel to the furnace. The COMPRESSOR switch will deactivate the compressor motor.

1.2 If an immediate system shutdown is desired, but cooling air is still required within the combustion chamber, the following should be done:

1.2.1 Turn the FLAME SAFEGUARD switch to the off position. The FLAME SAFEGUARD switch will stop the flow of gas and/or solid fuel to the furnace.

1.3 A fire extinguisher is located below the light switch, immediately inside the door of the combustion facility. All operators should know how to use it.

1.4 In case emergency help must be summoned, a phone is located in the hallway just outside the door of the furnace room.

Ordinary shutdown procedures may be found in Section V.

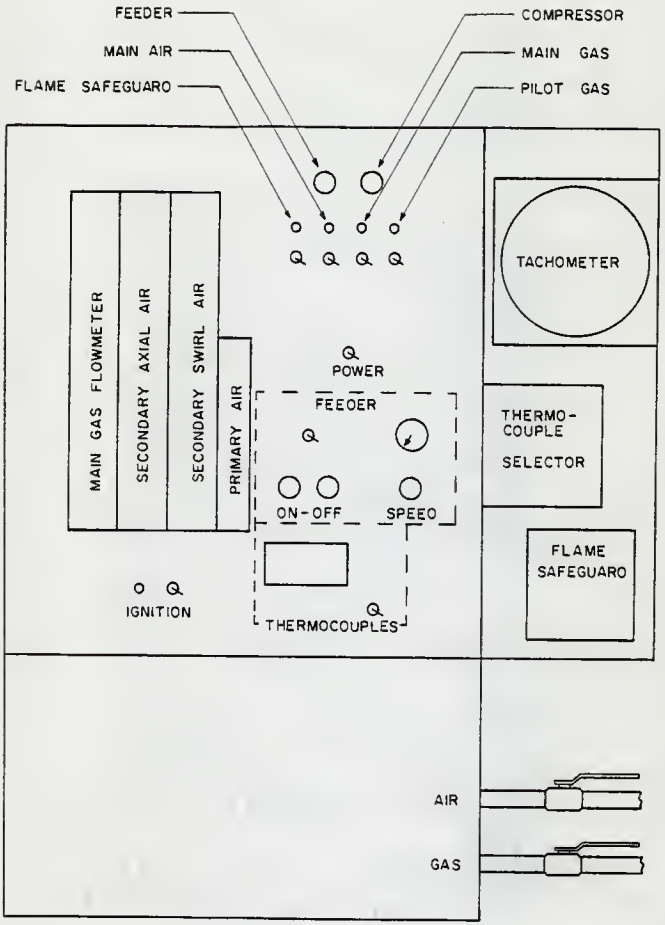

FIGURE F-I CONTROL PANEL

2. General Information

The plug flow drop furnace was designed to burn pulverized solid fuels, such as pulverized coal and finely ground wheat straw. Before a stable flame with these solid fuels can be achieved, the inside wall temperature of the furnaces must be brought up to about 1050 C through the use of a natural gas burner. Burning 80 CFH of natural gas, about 6 hours is required to attain this temperature. After the desired temperature is reached, the natural gas burner is withdrawn and the solid fuel injector inserted.

The flame is monitored continuously by an ultraviolet flame detector connected to a flame safeguard control. In the event of a flame failure the flame safeguard system will shut off supplies of gas and solid fuels to the furnace. The air to the furnace and the compressor itself must be shut down manually. Therefore, upon flame failure, air will remain flowing to cool the furnace walls.

A natural gas pilot burner is used to ignite the main gas flame. After the main gas flame has been stabilized, the pilot burner is extinguished. The pilot will be reignited at the time of change over from gas to solid fuel injectors in order to keep a flame present in the furnace at all times. Absence of a flame would cause the flame safeguard control to shut down the system.

Additional safety is provided by a low pressure limit switch on the compressed air supply line and a high temperature limit switch above the burner. Either of these switches can shut down or prevent

startup of the system by cutting off the power to the flame safeguard control. Restart can only be attempted after manually resetting these switches.

3. Startup

Before startup is attempted, the following checks should be made:

3.1 Verify that all control panel switches are in the off position, and all manual valves are closed.

3.2 Check the compressor oil level and safety pressure release valve.

3.3 Drain any condensate from the compressed air tank.

3.4 Clean the main air filter, as follows:

3.4.1 Turn on the POWER and MAIN AIR switches.

3.4.2 Open the manual drain valve, below and behind the control panel.

3.4.3 Open the manual main air valve. This should release all pressure in the air lines.

3.4.4 Remove, clean, and replace the filter bowl.

3.4.5 Close the two manual valves at the control panel.

3.5 Press the compressor START switch. The COMPRESSOR indicator lamp on the control panel should light as the compressor starts.

3.6 Open the manual valve at the compressor outlet.

3.7 Check the main air line regulator (308.0 kPa or 30 psig) and turn off the POWER and MAIN AIR switches.

3.8 Manually reset the high temperature limit switch, check to see that it is set 116 C (240 F), and see that it is positioned on top of the burner.

3.9 Manually reset the low pressure limit switch and check to see that it is set at 652.6 kPa (80 psig).

3.10 Check to see that the furnace is sealed. Seal any cracks with mortar or silicone sealant.

3.11 Make sure that all of the observation ports are sealed.

3.12 Turn on the cooling water, as follows:

3.12.1 Open the probe cooling valve about 1/4 turn (on bench, near door).

3.12.2 Open the flue cooling valve about 1/2 turn.

3.12.3 Fully open the burner cooling water valve.

3.13 Insert and clamp the gas injector in the main burner. Be sure it is properly positioned. Then open the manual valve on the injector.

3.14 Open the manual main gas valve.

3.15 Turn the following switches on:

POWER
IGNITION
PILOT GAS

No indicator lamps should light at this time.

3.16 Turn on the FLAME SAFEGUARD switch. The FLAME SAFEGUARD indicator lamp should light immediately. Within a few seconds, the following events should be observed:

3.16.1 The IGNITION and PILOT GAS lamps light. At this stage, the pilot flame should be ignited. If not,

the system will automatically shutdown. NOTE: Do not touch the body of the pilot burner assembly while the IGNITION lamp is lit. The assembly acts as a ground for the high voltage spark of the electrical ignition.

3.16.2 Upon ignition of the pilot flame, the IGNITION lamp will be extinguished and the PILOT GAS lamp will remain lit.

3.16.3 If both lamps go out (or if they never light) the sequence may be restarted by pushing the purple RESET button on the flame safeguard control box.

3.17 Turn the IGNITION switch off and the MAIN AIR switch on.

3.18 Open the manual air valve, adjust the secondary axial flowmeter valve to about 600 CFH, and adjust the secondary swirl flowmeter valve to about 200 CFH.

3.19 Open the main gas flowmeter about 1 1/2 turns.

3.20 Establish a main gas flame as follows:

3.20.1 Turn on the MAIN GAS switch.

3.20.2 Open the main gas flowmeter valve until the gas flow is about 80 CFH.

3.21 Turn off the PILOT GAS switch. At this stage, the control panel should show the following indicator lamps on:

FLAME SAFEGUARD
MAIN AIR
MAIN GAS
COMPRESSOR

All other indicator lamps should be off. The furnace wall

temperature may be monitored by switching on the readout meter and turning the thermocouple selector to the desired position.

3.23 Troubleshooting

3.22.1 If after switching on the FLAME SAFEGUARD switch, the FLAME SAFEGUARD lamp does not light, check to see that all the safety switches have been manually reset.

3.22.2 If the FLAME SAFEGUARD indicator light does light, but the PILOT GAS and IGNITION lamps do not, wait at least 15 seconds. Then press the purple RESET button on the flame safeguard control box.

3.22.3 If the PILOT GAS and IGNITION indicator lamps light and then go out without a pilot flame being established, check to see that the manual main gas valve and all pilot line valves are open. If they are open, the line of sight of the flame detector may need to be lined up with the pilot flame position. Be sure that the pilot burner is inserted in the proper port. If everything else checks out, the fuel/air mixture of the pilot may need adjustment.

4. Changeover from Gas to Solid Fuel

When the inner wall of the furnace has reached a sufficiently high temperature (1050°C) the combustion of solid fuel may be attempted. In order to burn solid fuel, a special injector must be inserted in

the place of the gas injector. The following steps should be observed:

4.1 Make sure that the feeder hopper contains a sufficient amount of the proper solid fuel.

4.2 Turn the PILOT GAS switch to the on position. The pilot flame should be ignited by the main gas flame.

4.3 Visually verify that the pilot flame is burning. The following steps need to be accomplished in as short a time as possible. Otherwise, after extinguishing the main gas flame, the furnace may cool below the temperature needed to establish a stable solid fuel flame.

4.4 Turn off the MAIN GAS and MAIN AIR switches.

4.5 Close the valve on the main gas flowmeter.

4.6 Close the manual valve on the gas injector and remove the injector from the burner.

4.7 Insert the solid fuel injector and make the proper connections to the air lines, feeder tube and burner.

4.8 Turn the MAIN AIR switch on. Open and adjust the valve on the primary air flowmeter to the proper position.

4.9 Press the feeder START button. The FEEDER indicator lamp at the top of the control panel should light and the tachometer should read about 25 rpm. Solid fuel should be observed feeding into the furnace. NOTE: The solid fuel flame is much more luminous than the gas flame, so it should be easy to visually verify. Also, the trails of individual burning solid fuel particles may be observed.

4.10 Turn on the FEEDER CONTROL switch and adjust the air pressure regulator until the desired feeder speed is attained. Important: the control pressure should not exceed 204.7 kPa (15 psig).

4.11 Stabilize the solid fuel flame by adjusting the air flow rates, through the three air flowmeters. NOTE: As an approximation, use 15% primary air, 45% secondary axial air, and 45% swirl air. These figures will give a very slightly lean mixture.

4.12 At this stage, only the following indicator lamps should be lit:

FEEDER
COMPRESSOR
FLAME SAFEGUARD
MAIN AIR
PILOT GAS

There should be flow indicated through all three air flowmeters, but no gas flow.

4.13 Troubleshooting.

4.13.1 If a shutdown occurs when the MAIN GAS switch is turned off the pilot flame probably failed. Make sure that the manual main gas valve has not been closed. Try to verify that the line of sight of the flame detector intersects the axis of the pilot flame. Reignite the pilot burner by turning on the PILOT GAS and IGNITION switches and pressing the purple RESET button on the flame safeguard control box.

4.13.2 If the main flame does not ignite, or is unstable, the furnace wall temperature may not be high enough. Re-insert the gas injector and resume natural gas heating.

4.13.3 If a pulsing phenomenon is noticed, try operating the feeder at a higher rpm setting. This, of course, will necessitate increasing the air flow in order to supply combustion air for the increased amount of solid fuel.

V. Shutdown

5.1 Shutdowns after short term operation.

5.1.1 Turn off the POWER switch. This will deactivate all components except the compressor.

5.1.2 Turn off all other switches on the control panel.

5.1.3 Close all flowmeter valves.

5.2 Shutdowns after long term operation.

5.2.1 Turn off the FLAME SAFEGUARD switch. This will deactivate all components except the main air and the compressor. The air needs to be left on only if it is required to aid in cooling down the furnace.

5.2.2 Turn off all other switches on the control panel except for the POWER switch and the thermocouple readout power switch.

5.2.3 Close the gas flowmeter valve and the manual main gas valve.

5.2.4 When the furnace has cooled sufficiently, close the manual main air valve and the air flowmeter valves.

5.2.5 If the compressor has been running for a long period, allow it to run free (with no load) for several minutes before shutting it off.

6. Restart

6.1 To restart after a routine shutdown, repeat Section 3.

6.2 To restart after a safety shutdown, the cause of the interruption must be identified and corrective action taken. After manually resetting all safety switches, restart can be attempted by following the procedures of Section 3.

DESIGN, FABRICATION, AND TESTING OF A PULVERIZED FUEL COMBUSTION FACILITY

by

Lawrence Patrick Nelson

B.S., Pittsburg State University, 1977

AN ABSTRACT OF A MASTER'S THESIS

submitted in partial fulfillment of the

requirements for the degree

MASTER OF SCIENCE

Department of Nuclear Engineering

KANSAS STATE UNIVERSITY

Manhattan, Kansas

1979

ABSTRACT

A laboratory scale combustion chamber was constructed and subsequently employed in studies of the gaseous emission characteristics of wheat straw co-fired with two coals. Tests of the chamber were performed to evaluate the degree of similarity to full scale boilers used in utility and industrial applications. The co-firing of wheat straw with coal was achieved at several different input air conditions to determine the effect of swirl and excess air on the levels of sulfur dioxide (SO_2) and oxides of nitrogen (NO_x) in the gaseous combustion products.

While increasing excess air increased NO_x emissions in all cases, the introduction of more swirl led first to a reduction in NO_x and then to an increase as the swirl percent increased past approximately 50%. Insofar as both of these parametric variations are in accord with results from other furnaces, the furnace operation was judged acceptable. Incomplete conversion of sulfur to SO_2 was obtained and some dependence on excess air and percent swirl was noted. This effect, anomalous in comparison with most other work, is explained on the basis of cooler temperatures in the current experiments, which from recent basic experimentation, have been shown to lead to comparable levels of sulfur conversion. Further reduction in the SO_2 levels may have been caused by relatively high ash loadings leading to absorbance of some SO_2.

Of most importance is the effect of wheat straw addition on NO_x emissions. Concurrent with the decrease in SO_2 levels, NO_x emissions

were increased by up to a factor of 4 over those observed from firing coal alone. The higher NO_x emissions are accounted for by the presence of nitrogen in weakly bound (compared to coal) functional groups in the straw which are easily evolved in the primary flame region and oxidized to NO_x. Although the firing of wheat straw is effective in suppressing SO_2 formation, the increased levels of NO_x emissions indicate that combustion modifications will be necessary to suppress this pollutant.